University of Windsor
Scholarship at UWindsor

Electronic Theses and Dissertations

2016

Experimental Investigations on Evaporation from Porous Media

Rafal Marynowski
University of Windsor

Follow this and additional works at: http://scholar.uwindsor.ca/etd

Recommended Citation
Marynowski, Rafal, "Experimental Investigations on Evaporation from Porous Media" (2016). *Electronic Theses and Dissertations.* Paper 5846.

This online database contains the full-text of PhD dissertations and Masters' theses of University of Windsor students from 1954 forward. These documents are made available for personal study and research purposes only, in accordance with the Canadian Copyright Act and the Creative Commons license—CC BY-NC-ND (Attribution, Non-Commercial, No Derivative Works). Under this license, works must always be attributed to the copyright holder (original author), cannot be used for any commercial purposes, and may not be altered. Any other use would require the permission of the copyright holder. Students may inquire about withdrawing their dissertation and/or thesis from this database. For additional inquiries, please contact the repository administrator via email (scholarship@uwindsor.ca) or by telephone at 519-253-3000ext. 3208.

EXPERIMENTAL INVESTIGATIONS ON EVAPORATION FROM POROUS MEDIA

By

Rafal Marynowski

A Thesis
Submitted to the Faculty of Graduate Studies
through the Department of Civil and Environmental Engineering
in Partial Fulfillment of the Requirements for
the Degree of Master of Applied Science
at the University of Windsor

Windsor, Ontario, Canada

2016

© 2016 **Rafal Marynowski**

EXPERIMENTAL INVESTIGATIONS ON EVAPORATION FROM POROUS MEDIA

By

Rafal Marynowski

APPROVED BY:

_____

G. Rankin
Department of Mechanical, Automotive and Materials Engineering

_____

R. Carriveau
Department of Civil and Environmental Engineering

_____

T. Bolisetti, Advisor
Department of Civil and Environmental Engineering

_____

R. Balachandar, Co-Advisor
Department of Civil and Environmental Engineering

September 21, 2016

DECLARATION OF ORIGINALITY

I hereby certify that I am the sole author of this thesis and that no part of this thesis has been published or submitted for publication.

I certify that, to the best of my knowledge, my thesis does not infringe upon anyone's copyright nor violate any proprietary rights and that any ideas, techniques, quotations, or any other material from the work of other people included in my thesis, published or otherwise, are fully acknowledged in accordance with the standard referencing practices. Furthermore, to the extent that I have included copyrighted material that surpasses the bounds of fair dealing within the meaning of the Canada Copyright Act, I certify that I have obtained a written permission from the copyright owner(s) to include such material(s) in my thesis and have included copies of such copyright clearances to my appendix.

I declare that this is a true copy of my thesis, including any final revisions, as approved by my thesis committee and the Graduate Studies office, and that this thesis has not been submitted for a higher degree to any other University or Institution.

ABSTRACT

Evaporation is an important component of hydrological cycle. With rising global temperatures it is important to gather knowledge about evaporation and the physics involved. In this investigation, the evaporation from fully saturated bare soils was conducted to determine the drying process of porous media. It is defined that evaporation from fully saturated bare soils is categorized into two main stages Stage 1 and Stage 2 and an intermediate stage called the falling rate period. The evaporation process from fully saturated porous media begins with Stage 1 evaporation. At this stage the evaporation is constant with high evaporation rate, this is caused by the capillary action transporting the water molecules up to the surface of the porous media. Next, the evaporation enters the falling rate period where the evaporation drops over time with capillary forces growing weaker. After the falling rate period the evaporation enters Stage 2 evaporation where the evaporation rate is really low. In this investigation, experiments were conducted in order to gather a database to predict the evaporation model based on the ambient and soil conditions. The investigation was done using both traditional method of evaporation estimation and infrared imagery. Infrared imagery was introduced as a non-intrusive way of determining the temperature changes of the surface of the porous media. The experiments also focused on the evaporation behaviour due to different boundary conditions and variety of turbulent air flow velocities. A mathematical model was used to analyse the evaporation rates as a function of temperature, air flow velocity, humidity and porous media characteristics. The model was able to predict the observed evaporation rates successfully during Stage 1 and Stage 2 evaporation.

DEDICATION

To Mom, Dad and Pat

ACKNOWLEDGMENTS

I would like to thank all of those who have helped in the completion of this thesis. I would like express deepest appreciation and special thanks to my supervisor Dr. T. Bolisetti, for his assistance, guidance, support and patience throughout the over the past three years. I would also like to thank my co-advisor Dr. R. Balachandar for his input and support throughout the project. I would also like to thank my committee members, Dr. R. Carriveau and Dr. G. Rankin for their comments and suggestions.

I would also like to thank Dr. V. Roussinova in providing her input of the design of the wind tunnel models.

I would like to express my gratitude to the University of Windsor technician Matt St. Louis for his support and help in constructing my testing apparatus.

I would also like to thank Mehdi Heidari and Vimaldoss Jesudhas for their assistance and input throughout the duration of the thesis.

I would also like to thank my parents Hanka Marynowska and Robert Marynowski, and my brother Patryk Marynowski for their support and patience.

TABLE OF CONTENTS

LIST OF TABLES

LIST OF FIGURES

NOMENCLATURE

A – Evaporating area, (m^2)

Bias – Uncertainty of the measuring device

e – Experimental evaporation, (mm/d)

ė – Evaporation of water, (mm/d)

e_p – Potential water evaporation, (mm/d)

e_{s1} – Stage 1 evaporation, (mm/d)

e_{s2} – Stage 2 evaporation, (mm/d)

g – Acceleration due to gravity, (m/s^2)

H – Height of liquid column, (m)

h_a – Thermal conductivity of fluid air, (W/m^2K)

L_C – Characteristic length, (cm)

L_G – Gravitational characteristic length, (cm)

L_V – Viscous characteristic length, (cm)

L_W - Latent heat of vaporization, (J/Kg)

P_S – Static pressure, (Pa)

P_T – Dynamic pressure, (Pa)

Pv_a - Ambient vapour pressure, (Pa)

Pv_s – Saturation vapour pressure, (Pa)

r_2 – Large pore size, (mm)

r – Soil pore radius, (m)

r_{BL} – Boundary layer resistance, (Pa d mm^{-1})

Re_x – Reynolds number

RH – Relative humidity, (%)

r_{s1} – Stage 1 vapour flow resistance, (Pa d mm^{-1})

r_{s2} – Stage 2 vapour flow resistance, (Pa d mm^{-1})

S_{RH} – Standard deviation of relative humidity, (%)

S_T – Standard deviation of ambient temperature, (°C)

S_x –Standard deviation

t_{95} – Student's t variable

T_a – Ambient temperature, (°C)

T – Ambient temperature, (°C)

T_s – Surface temperature, (°C)

u_0 – Zero uncertainty

u_a – Instrument uncertainty

u_d – Design uncertainty

UN – Total uncertainty

V – Fluid velocity, (m/s)

V_∞ – Air flow velocity, (m/s)

x – Distance of the downstream start of the boundary layer, (mm)

Greek Letters

γ – Small to large pore size ratio

Δm – Change in mass, (g)

δ – Boundary layer thickness (mm)

ε – Reduction factor

η – Dynamic viscosity, (Pa-s)

Θ_s – Saturated water content

Θ_r – Residual water content

κ – Permeability of porous medium, (m^2)

ρ_w – Density of water, (kg/m^3)

σ – Surface tension, (N/m)

CHAPTER 1

INTRODUCTION

1.1 General

Evaporation is a process in which liquid water is transferred from land and water masses into the atmosphere (Veissman et al. 1989). Water in the soil can be found in various forms which exhibit varying degrees of binding with the soil particles. Drying of porous medium is the expression of evaporating water being replaced by the surrounding air infiltrating the soil particles. Evaporation is the largest component of hydrological cycle (Linsley et al., 1982). Evaporation plays an important role in plant transpiration and organisms living beneath the soil surface. With increasing global evaporation a significant impact will be felt by various sectors, mainly agriculture as it primarily thrives on hydrological cycle (Neriah et al., 2014). As the temperatures around the globe are rising and are projected to continue to rise over the next century, the earth is bound to see significant changes in its natural environment. These include droughts, extreme weather (rise in hurricane intensities and tropical cyclones etc.) and increase in evaporation. Furthermore, evaporation is of significance in many engineering and industrial processes, such as construction, fuel cell technology, and food processing.

The main complexity of predicting evaporation rates is due to its dependence on a variety of factors e.g., humidity, air temperature, air velocity, sun radiation and characteristics of the porous medium, such as porosity, angularity and grain size (Davarzani et al. 2014). It is also important to take into consideration bonds between water particles as well as capillary and gravitational forces. Capillary action occurs when capillary forces of the soil particles are stronger than the forces between the water particles (Lehmann et al. 2009). This occurs when the evaporating surface of the soil sample draws the water from the saturated layers in order to stay moist. The height from which the water can be drawn depends on the capillary forces as well as the forces of gravity. Water that is subject to gravitational forces typically moves in the soil from top to bottom.

The cause of evaporation is the difference in water vapour pressure at its evaporating surface and the surroundings. During the evaporation stage, the difference in water pressure slowly equalizes itself. Another phenomenon that can cause vaporization of water is air flow; this causes

the humid and dry air to exchange water particles, meaning that less humid air becomes more humid as it passes over the saturated soil. The velocity at which the air is moving has a significant effect on the drying process of the saturated porous media (Haghighi et al. 2013). Faster air that is less humid than the soil will exchange the water particles quicker than a slow moving air as it flows over the soil. In order for the evaporation to occur, energy is required and this energy is usually delivered by direct sun radiation or change in ambient temperature. Although hard to predict, the phenomena of evaporation is an important component in energy balance of bare soil surface (Aluwihare and Watanabe 2003).

There has been a renewed interest in the recent years on water evaporation due to extended dry spells. There has been a significant progress in developing the knowledge on the evaporation process, although no concrete method of evaporation estimation has been developed (Smits et al. 2012). Thus it is necessary to discover more tools that can help in estimating water evaporation. Research on this problem has progressed significantly in both experimental and modeling frameworks. Mathematical modelling involves the use of complex variables and equations accompanied by computational tools. On the other hand, the estimation of evaporation by experimental testing, another commonly used method, is a valuable approach to investigate the processes occurring at the interface of the porous media and the atmospheric surface. Different soil samples are subjected to direct sunlight or other conditions, such as convection drying or combination of both direct sunlight and air flow. Experimental testing is usually done in the lab where most of the parameters are known and all the variables are measured using various devices, such as scales, Pitot-static tubes, humidity sensors and temperature sensors.

1.2 Objectives

The main objectives of this thesis are

- to experimentally investigate the phenomenon of evaporation from porous media based on forced convection via thermal imagery and establish a model based on the results
- to develop experimental datasets that can be used for mathematical modeling studies
- to analyze the evaporation rates of different soils through the use of a mathematical model

The sub-objectives of this research are to:

- Evaluate the effects of convection due to air flow, at different velocities, over different soils (fine, coarse and mixed sands) through wind tunnel experiments.
- Investigate the boundary effects of different tunnel models.
- Establish a model based on the experimental results.
- Analyze the evaporation using temperatures from infrared imagery.

The basic idea of the experiment is that as the water evaporates from the soil sample the soil itself changes temperature thus indicating that water is evaporating. In order to analyze the evaporation, a series of infrared images were taken. These images were then analyzed for the temperature changes and eventually for obtaining an estimate of the evaporation.

1.3 Scope of Work

The present research work, consisting of 42 individual experiments, was conducted at the University of Windsor's Ed Lumley Center of Engineering Innovation. The experiments were carried out in two different tunnels on three different soil conditions and four different air speeds. The surface temperatures of the soils were obtained using an infrared camera. The data were analysed using analytical expressions to estimate the evaporation and were compared with the actual estimates of evaporation rates obtained from the water loss measurements.

CHAPTER 2

LITERATURE REVIEW

2.1 General

In this chapter, the literature on water evaporation is reviewed. The literature review consists of an overview of the evaporation process and its methods of estimation, the mechanisms of the drying stages, experimental methods of evaporation rate estimation and the mathematical models used.

2.2 Evaporation

Evaporation is often characterised as the removal of moisture from the soil or capillary porous media. The evaporation phenomenon occurs at the surface of the porous medium where the water gets vaporised into water vapour and the pores within the soil get replaced with ambient air. Evaporation is caused by factors such as convection of air, relative humidity, air temperature and infrared radiation. After the water from the surface turns into vapour it gets either replaced with ambient air that fills the soil pores or the soil draws the water from layers below the surface. This phenomenon is caused by the capillary flow inside the porous media where the water flows through hydraulic paths (Lehmann et al., 2009) in the saturated zone of the sample. The capillary action is often expressed as

$$H = \frac{2\sigma cos\theta}{\rho_w g r} \qquad (2.1)$$

where, H is the height of the liquid column (m), σ is the liquid-air surface tension (N/m), θ is the angle of contact, ρ_w is the density of water (kg/m^3), g is the acceleration due gravity (9.81m/s^2) and r is the radius of soil pores (m). One of the reasons that the capillary action is possible is due to the bonds between the water particles; this means that as long as the surface tension of water is strong enough the capillary flow will occur. Gravitational force acts opposite to the capillary flow meaning that the water not only has to sustain the water surface tension but also conquer the gravitational forces acting upon it. Gravitational forces make it more difficult for the water to travel vertically thus slowing down the evaporation phenomena. Other variables that can affect the rate of evaporation are temperature, humidity, wind velocity, pressure, soil conditions (fine, coarse and/or mix sands) and saturation level (Ghosh et al., 2008).

2.2.1 Drying Process

The drying process of a fully saturated soil sample is considered, to be a removal of moisture from its surface. Evaporation is controlled by several atmospheric elements that affect the rate of evaporation they include, wind velocity, ambient air temperature, atmospheric pressure, solar radiation, humidity, water temperature and characteristics of porous medium (grain size distribution, pore size and capillary forces etc.) (Gupta, 1989; Shokri et al., 2009; Veissman et al., 1989). It is observed that the rates of evaporation are affected by the changes of heat flux of the ambient temperatures and differences of vapour pressures (Aoki, 2000; Zhang et al., 1997), wind effects such as laminar and turbulent flows and difference in humidity also have a significant effect on the drying process of porous media (Mahfouf and Moilhan, 1991). Soil characteristics such as angularity and grain size distribution affect the water transfer system inside of the porous medium (Mahfouf and Moilhan, 1991).

The drying process of porous media is categorized into two drying stages Stage 1 and Stage 2 and an intermediate falling rate period (FRP) (Smits et al., 2012). In Stage 1, evaporation occurs at the beginning of the evaporation period when a sample of soil is fully saturated. During this stage the evaporation remains constant with high evaporation rate (Shahraeeni et al., 2012). The high evaporation rate is caused by the capillary action that transports the water up to the evaporating surface from hydraulically connected drying front (Shokri and Or, 2013). The capillary action of Stage 1 evaporation can be mathematically modelled by knowing the soil and ambient conditions (Neriah et al., 2014). With the ambient conditions determined experimentally. Capillary action continues until the hydraulic continuity between the evaporating surface and the receding drying front of the water transport is broken; changes in evaporation are then observed (Haghighi et al., 2013). At the end of Stage 1 evaporation the drying enters into the falling rate period. Falling rate period is defined as the intermediate stage between Stage 1 and Stage 2 evaporation (Nachshon et al., 2011). Over the duration of the FRP the evaporation from porous media decreases significantly. At this stage the drying front recedes into the soil drawing the water from the saturated zones underneath the drying front (Shokri and Or, 2013). This process continues until there is an equilibrium between the capillary and gravitational forces therefore the capillary action seizes to transport the water molecules up to the drying front (Scherer, 1990; Shokri et al., 2008). Stage 2 evaporation begins after the FRP. At this stage of

evaporation the effects of wind velocity are minimal and most of the evaporation happens at the secondary drying front which forms after the capillary action no longer supplies the water to the evaporating surface (Shokri and Or, 2011; Davarzani et al., 2014). During Stage 2 most of the evaporation is done by slow exchange air particles infiltrating the soil depth at the Stage 2 drying front (Nachshon et al., 2011).

2.3 Evaporation Estimation

2.3.1 Analytical Approach

As discussed above the evaporation is a two step process where the water molecules require enough energy in order to breach through the water surface and escape into the atmosphere (Gupta, 1989). During that process most of the energy is provided by solar radiation, after which the water molecules get transported out of the evaporating surface into the atmosphere by the means of the air convection (Laurindo and Prat, 1996).

The simplest method of evaporation estimation is the pan method which is used to find the evaporation from the body of water. In this method a galvanized iron pan 4 ft in diameter and 10 inches deep is filled with water to a depth of 8 inches and mounted 12 inches above the ground. The readings are then taken manually by a hook gage. The evaporation is then found by computing the difference of the measured levels during the observation. Another method of estimating evaporation is the energy budget method. The energy budget equation of estimating the evaporation accounts for the incoming and outgoing radiant energy stored in the system (Veissman et al., 1989). This method requires sophisticated and often expensive measuring instruments such as lysimeters. The energy budget equation is highly dependent on the precision and reliability of the collected data. This method of estimating evaporation is not commonly used. Another method of estimating evaporation from porous media is the mass transfer method, which is widely used in many processes, such as drying, humidifying, precipitation and dispersion of contaminants. In this thesis the mass transfer method is used for the computation of the evaporation and drying process of the porous media. A simple equation of mass transfer can be written as:

$$\dot{m} = f(u)(p_s - p_a) \qquad (2.2)$$

where, $\dot{m}$ is the evaporative flux of water, $f(u)$ is a function of wind velocity, temperature and relative humidity, p_s and p_a are the saturation vapour pressure and vapour pressure an ambient air. The air that flows over the evaporating surface creates what is defined as boundary layer, where its thickness is governed by the air flow velocity. Another way of expressing the free-water evaporation estimation is with the combination of mass transfer method which is defined as the potential evaporation (e_p) of water vapour (Veissman et al., 1989). Evaporation of surface water from porous media is a two step process. The water molecules are transported by the capillary action or molecular diffusion in the soil from the water surface up to the drying front or land surface (Kondo et al., 1989). The second process involves the surface water to be transformed into water vapour where it is transported from the land surface into the atmosphere by laminar or turbulent air flows (Aluwihare and Watanabe, 2003; Veissman et al., 1989). With only surface water present at the surface of the soil the expression for evaporation can simply be written as:

$$e_p = \frac{(Pv_s - Pv_a)}{r_{BL}} \qquad (2.3)$$

where, (r_{bL}) is the resistance of the boundary layer due to a combination of boundary layer thickness over the vapour diffusion coefficient, (Pv_s) is the saturated vapour and (Pv_a) is the atmospheric vapour pressure.

Modelling of evaporation from porous media has proven to be a problematic task at hand, where there is no agreement as to what is the best method of evaporation estimation from porous media (Smits et al., 2012). The evaporation from bare soils depends on the properties of the characteristics of the porous media and the ambient conditions (Smits et al., 2011). Due to soil characteristics the evaporation rates can differ substantially. Budyko, 1955 developed an evaporation reduction factor (ε) that reduces the potential evaporation (e_p) giving an estimate of evaporation from soils ($\dot{e}$):

$$\dot{e} = \varepsilon e_p \quad (2.4)$$

where, ε is the reduction factor associated with the soil properties and water content and $\dot{e}$ is the water evaporation from soil. For fully saturated bare soil surface the $\varepsilon = 1$ however, when the water content in the soil decreases so that $\varepsilon < 1$, $\dot{e} < e_p$ (Brutsaert, 2005). As described, the

process of drying involves two stages Stage 1 and Stage 2 and many variables are involved. During the Stage 1 evaporation, the water diffusion is the same as the evaporation rate at the surface of the bare soil (Yiotis et al., 2007), therefore the Stage 1 evaporation can be expressed as:

$$e_{s1} = \frac{(Pv_s - Pv_a)}{r_{s1}} \qquad (2.5)$$

where, e_{s1} is the evaporation during stage 1, Pv_s is the saturated vapour pressure, Pv_a is the atmospheric vapour pressure and r_{s1} is the combination of air flow boundary layer and surface resistance. The constant evaporation of Stage 1 continues up until the hydraulic continuity in the soil breaks, after which the effects of air flow are minimal on the evaporation (Davarzani et al., 2014) and the evaporation is mostly controlled by the diffusive mass transfer of porous media (Prommas, 2011; Schultz, 1991). During that stage the evaporation is substantially lower than the Stage 1 evaporation and it is expressed as:

$$e_{s2} = \frac{(Pv_s - Pv_a)}{r_{s2}} \qquad (2.6)$$

where e_{s2} is the evaporation rate of Stage 2 evaporation and r_{s2} is the combination of the Stage 1 resistance and viscous resistance.

When modelling the evaporation of Stage 1, the duration is mainly dependant on three factors: gravitational length, viscous length and characteristic length (Neriah et al., 2014) and it is expressed as:

$$\tau = \frac{L_C(\theta_s - \theta_r)}{e_{s1}} \qquad (2.7)$$

where, θ_s is the saturated water content, θ_r is the residual water content and e_{s1} is the Stage 1 evaporation. The characteristic lengths determine the extent of the hydraulically connected evaporating surface and the receding drying front (Lehmann et al., 2008). As stated before, Sage 1 depends on the hydraulic capability of the soil to rehydrate the evaporating surface by capillary action. This is determined by the gravitational characteristic length (L_G) where it defines the maximum vertical length that the liquid-filled pores connect to the drying front and the

evaporating surface sustaining the constant evaporation (Lehmann et al., 2008). This force balance between the capillary action and the gravitational force is expressed as:

$$L_G = \frac{\sigma}{\rho g r_2}\left(\frac{2}{\gamma} - 2\right) \quad (2.8)$$

where ρ is the density of water (kg/m^3), σ surface tension (N/m) and r_2 large pore size (mm). Another variable that affects the duration of Stage 1 evaporation is the viscous length, it represents the viscous dissipation. The viscous length is represented as:

$$L_V = \frac{\sigma\kappa}{\eta e_0 r_2}\left(\frac{2}{\gamma} - 2\right) \quad (2.9)$$

where κ is the permeability of the porous medium, η is dynamic viscosity (Pa-s) and e_0 is the potential evaporation (mm/d). Combining both the gravitational and viscous length the critical length (L_C) can be found (Lehmann et al., 2008; Lehmann and Or, 2009). Critical length marks the end of stage 1 and the beginning of the falling rate period and it is expressed as:

$$L_C = \frac{L_G}{\frac{L_G}{L_V}+1} \quad (2.10)$$

2.3.2 Experimental Approach

2.3.2.1 Investigations of Effects of Ambient Conditions on Evaporation

The rate of evaporation is greatly affected by the ambient conditions one of which is the air temperature. Having warmer air with lower vapour concentration pass over the saturated sample it is more likely that the surface moisture will be removed faster (Davarzani et al., 2014). Bittelli et al., 2008 claimed that heat and mass transfer of the soil is controlled by the dynamics of the drying surface and the atmospheric temperature boundary layer. A model was developed by (Jassal et al., 2003) that incorporates the atmospheric temperature boundary layer and determination of mass transfer in the soil surface. Similarly an experiment done by Davarzani et al., 2014 and shown in **Figure 2.1** illustrates how wind velocity combined with different air temperatures affect the initial stages of evaporation over a certain period of time. From the graph it is shown that as the air temperature is increased the initial evaporation (first linear portion of the graph) changes as well. With a higher temperature the initial evaporation of porous media reaches its maximum rate much quicker than with the lower temperatures. During the initial

evaporation the rate of drying is controlled by the high atmospheric demand such as high temperatures and wind velocities (Bittelli et al., 2008).

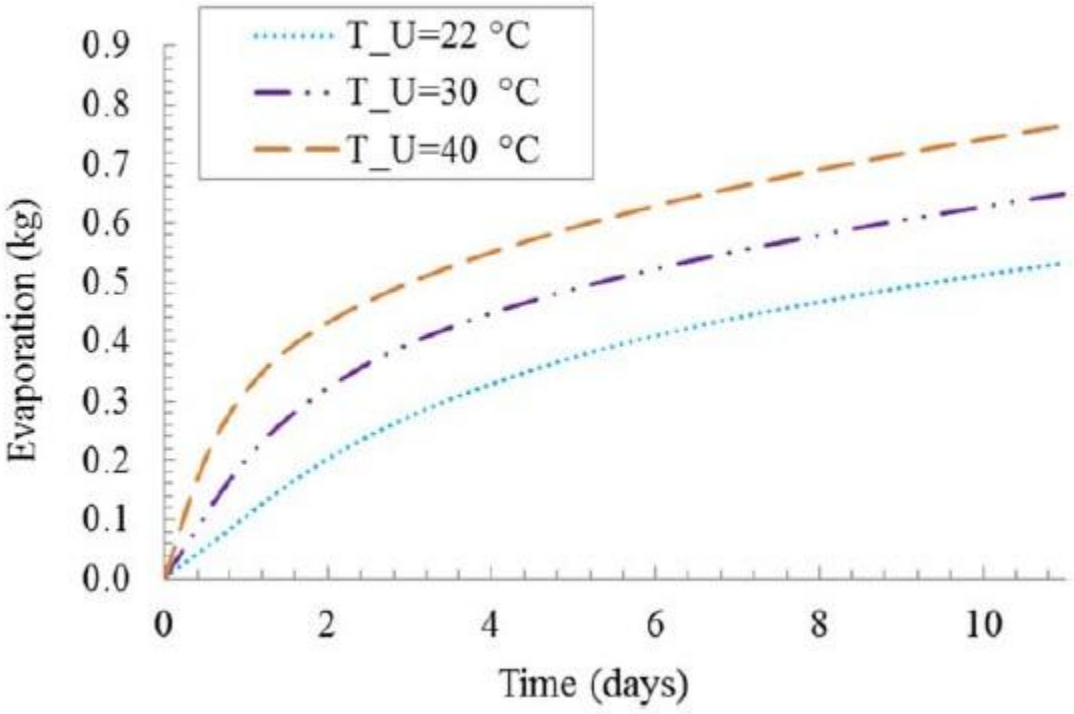

Figure 2.1 Variation in temperature with constant wind velocity (Davarzani et al., 2014)

As the water evaporates from the fully saturated porous medium the drying front moves deep into the soil, it is presumed that the top surface is dry (Nachshon et al., 2011). The occurrence of drying front receding into the porous medium affects the temperature of the soil. One of the hypotheses is that as the soil dries it warms up making it possible to see the transitions from Stage 1 to Stage 2. With the top surface of the soil drying, it is seen from **Figure 2.2** that the temperatures increase over time. With the sensor 3 being 2.5 cm below the soil surface the figure shows the temperature of the porous medium. The hypothesis is that if the soil temperature increases the surface temperature increases as well (Shahraeeni and Or, 2010). During the experiment, Davarzani et al. 2014 kept the ambient relative humidity relatively constant. Humidity and vapour changes are the two important factors that affect the rate of evaporation (Sakai et al., 2011).

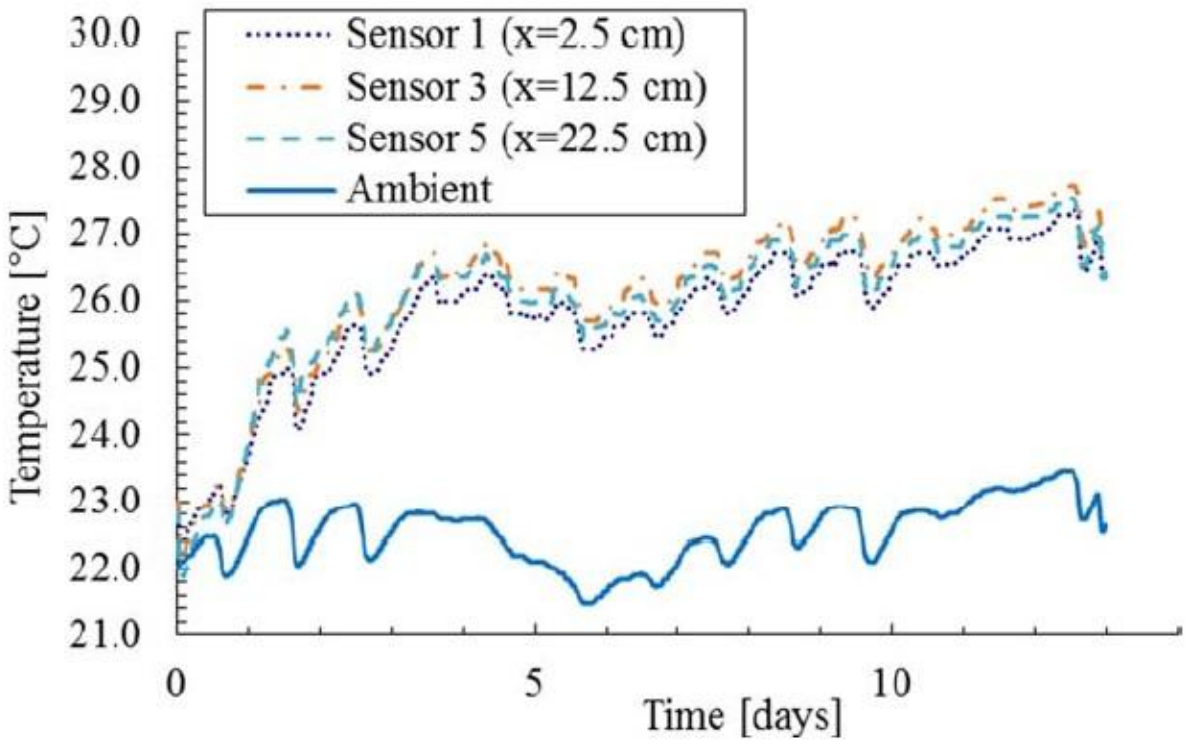

Figure 2.2 Increase in temperature over time (Davarzani et al., 2014)

A model developed by Mahfouf and Moilhan, 1991 was used to estimate the evaporation of surface water in terms of the absolute humidity at the vapor interface level. This model was then used by Daamen and Simmonds 1996 to estimate the evaporation from bare soil based on humidity measurements. The model included the in-situ determination of evaporation based on the saturated absolute humidity. In **Figure 2.3** an experiment performed by Mahfouf and Moilhan, 1991 shows that the changes in humidity affect the evaporation of water from bare soils. Test 1 shows the case of high relative humidity and Test 5 shows the evaporation rate based on low relative humidity. Therefore, changes in evaporation are closely related to the changes in vapour pressure (Kohsiek, 1980; Seymour and Hsiao, 1984).

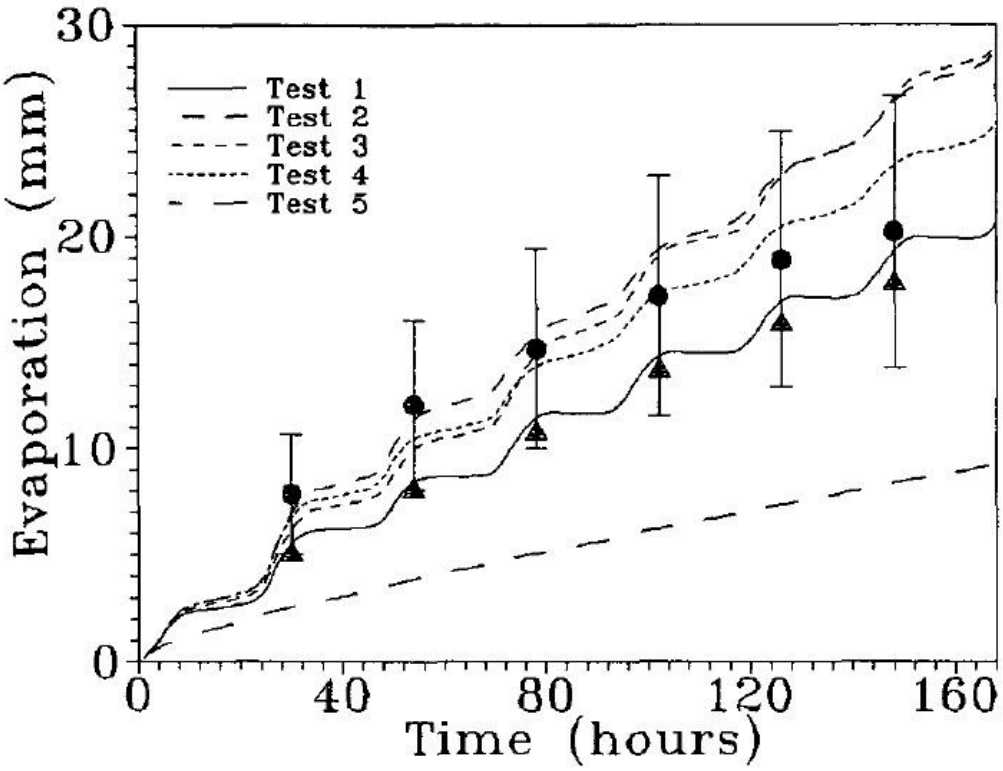

Figure 2.3 Evaporation based on the changes in humidity (Mahfuf, 1990)

The wind velocity is yet another factor affecting the rate of water evaporation. An increase of air flow velocity increases the Stage 1 evaporation rate which shortens the duration of Stage 1 evaporation while decreasing the air velocity decreases the Stage 1 evaporation and lengthens the duration of Stage 1 (Davarzani et al., 2014). One way of determining evaporation due to wind flow velocity is establishing the wind velocity profiles which give an insight into the boundary layer thickness of the flow. Boundary layer due to a non-slip condition is a region where the viscous forces predominate (Cengel et al., 2011). There are multiple ways of obtaining wind velocity profiles, these methods range from hotwire, Pitot-static tube and LDV (Prichard and Leylegian, 2011). **Figure 2.4** shows a typical velocity profile for the laminar flow of air in a duct. Velocity profiles in the wind tunnel experiments are usually symmetrical when surfaces of the top and bottom of the tunnel are made out of the same material. One of the more accurate methods to capture the velocity profile is the Laser Doppler Velocimetry or (LDV) (Aksel and Schmidtchen, 1996), LDV works by the use of laser in order to record the velocity of the fluid.

Although LDV is the most accurate it requires expensive equipment and proper seeding devices. One of the most challenging tasks in LDV is the proper seeding which ranges from consistency, density and particle size.

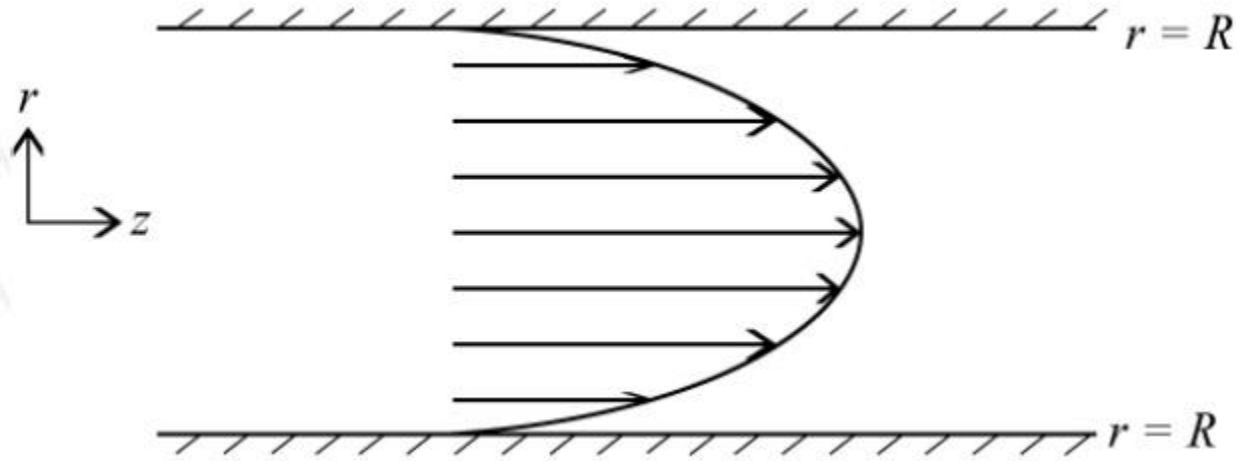

Figure 2.4 Velocity profile in a duct pipe (Libii, 2013)

Another tool that is used to record the velocity profiles is the Pitot tube, although less accurate than the LDV it is still widely used. A simple Pitot tube is used to measure the stagnation pressure of a moving fluid. Pitot-static tube on the other hand measures the dynamic pressure of the moving fluid which is the difference between the stagnation pressure and the static pressure of the fluid (Wecel et al., 2008; Prichard and Leylegian, 2011). The dynamic pressure is then displayed on the pressure transducer that the Pitot-static tube is connected to. In order to record the whole profile, the Pitot-static tube is moved from the bottom of the duct all the way to the top in equal increments which results in establishing a appropriate velocity profile. The two recorded pressures are converted to velocity using a simple equation:

$$V = \sqrt{\frac{2(P_T - P_S)}{\rho}} \quad (2.11)$$

where, V is the velocity of the fluid (m/s), P_T is the total pressure of the fluid (Pa) P_S is the static pressure of the fluid (Pa) and ρ is the density of the fluid (kg/m^3). The velocities are then plotted on a graph against a flow depth.

Theoretical assumptions of the boundary layer thickness can also be obtained from the following equation (Prichard and Leylegian, 2011):

$$\delta = 0.382 \frac{x}{Re_x^{1/5}} \quad (2.12)$$

where, x is the distance of the downstream start of the boundary layer, Re_x is the Reynolds number for turbulent flow. One of the important aspects in convective drying of porous media is to obtain an accurate turbulent wind velocity profile; this is achieved by tripping the laminar boundary layer by the use of the trip wire (Prichard and Leylegian, 2011). One of the ways to determine if the turbulent boundary layer has been achieved is by checking the Reynolds number. High Reynolds number signifies that the flow in the tunnel is more turbulent and lower number means that the flow is more laminar. A study by Shahraeeni et al., 2012 was done where a variety of different wind velocities were used. The study concluded that there is a difference in evaporation rates with increasing velocities as shown in **Figure 2.5**. With the velocities ranging from 0.75, 1.5, 2.5 and 3.5 m/s there seem to be an impact on the amount of the water lost during the initial evaporation (Stage 1). With increased velocities the Stage 1 evaporation duration appeared to decrease (Davarzani et al., 2014). Another experiment by conducted by (Haghighi et al., 2013) had shown that the increase in velocity over a surface of porous media decreases the duration of Stage 1 evaporation. This signified that there is an impact on the Stage 1 evaporation with increased air flow. One aspect of evaporation with forced air flow is the affect of wall boundaries on the tunnel conditions. The hypothesis is that with the smaller tunnel there is much more interference between the wall boundaries thus affecting the rate of evaporation of water from porous media. A study done by Mokhtari and Bradshaw, 2016 where the interference of the boundary walls was studied. The study found that there is a presence of longitudinal vortices in the wind tunnel boundary layers. Another study done by Hottner, 1995 to determine the disturbances in air flow velocity by a single wall adaptation. From the experiment conducted by Hottner, 1995 it was shown that there is some interference with the adaptation of the single wall boundary condition. Bouriga et al., 2014 studied the interference of the wall boundary conditions due to contractions in the tunnel. The experiment concluded that there were slight non-uniformities in the tunnel's boundary layer.

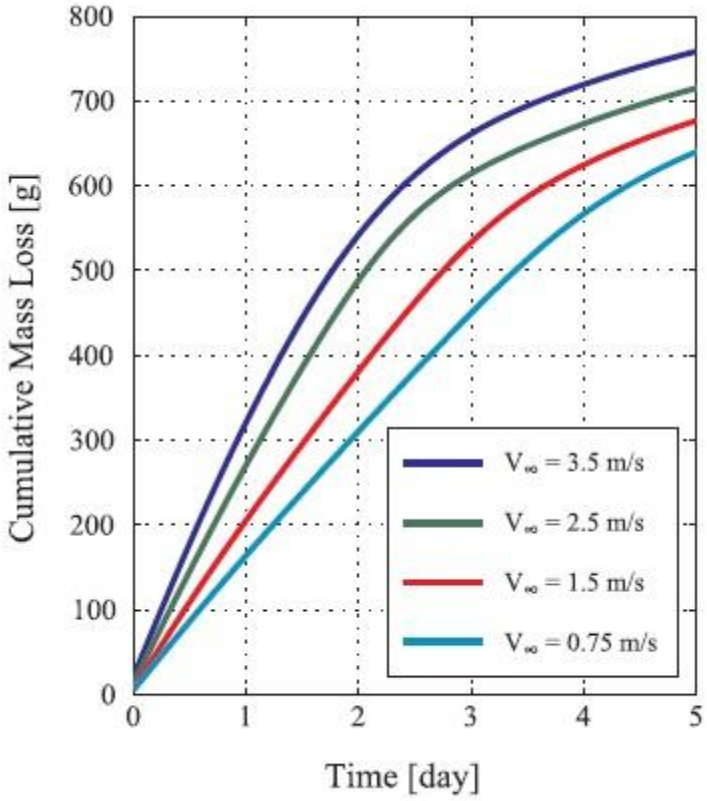

Figure 2.5 Effect of an increase of air velocity on the saturated sample (Shahraeeni et al., 2012)

2.3.2.2 Investigations of Experimental Determination of Evaporation

There are number of other experimental determinations of evaporation one of which is the pan method (Gupta, 1989; Veissman et al., 1989), as discussed earlier the pan method is widely used method of determining the surface water evaporation. In order to experimentally determine the evaporation from porous media some have resulted to obtaining gravitational samples, where a sample of soil is taken out of the ground at different depths and time intervals (Jackson et al., 1974). The wet and dry mass of the samples are then obtained giving an idea of amount of water in the soil during the certain time interval. Although it is an easy method of obtaining evaporation due to its simplicity, challenges arise when it comes to obtaining a consistency of a sample (Aluwihare and Watanabe, 2003). This method also poses and an intrusive way of obtaining evaporation. The "chambers" method is a way of obtaining the evaporation at any

moment in time. In this case, the a sample of soil is kept inside a closed chamber where the air temperature and humidity are kept constant (Kohsiek, 1980). The air inside the chamber is circulated vigorously where temperature and humidity sensors record any changes inside the chamber; based on these changes the evaporation of the porous media is developed. Although a popular method of obtaining experimental evaporation it was determined that errors exist due to alterations of natural radiation, turbulence, humidity and temperature (Leuning and Foster, 1981; Aluwihare and Watanabe, 2003). With advances of the in-situ methods of obtaining evaporation a microlysimeter has been introduced to obtain the evaporation from porous media (Boast and Robertson, 1982). The method works by inserting a thin walled cylinder into the ground of the in-situ soil, then removing the container containing the soil out of the cavity and capping the bottom of the container. The capped container (microlysimeter) is then water proofed and weighted. Before the microlysimeter is placed back into the cavity a load cell is inserted, microlysimeter is then rested on top of the load cell which then records the changes in microlysimeter's mass (Daamen and Simmonds, 1996; Uclés et al., 2013). The changes in mass are then recorded remotely over a certain period of time. Although this method introduces a less destructive and slightly more accurate method of obtaining the evaporation than the gravity sample method it still uses an intrusive methodology. Over the years new developments in infrared cameras have sparked a debate on the use of infrared remote sensing technology on determining the water behaviour in porous media (Avdelidis et al., 2003). With water evaporation being a very basic phenomenon, there is still a lack of experiments that give a direct insight of the process (Innocenzi et al., 2009). The use of infrared camera technology (IR) can give you an insight process of the thermal signature of the evaporative fluxes of the bare soils (Shahraeeni and Or, 2010). Thus far only few experiments have been performed using the infrared technology a study done by Innocenzi et al., 2009 was done on the evaporation of water droplets on a flat surface. The objective of the experiments was to find the chemical-physical process of evaporation of the water droplet exposed to different values of relative humidity. Another study by Chauvet et al., 2010 was done to determine the drying from square capillary tube. The study involved the observation of the bulk meniscus as the drying front receded into the capillary tube. The study found that as the drying front receded into the soil the surface of the soil heated up defining the location of the bulk meniscus. A study of surface temperatures via infrared thermography was done Nachshon et al., 2011 it was used to determine the evaporation

from porous media with salt deposits subject to natural convection. A model established by Nachshon et al., 2011 showed that the changes in ambient and surface temperatures are proportional to the changes in evaporation. From **Equation 2.13** we see that the difference in temperature combined with the thermal conductivity, latent heat of vaporization and water density can establish an evaporation model based on the knowns:

$$\dot{e} = \frac{h_a}{\rho_w L_w}(T_a - T_s) \qquad (2.13)$$

Equation 2.13 represents the evaporation of water in m/s where h_a is thermal conductivity of fluid air depending on its speed (W/m^{2}K), ρ_w is the density of water (1000kg/m^3), L_w is the latent heat of vaporization (2450J/Kg).

2.4 Summary

Evaporation is the process of removing water from porous media, often governed by atmospheric conditions. There are numerous mathematical models that allow the estimation of evaporation whether based on surface water evaporation of porous media drying, although there is no concrete method of estimating evaporation (Smits et al., 2012). Most of the analytical models already established use the mass transfer method as a basis of their evaporation estimation. The mass transfer of water vapour in fully saturated porous media is controlled by capillary action, gravitational forces and viscous losses. Evaporation is typically divided into two stages Stage 1 where the evaporation rate is relatively high and constant and Stage 2 where the evaporation rate is low and also constant. There is also the falling rate period that transitions the Stage 1 evaporation into Stage 2. Stage 1 is generally governed by the ambient conditions such as wind velocity and temperature changes. These conditions were tested in multiple experiments conducted over the years. The effects of temperature, wind velocity and relative humidity were among elements that affect the evaporation rates in porous media. There are also several experimental methods of determining the evaporation; most of these methods are determined to be an intrusive way of determining evaporation. These include but are not limited to gravitational samples and microlysimeter, there are also several less accurate but non intrusive methods of determining evaporation. They include the pan method and chambers method.

CHAPTER 3

EXPERIMENTAL PROCEDURE

3.1 General

The objective of the present research is to investigate the evaporation behaviour of porous media subject to forced convection through an experimental setup. In order to achieve this objective, two separate wind tunnels were designed and constructed. The main difference between the tunnels is the dimension of the cross-section. The idea behind the use of two different cross-sections was to study the effects of the boundary conditions that may be present during the testing. All of the experiments were conducted at the University of Windsor's Ed Lumley Center for Engineering Innovation.

The present chapter of the thesis describes the details of the experimental setup, sand material, experimental plan and experimental procedure followed. The section on the Experimental Setup describes the apparatus used in the experiment as well as the instruments used to gather the data. For the testing of evaporation of water from the porous media different types of sand were used. The sand material is described by the sieve analysis and the grain size distribution. Furthermore the ambient temperature and humidity were monitored during the entire duration of the experiment. Experimental plan and procedure describe the approaches taken in order to conduct the following experiments.

3.2 Experimental Setup

The experiments were conducted in two separate tunnels of varying dimensions which were constructed as an open loop system to facilitate easier accessibility to the inside of the tunnels. The schematic of the components of the tunnels is shown in **Figure 3.1** for the small tunnel and **Figure 3.2** for the large tunnel. The assembly of the tunnels consisted of three major parts 1) Fan chamber 2) Extension chamber/Air flow reducer and 3) Air flow straighteners. Fan chamber was constructed mainly to mount a fan at the entrance of the tunnel and give the air entering the tunnel some distance before flowing through the straighteners. The next part of the tunnels consisted of air flow reducer (2) for the small tunnel and an extension chamber (2) for the large tunnel. The air flow reducer was constructed in order to help the air transition from the

larger fan chamber to the small test chamber. The test chamber was constructed to hold the sample box. The sample box (6), filled with sand, was placed through a rectangular hole at the bottom of the chamber such that the top of the sample was aligned with the bottom of the test chamber. The test chambers were constructed using acrylic with the cross-sectional dimensions of 200 x 200 mm for the small tunnel and 610 x 1220 mm for the large tunnel. The sample box was also made out of acrylic material with the dimensions of 200 x 200 x 150 mm.

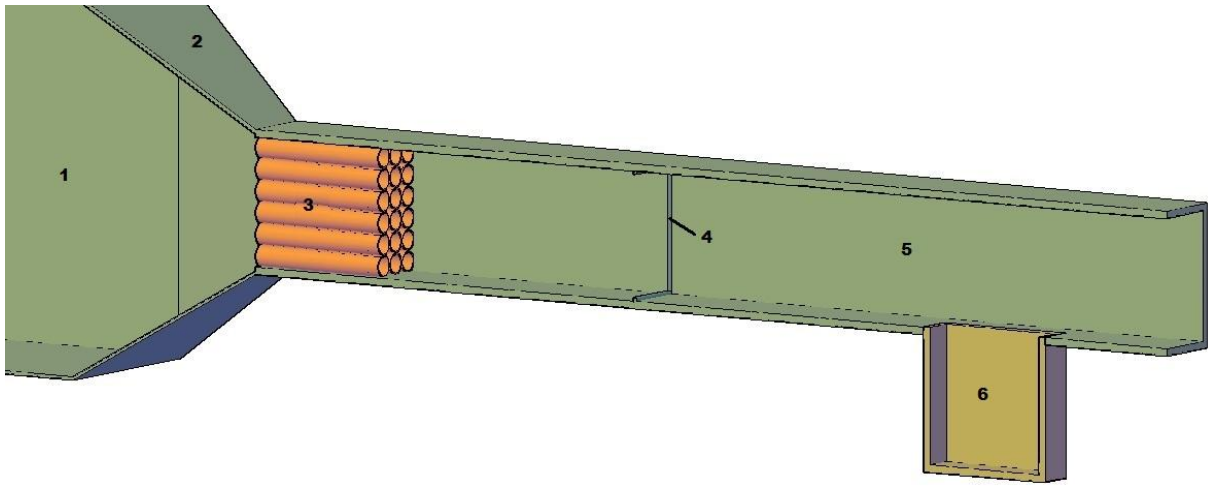

Figure 3.1 Schematic of cross-section of small tunnel showing fan chamber (1), air flow reducer (2), air flow straighteners (3), trip wires (4), test chamber (5), and sample box (6)

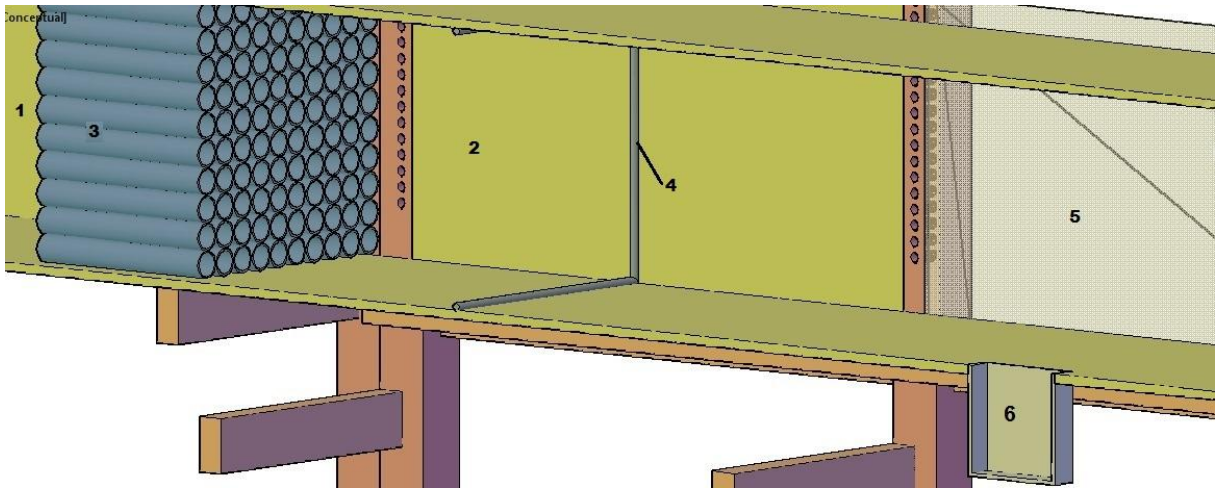

Figure 3.2 Schematic of cross-section of the large tunnel consisting of fan chamber (1), extension chamber (2), air flow straighteners (3), trip wires (4), test chamber (5), and sample box (6)

3.2.1 Velocity Profiles

The determination of evaporation from forced air convection indicated that velocity profiles had to be taken into consideration. Velocity profiles were obtained by the use of the Pitot-static tubes (Dwyer Instruments, Series 160E, USA). To obtain the velocity curves the Pitot-static tubes were inserted inside of the tunnel through small openings at the top of the test chambers. The readings were taken at small vertical intervals of 2.5 mm for the small tunnel and 5 mm for the large tunnel. The readings were taken at four different locations of the tunnels, the centre of the tunnel just above the sample box, 300 mm and 50 mm from the sidewalls for the large and the small tunnel, respectively, and just ahead of the sample box at the centre of the tunnel. Due to the scale of the tunnels two different Pitot-static tubes were used to obtain the curves; for the small tunnel a tube of diameter of 3 mm was used and for the large tunnel a tube with diameter of 8 mm was used. The tubes were attached to the pressure transducer (Dwyer Instruments, MS2 Magnesense, USA) that read the pressure of the wind velocity in Pascals (Pa) which was later converted into velocity in meters per second (m/s) using **Equation 2.11** In order to promote air flow inside the tunnels, two different fans were used, a 21" box fan (Lasko, B20201, USA) for the small tunnel setup and a 20" exhaust fan (TPI Corp, CE20-DS, USA) for the large tunnel setup.

To ensure turbulent velocity profiles, both tunnels were equipped with air flow straighteners (d = 20 mm and d = 50 mm for small and large tunnels, respectively) and trip wires (d = 4 mm and d = 15 mm for small and large tunnel) as shown in **Figures 3.1** and **3.2**. Air flow straighteners were installed to regulate the flow of air and trip wires were installed to ensure the wind transitioned into a turbulent flow. Four different velocities were tested, 2.3, 2.8, 3.2 and 3.6 m/s which were controlled by the fan velocity regulator to ensure that both tunnels experienced the same velocity.

The velocity measurements were taken after the installation of the trip wires to ensure that the flow in the tunnels was turbulent in order to simulate the real world wind flow pattern. **Figure 3.3** shows the turbulent velocity profiles for the tunnel section above the sample box for the velocities tested. As defined earlier, the boundary thickness δ is located within 1% of the free stream u~99U, from the graphs it is seen that the boundary layer thickness occurs close to the wall and subsequently the air flow matches the free stream velocity. The boundary layer

thickness as read from **Figure 3.3** is the distance between the wall and the point where the wind velocity reached the free flow velocity, the results are summarized in **Table 3.1**.

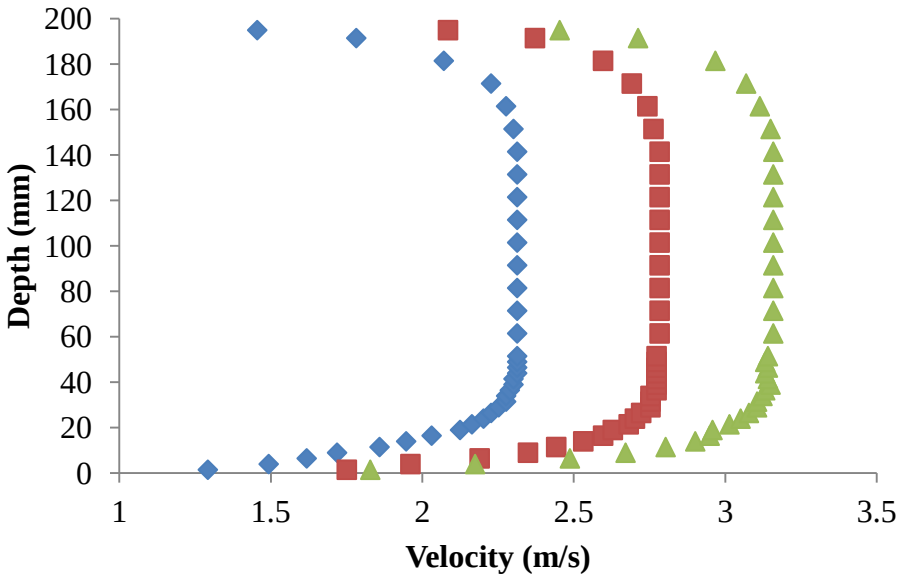

(a)

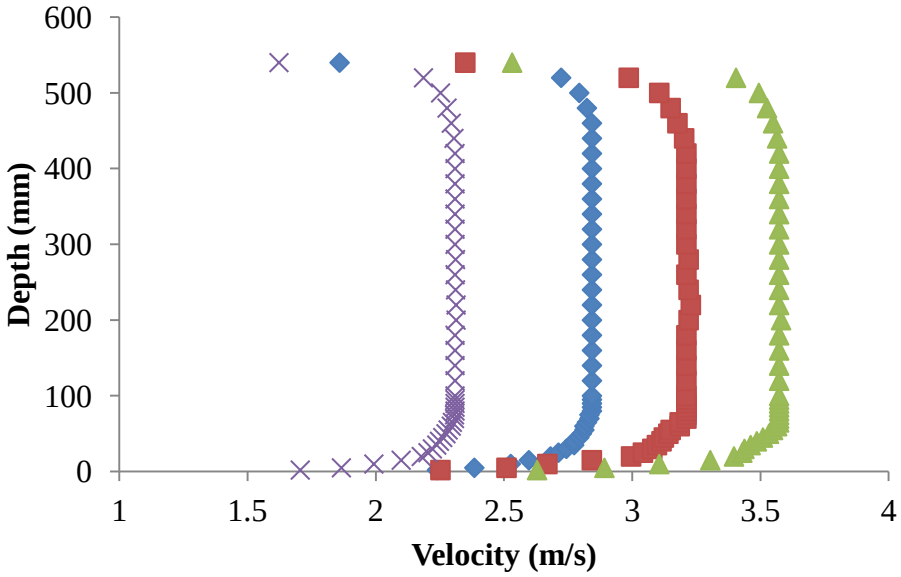

(b)

Figure 3.3 Velocity profiles with the trip wire in the (a) small tunnel and (b) large tunnel

Table 3.1 Boundary layer thickness

Velocity, U (m/s)	Boundary Layer Thickness, δ (mm)	
	Small Tunnel	Large Tunnel
2.3	41.5	80
2.8	34	75
3.2	31.5	65
3.6	-	60

From the table above, it is seen that as the velocity of the air increases the boundary layer thickness decreases. When comparing the average boundary layer thicknesses of the small and the large tunnel the large tunnel is about 2.02 times larger than the small tunnel. This indicates that the small tunnel has a greater rate of air displacement within the close proximity of the sand sample. **Figure 3.4** shows the nondimensionalized velocity profiles of the boundary layer thickness. When comparing the nondimensionalized velocity profiles, we see that the small tunnel profile is much more blunt than that of the large tunnel. Large tunnel's boundary layer is significantly thicker than that of the small tunnel which indicates that different evaporation rates might occur during initial (Stage 1) evaporation. With the thinner boundary layer the velocity close to the surface increases much quicker with distance from the bottom of the chamber. Thus with the higher velocities close to the bottom of the chamber where the humid air is present above the sample gets replaced faster allowing the sand sample to dry quicker. The thicker boundary layer in the large tunnel indicates that the air close to the sample does not travel as fast as the small tunnel's air therefore the less humid air will not infiltrate the soil at the same rate as the small tunnel. This means that the mass transfer in the large tunnel will occur much slower than the faster moving air in the small tunnel.

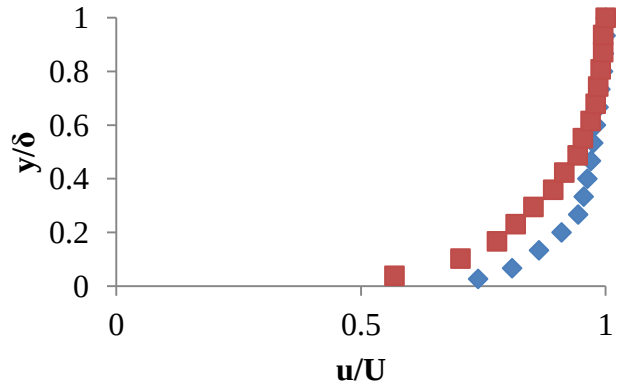

(a)

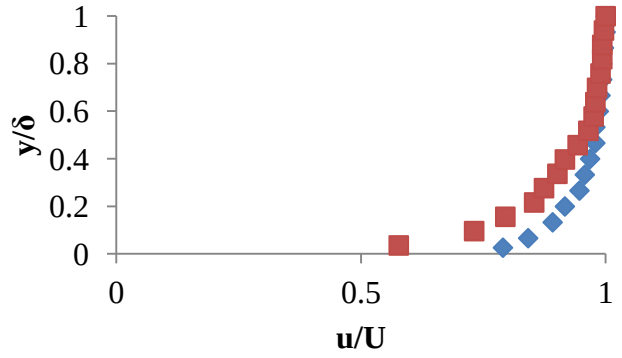

(b)

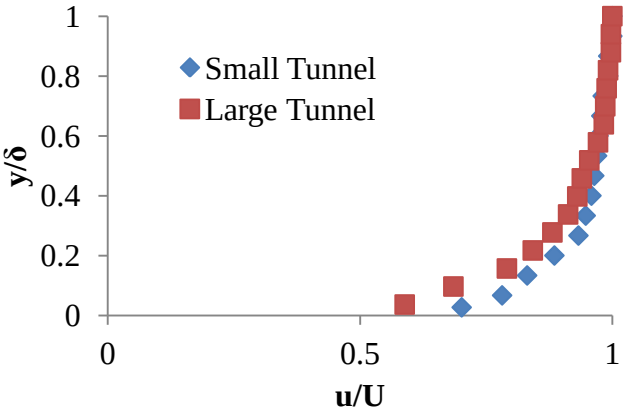

(c)

Figure 3.4 Nondimensional velocity profile for the (a) 2.3 m/s (b) 2.8 m/s, and (c) 3.2 m/s

3.3 Sand Material

A sieve analysis was performed on three different types of soils - coarse, fine and mixed sands; this was done to determine the grain size distribution (**Figure 3.5)** and to find the characteristics of each soil sample. From the grain size distribution it was found that the d_{50} values are 2.6 mm for the coarse sand, 0.23 mm for the fine sand and 0.57 mm for the mixed sand. From the figure we see that 50 % of the mixed sand particles are finer soils and 5 0% of the mixed sand are coarser soils thus representing uniform distribution of grain sizes for the mixed sand.

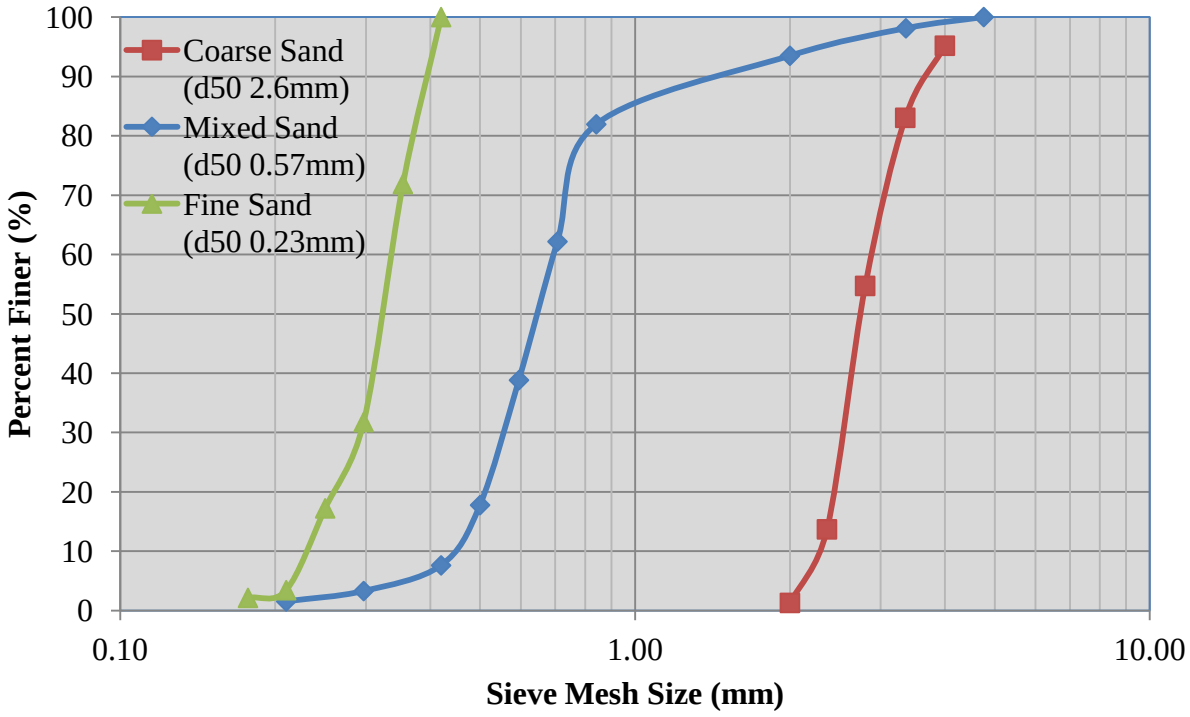

Figure 3.5 Sieve analysis with fine sand (d_{50} = 0.23 mm), mixed sand (d_{50} = 0.57 mm) and coarse sand (d_{50} = 2.6 mm)

3.4 Experimental Plan

The experimental plan consists of two phases where each phase contained a series of experiments. Phase 1 consisted of 18 experiments for the small tunnel where three sands, coarse d_{50} = 2.6 mm, fine d_{50} = 0.23 mm and mixed d_{50} = 0.57 mm, were subjected to three different

velocities of 2.3, 2.8 and 3.2 m/s. Phase 2 consisted of 24 experiments for the large tunnel with three different sands exposed to velocities of 2.3, 2.8, 3.2 and 3.6 m/s. Each of the experiments was repeated twice in order to verify the validity of the experiments.

3.5 Experimental Procedure

In order to determine the appropriate length of time required for the experiments to be conducted multiple preliminary tests were done. This ensured that the water inside the sample box was mostly evaporated. From the preliminary experiments it was determined that in order for the fine and mixed sand to reach the end of stage 1 evaporation at least 30-hours were required with another 10-hours for the falling rate period to reach the stage 2 evaporation. Thus the duration of the experiment was chosen to be a 72-hour period.

To make sure that no sand was lost during the testing period, prior to each experiment each sample of sand was oven dried with its dried mass recorded. After the 72-hour experimentation period the sample was emptied out of the sample box and placed in an oven for a 24-hour period where a dry mass after the testing was recorded. In order to determine if any sand was lost during the experiment, the mass of sand in the sample box was determined before and after each of the experiments. The difference was found to vary between 0.05% and 0.1%.

Each of the test series had the appropriate sand mixtures placed in the sample box which was then placed on top of a bench scale (OHAUS, Valor700, Canada) located underneath the test chamber (**Figure 3.6**). Water was added to the sand sample box; in order to make sure the sample was fully saturated, the manometers were mounted to measure the water level inside of the soil sample. The manometers were made out of flexible plastic tubes (d=4.7 mm) that were mounted at three different locations of the sample box 20, 60 and 100 mm (**Figure 3.7**) from the top of the sample. The water levels were monitored over the 72-hour period and with the mass of the sample box recorded every 15 minutes during the entire duration of the experiment.

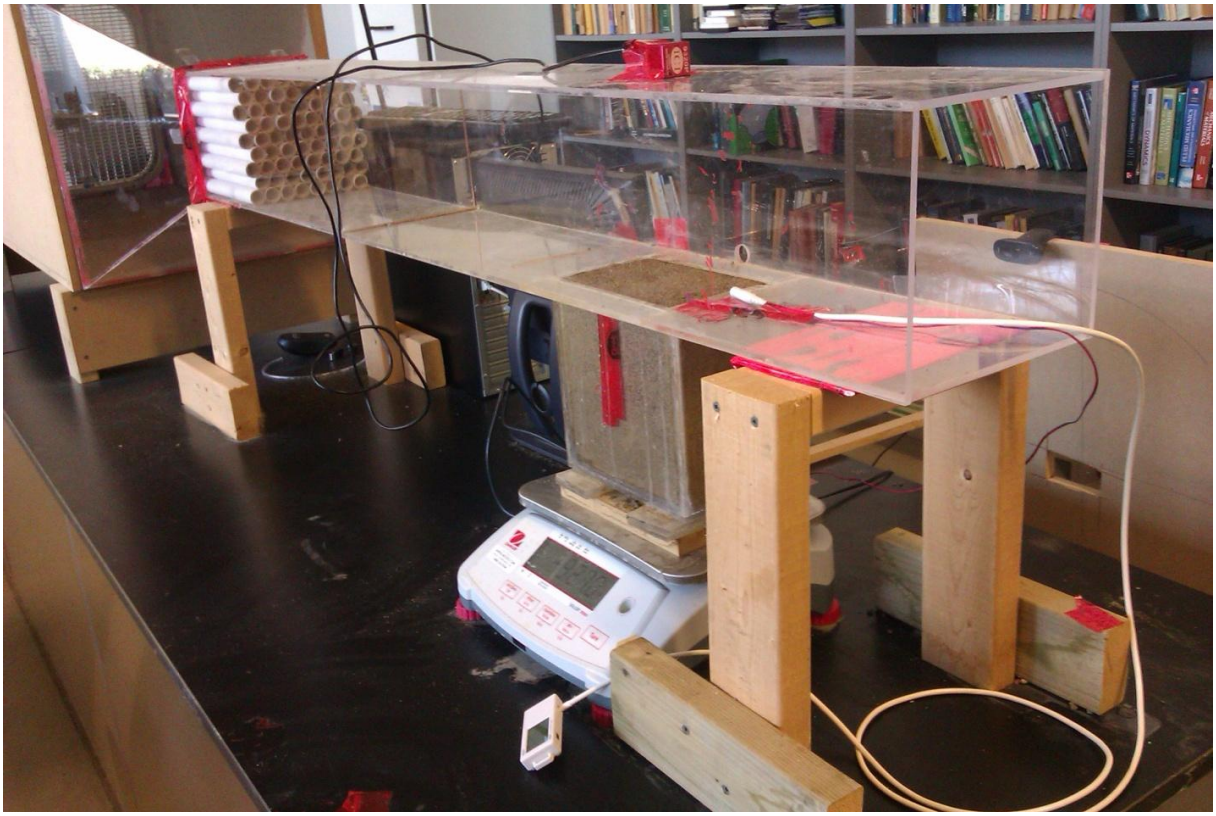

Figure 3.6 Experimental setup of the small tunnel

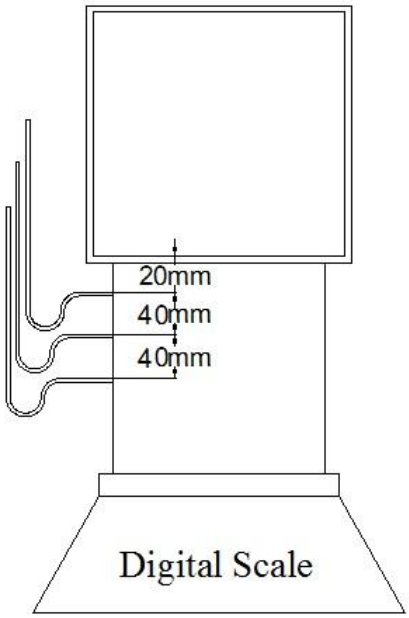

Figure 3.7 Locations of the manometers in the sample box

Humidity is an important aspect of evaporation with more humid air an evaporation of water is expected to drastically reduce; therefore humidity had to be monitored during the experimentation. Humidity was monitored inside of the test chamber with a humidity sensor (HOBO UX100-023, USA) which was placed inside the test chamber just after of the soil sample. Another humidity sensor was placed outside the test chamber in order to monitor the relative humidity in the room.

To monitor the ambient temperature inside the chamber a thermocouple temperature sensor (Measurement Computing, USB-TEMP, USA) was placed 2 mm above the soil sample. During the experimentation the temperature of the ambient room temperature was taken using thermocouples.

An infrared camera (Infrared Cameras Inc, ICI 9320 P-Series, USA) was mounted on top of the test chamber to monitor the temperatures of the surface of the porous media. The pictures of the soil were taken from the top of the test chamber showing the full profile of the sample. Pictures were taken over the course of the 72-hours. The infrared pictures were then analyzed in software IR Flash provided by the camera manufacturer to identify the changes of the surface temperatures.

CHAPTER 4

EXPERIMENTAL RESULTS AND DISCUSSIONS

4.1 General

This section covers the findings derived from the experimental study outlined in chapter 3 of this thesis. The results and discussions evaluate the rates of evaporation from soils subject to different wind velocities, investigation of the tunnel boundary effects of two tunnels, and investigation of infrared imagery based on the surface temperatures of porous media. The experiments were performed over the 72 hours period with the exception of the small tunnel of the test 2 where the experiments were performed over a 48 hour period due to the insignificant changes in mass. All plots in this section contain the results from two different experiments for each case.

4.2 Infrared Analysis

The infrared images were captured every 30 minutes to understand the process during the evaporation. **Figure 4.1** demonstrates the time transition of surface temperature of a drying coarse sand sample subject to 2.3 m/s air flow in the small tunnel. During the initial stage of evaporation (Stage 1) the capillary action rehydrates the surface of the soil. This keeps the evaporation constant up to the falling rate period. The constant rehydration also keeps the temperatures of the evaporating surface at a steady temperature. From the figure we can see that the temperatures for the first 10 hours of the drying cycle stays constant throughout the 10 hour period. At the 20 hour mark, visible changes in the surface temperature are noticed. From the figure we see that the soil still has some wet spots (blue region) still visible. These wet regions indicate that capillary action is still present at these locations, although the evaporation process has now entered the falling rate period. During this period the evaporation rate of water significantly drops. After the 30 hour mark, most of the water has evaporated from the surface of the sand and we start seeing dry spots appear on the surface (red regions), this indicates that the capillary action of the water transport has been broken. After 40 plus hours most of the moisture is gone from the surface and the evaporation entered Stage 2 evaporation at this stage we see distinguishable dry spots signified by the red regions on top of surface. At this stage of evaporation capillary action is no longer supplying the water to the surface and the effects of

wind velocity are minimal. During Stage 2 the evaporation is controlled by the slow exchange of infiltrating ambient air particles.

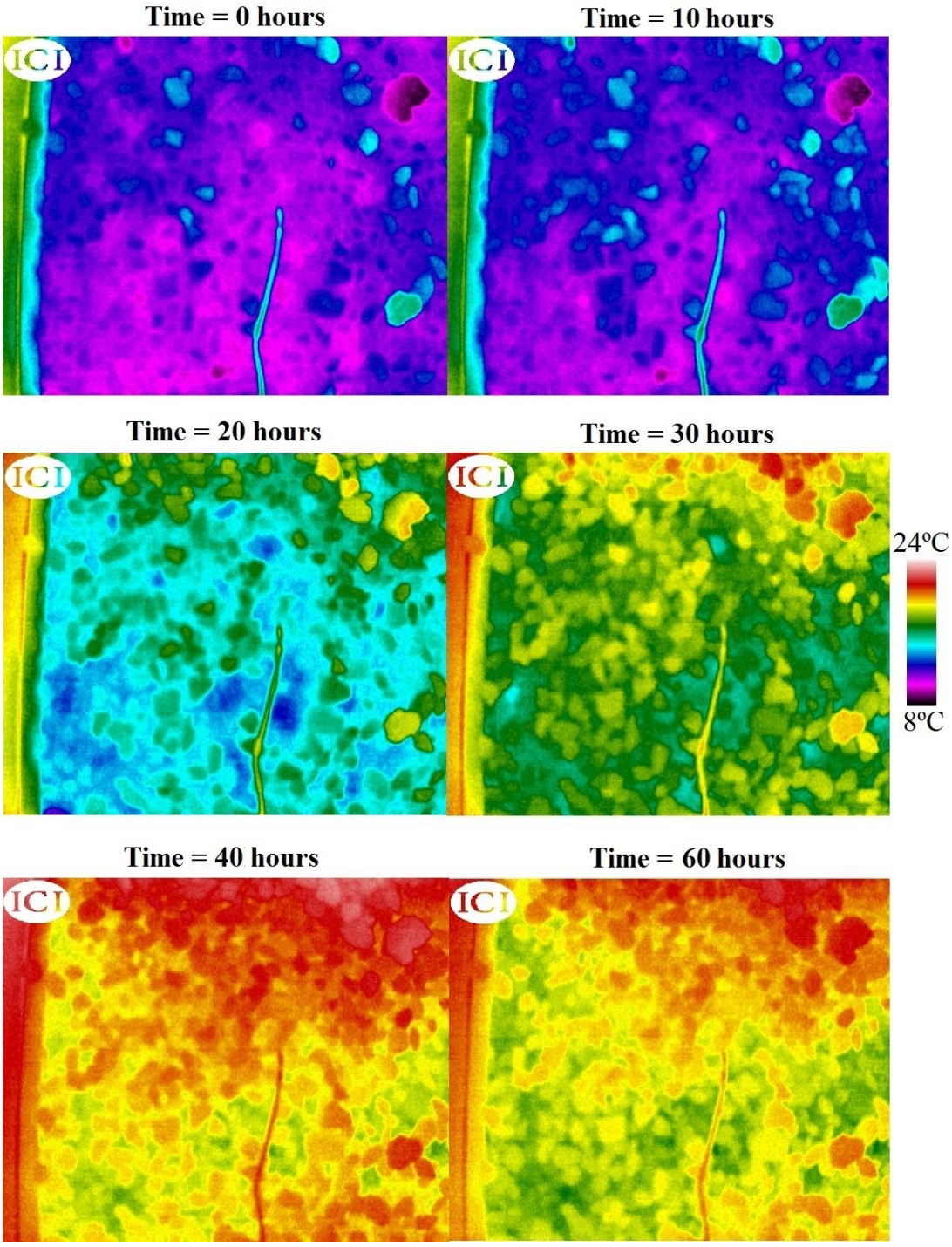

Figure 4.1 Changes of surface temperature of coarse sand subject to a air flow velocity of 2.3 m/s

The infrared imagery analysis was performed on the porous media to determine the behaviour of drying patterns of the soil surface based on the forced convection. **Figure 4.2** shows the average surface and ambient temperatures of the coarse soil subjected to forced convection in a large and small tunnel. From the graphs we can see that for the first 8-10 hours the temperatures are relatively constant. This indicates that coarse sand is experiencing Stage 1 evaporation. About 8-10 hours later the evaporation enters the falling rate period (FRP). From the experiments the FRP was found to be dependent on the wind velocity, meaning with increasing air flow the duration of the falling rate period shortens. From **Figure 4.2(a)** it was observed that the FRP is about 25 hours for the 2.3 m/s wind velocity and 20 hours for the 3.6 m/s velocity (**Figure 4.2(d)**). Comparing the surface temperatures of the large and the small tunnel for the coarse sand, we see that the FRP is much steeper in the small tunnel than the large tunnel. This may be due to the fact that the boundary layer in the small tunnel is much smaller than the large tunnel. This means that the water evaporates much quicker in the small tunnel due to thinner boundary layer. After reaching the stage 2 evaporation the temperature of the surface is almost identical to the ambient temperature of the room after which the soil temperature behaves with the same pattern as the ambient temperature.

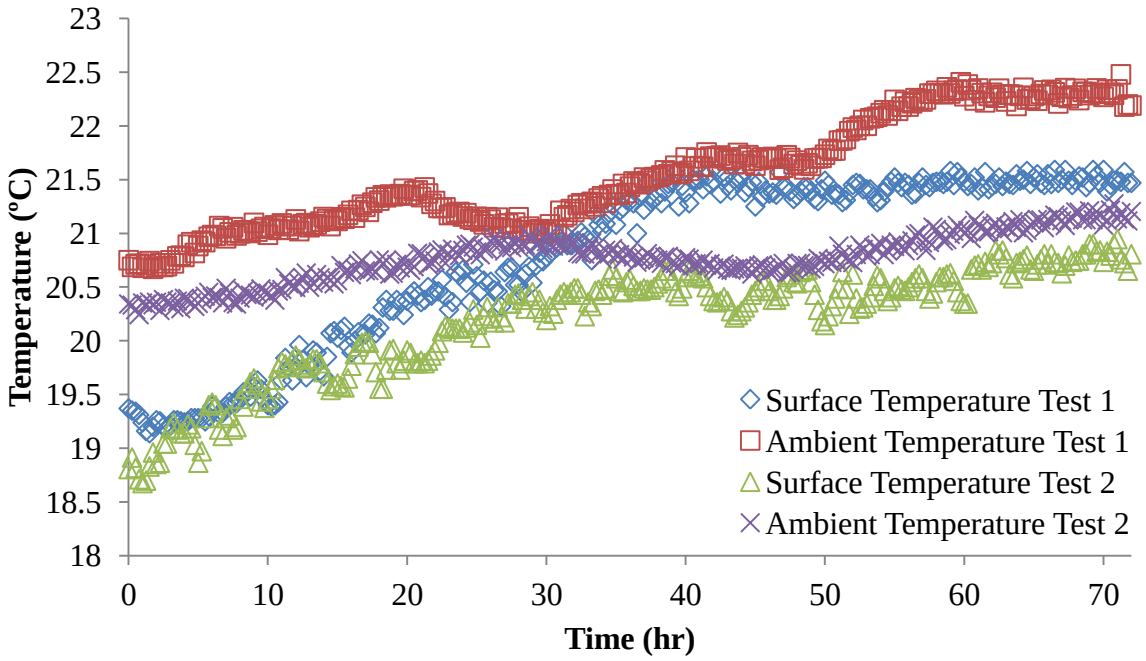

(a)

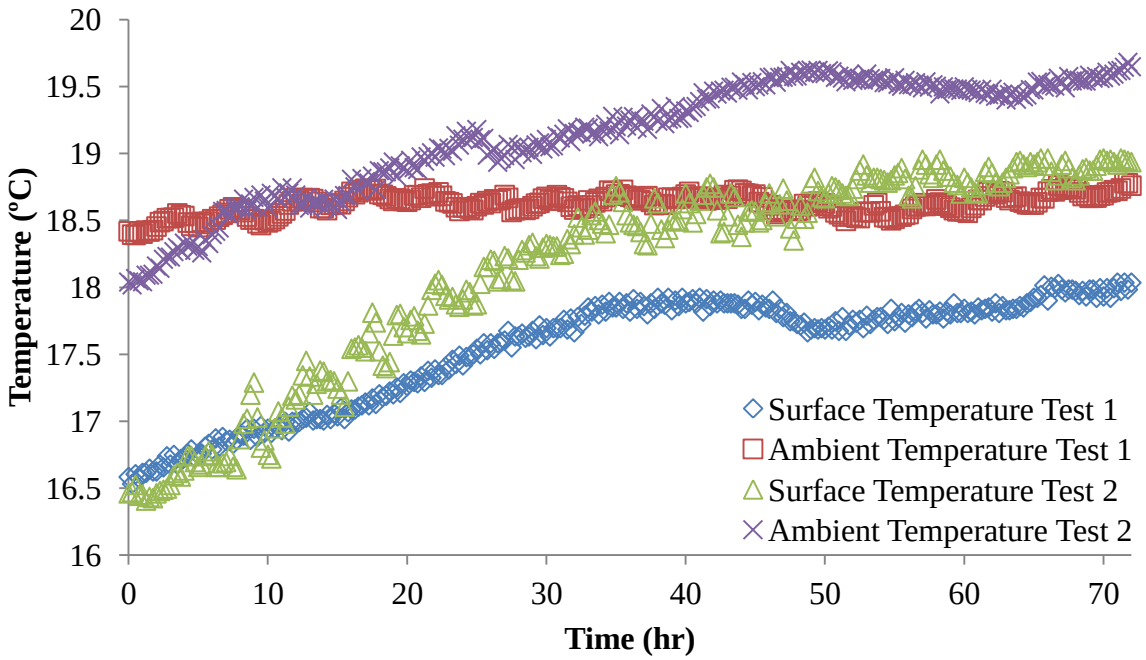
Temperature (°C)
20
19.5
19
18.5
18
17.5
17
16.5
16
0
10
20
30
40
50
60
70
Time (hr)
Surface Temperature Test 1
Ambient Temperature Test 1
Surface Temperature Test 2
Ambient Temperature Test 2

(b)

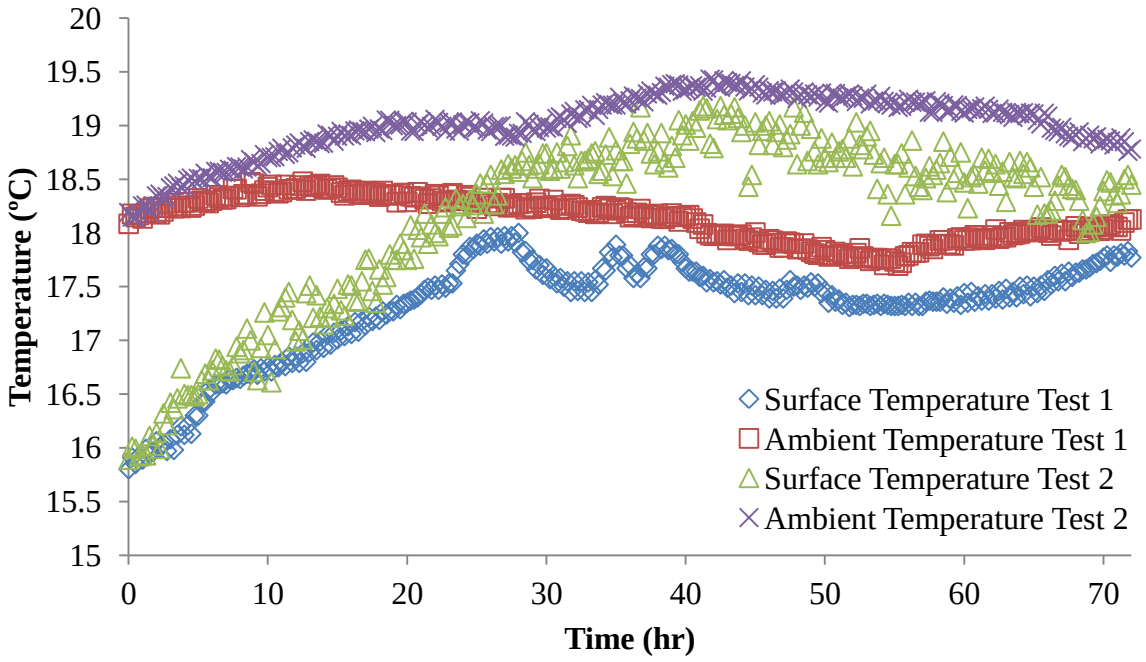
Temperature (°C)
20
19.5
19
18.5
18
17.5
17
16.5
16
15.5
15
0
10
20
30
40
50
60
70
Time (hr)
Surface Temperature Test 1
Ambient Temperature Test 1
Surface Temperature Test 2
Ambient Temperature Test 2

(c)

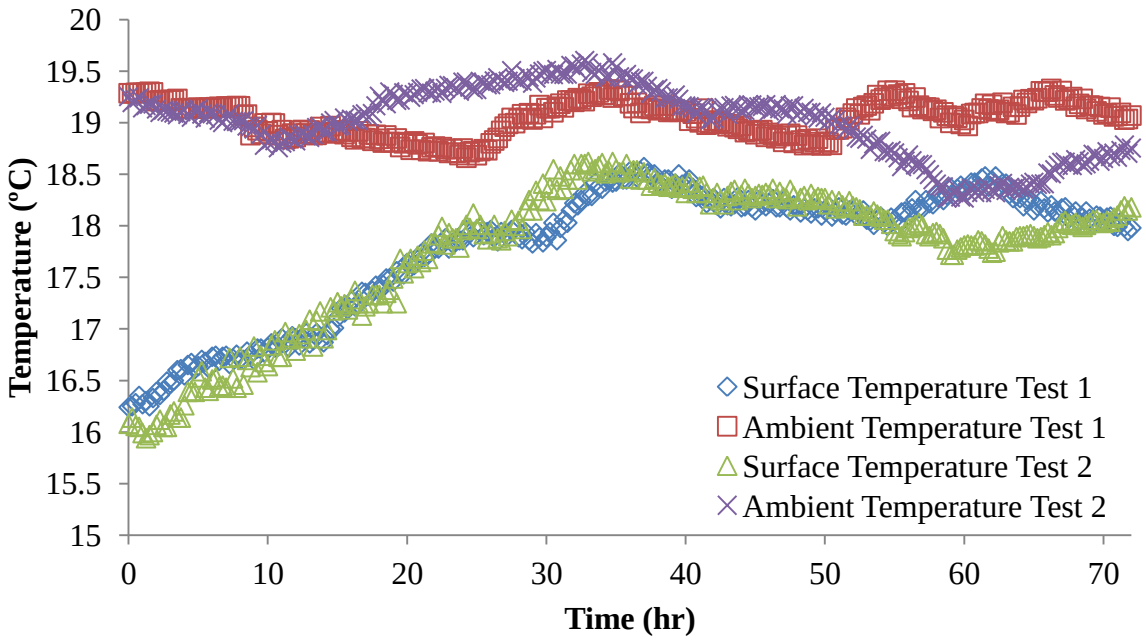

(d)

Figure 4.2 Infrared temperatures of the coarse sand surface in the large tunnel for air flow velocities of (a) 2.3 m/s, (b) 2.6 m/s, (c) 3.2 m/s and (d) 3.6 m/s

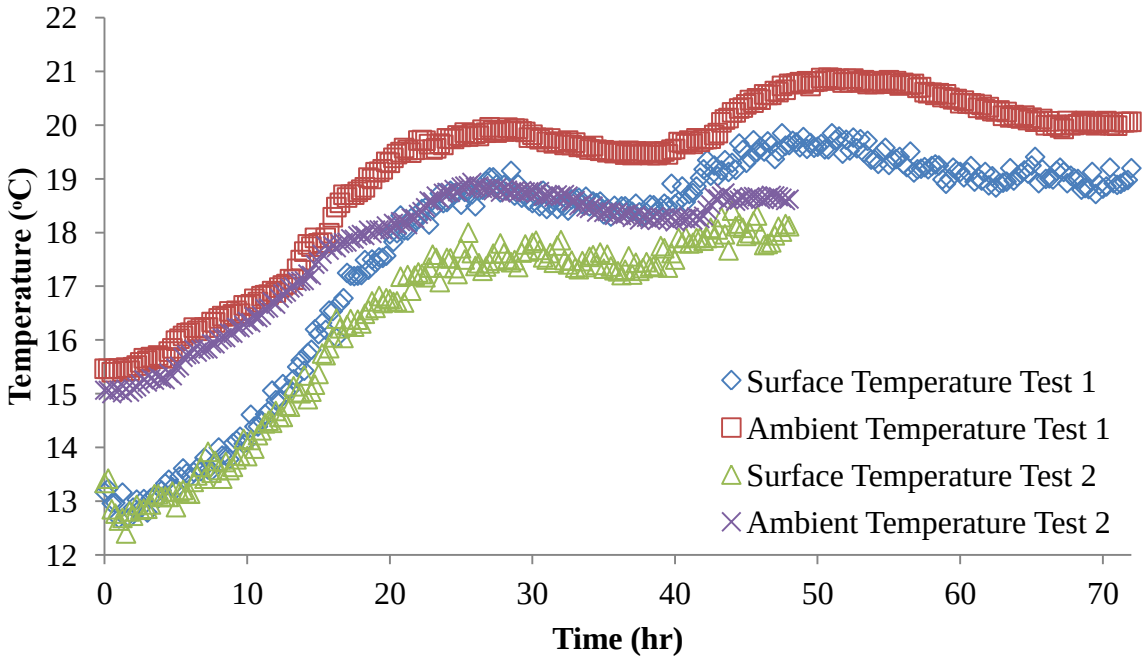

(a)

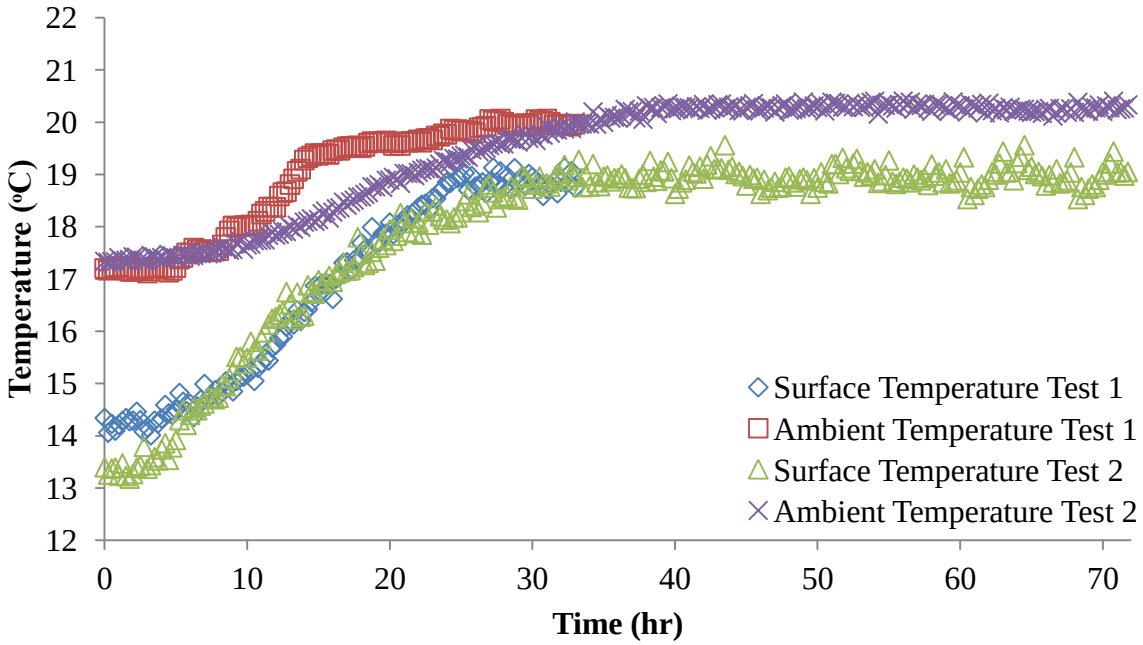

(b)

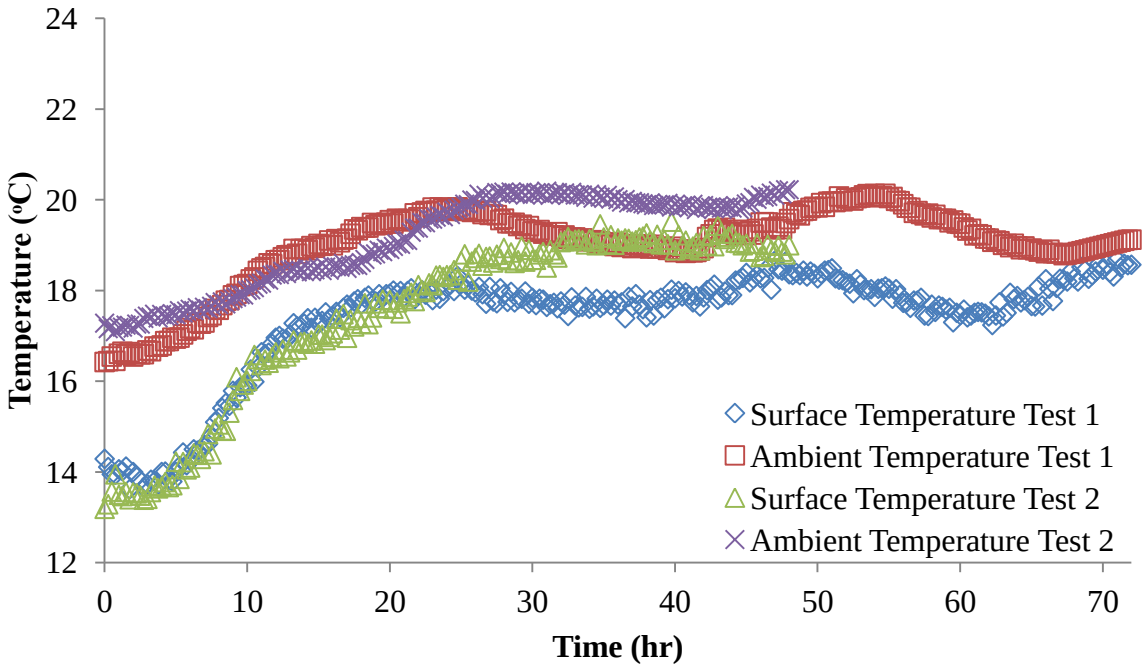

(c)

Figure 4.3 Infrared temperatures of the coarse sand surface in the small tunnel for air flow velocities of (a) 2.3 m/s, (b) 2.6 m/s and (c) 3.2 m/s

Fine and mixed sand exhibit much different phenomenon. **Figures 4.4** and **4.5** show the surface temperature changes for the fine sand and **Figures 4.6** and **4.7** show the surface temperature changes of the mixed sand for the small tunnel and the large tunnel. From figures we see that there is a distinguishable representation of the different stages of evaporation. Looking at the figures we see that the temperature of the surface of the fine and the mixed soil stays at a constant level during the early hours of the experiment. With the Stage 1 evaporation being constant at the beginning and sudden rise of the surface temperatures indicates the FRP and constant temperatures at the end of the experiment refer to the Stage 2 evaporation. The temperature of the surface remains constant due to the constant rehydration of the surface of the soils from the bottom layers of the soil. The water from underneath the drying front gets risen to the surface by the capillary action filling the dried pores. This action continues until the capillary action forces get overtaken by the gravitational forces. When the surface of the soil stops being rehydrated, the surface of the soil begins to warm up thus entering the FRP as stated before the stage 1 depends on the wind velocity and the ambient conditions FRP on the other hand is the ambient conditions such as the wind start to have a minimal effect on evaporation. The rise in temperatures shows that the drying front is slowly receding deeper into the soil. After the FRP, the evaporation enters Stage 2 from which the surface temperatures are constant indicating that the evaporation is no longer dependent on wind velocity. When comparing the behaviour of the surface temperatures at the initial stages of the evaporation for the coarse, fine and mixed soils we can say that the pore size also affects the length of the Stage 1 evaporation. With larger pore sizes the coarse sand had significantly less capillary action for the Stage 1 evaporation.

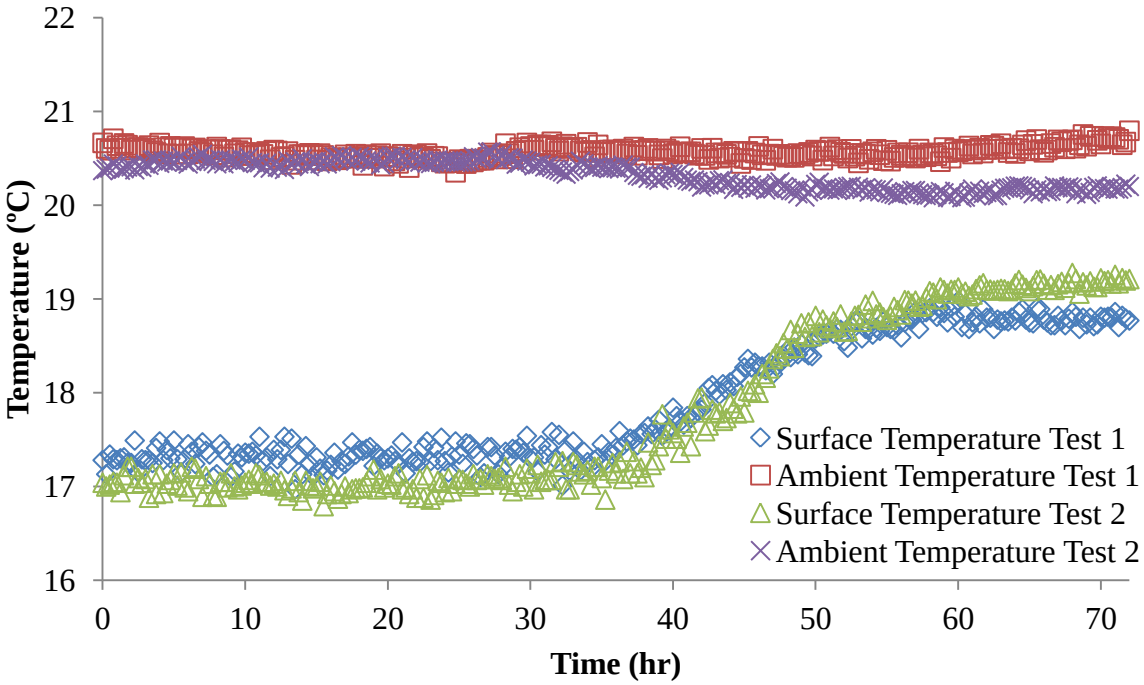
22
21
20
19
18
17
16
Temperature (ºC)
0
10
20
30
40
50
60
70
Time (hr)
Surface Temperature Test 1
Ambient Temperature Test 1
Surface Temperature Test 2
Ambient Temperature Test 2

(a)

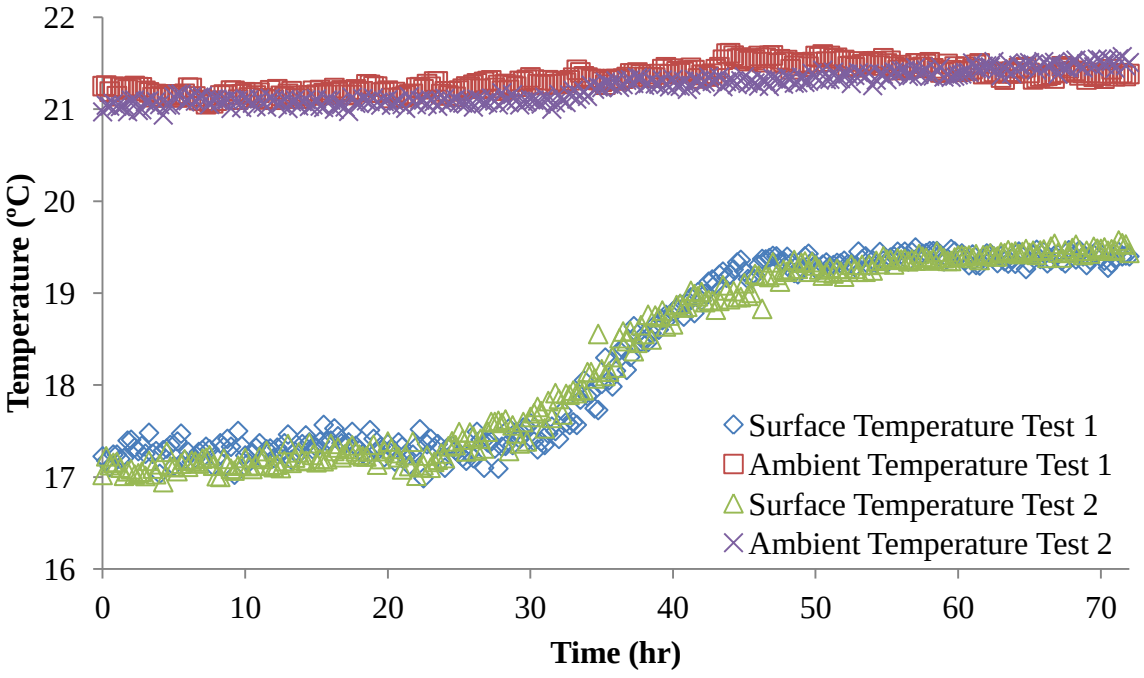
22
21
20
19
18
17
16
Temperature (ºC)
0
10
20
30
40
50
60
70
Time (hr)
Surface Temperature Test 1
Ambient Temperature Test 1
Surface Temperature Test 2
Ambient Temperature Test 2

(b)

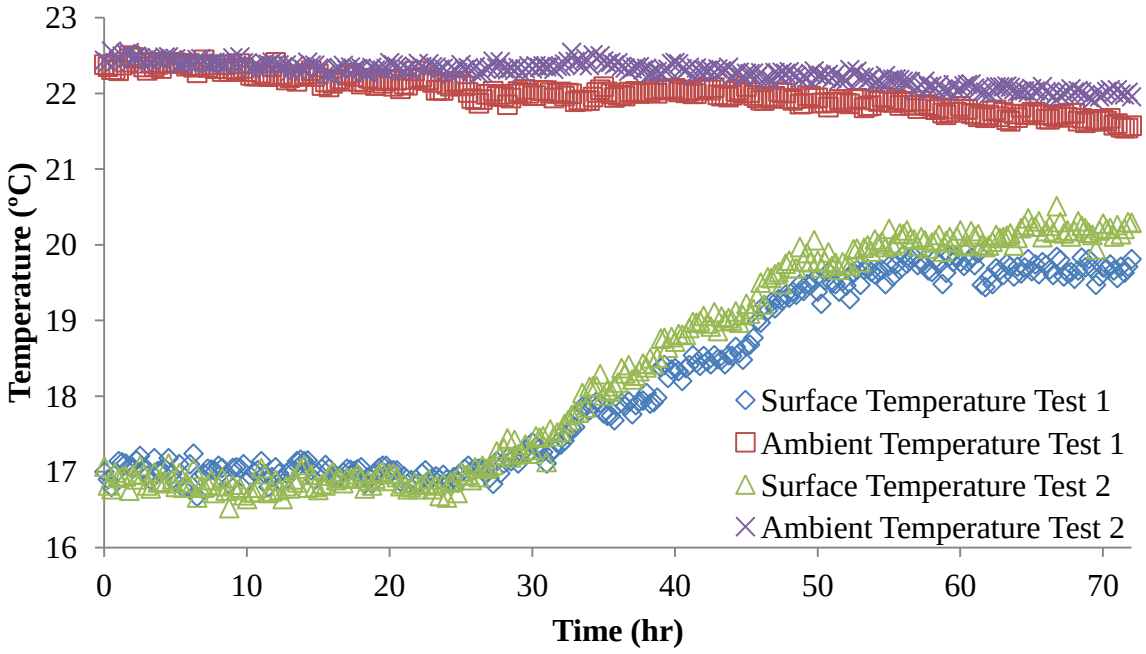

(c)

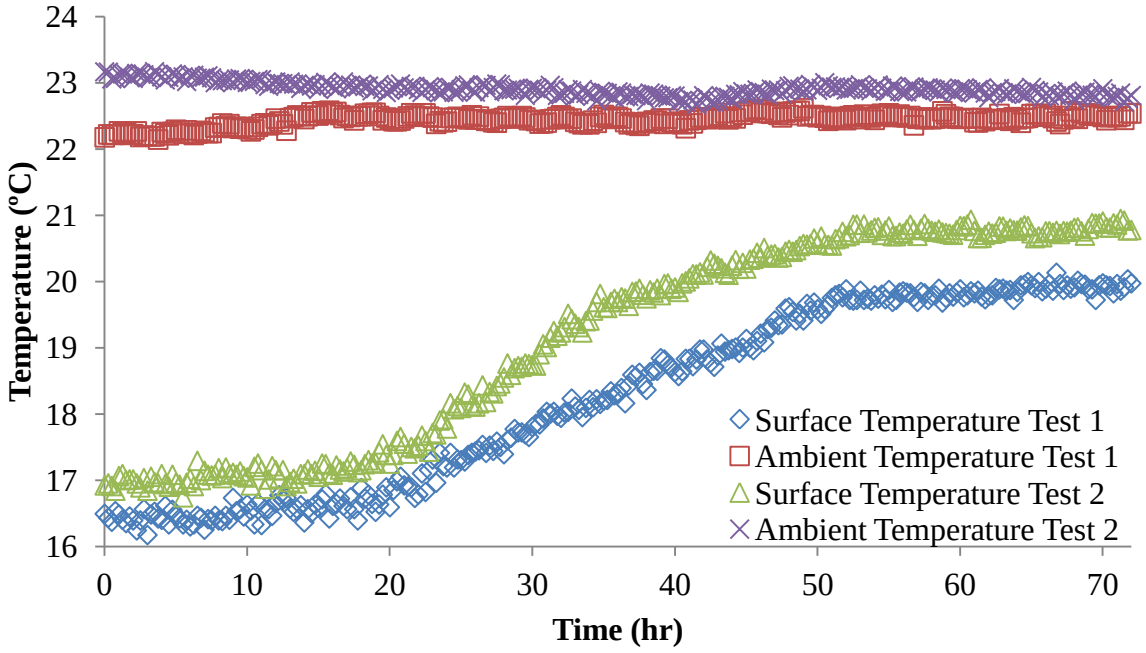

(d)

Figure 4.4 Infrared temperatures of the fine sand surface in the large tunnel for air flow velocities of (a) 2.3 m/s, (b) 2.6 m/s, (c) 3.2 m/s and (d) 3.6 m/s

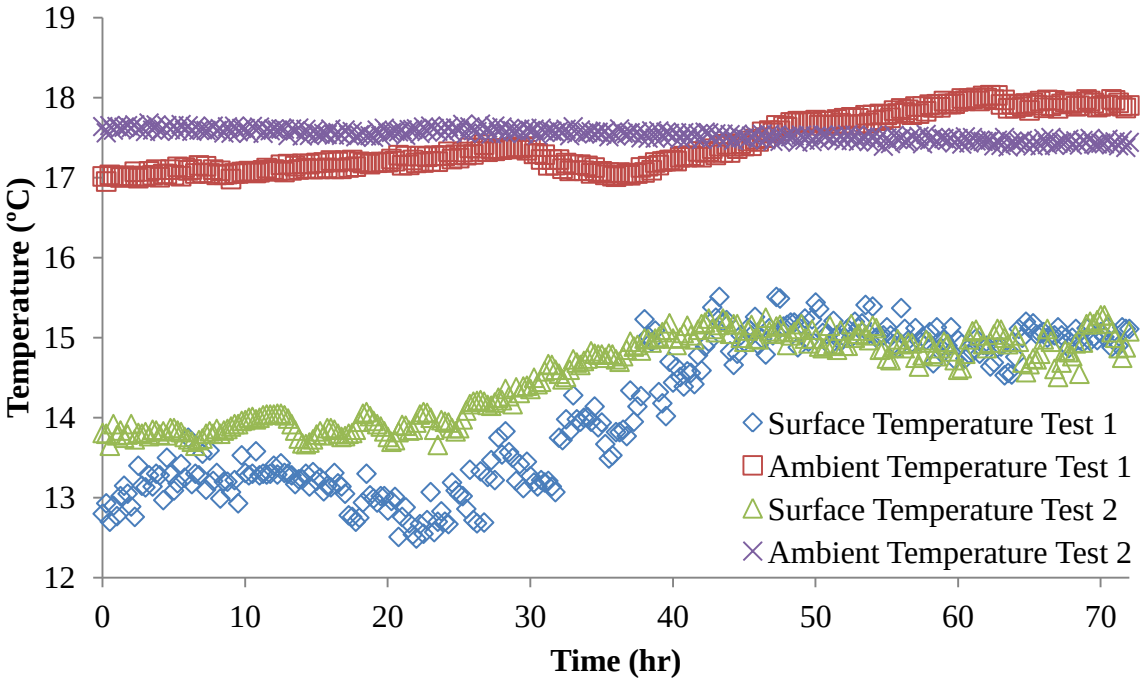
Temperature (°C)
19
18
17
16
15
14
13
12
0
10
20
30
40
50
60
70
Time (hr)
Surface Temperature Test 1
Ambient Temperature Test 1
Surface Temperature Test 2
Ambient Temperature Test 2

(a)

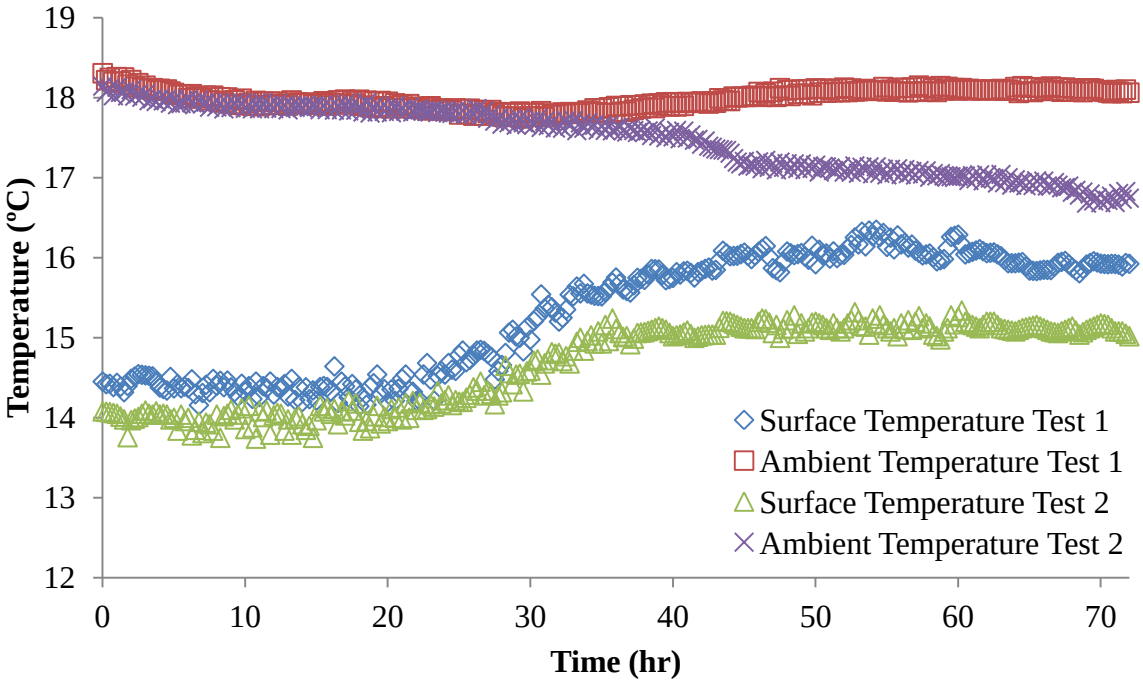
Temperature (°C)
19
18
17
16
15
14
13
12
0
10
20
30
40
50
60
70
Time (hr)
Surface Temperature Test 1
Ambient Temperature Test 1
Surface Temperature Test 2
Ambient Temperature Test 2

(b)

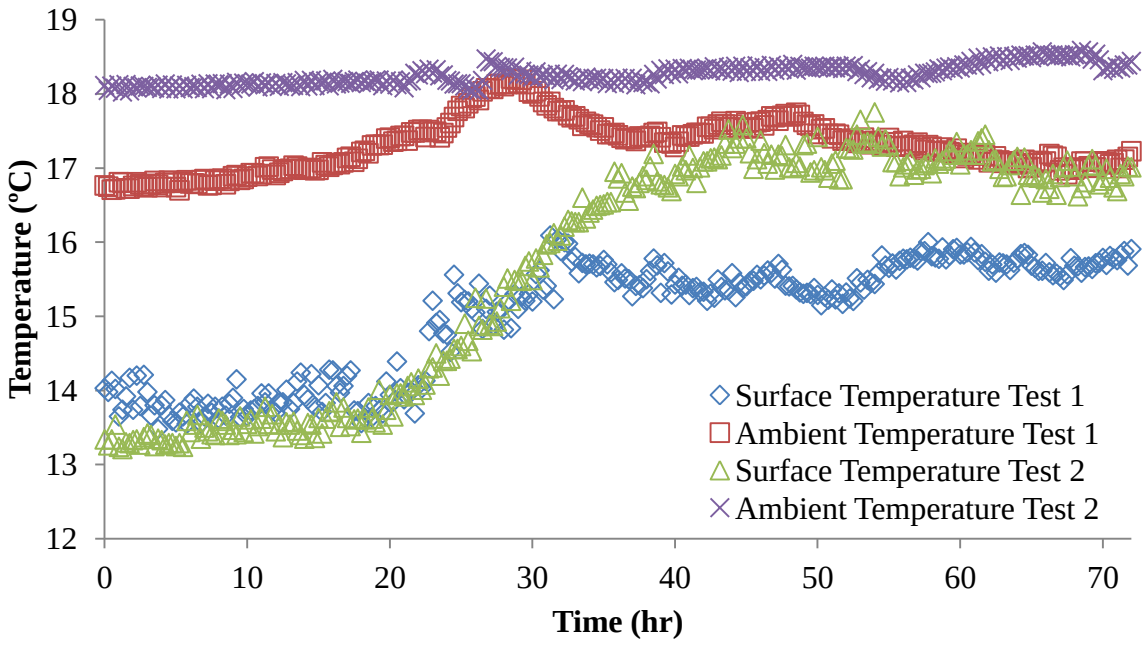

(c)

Figure 4.5 Infrared temperatures of the fine sand surface in the small tunnel for air flow velocities of (a) 2.3 m/s, (b) 2.6 m/s and (c) 3.2 m/s

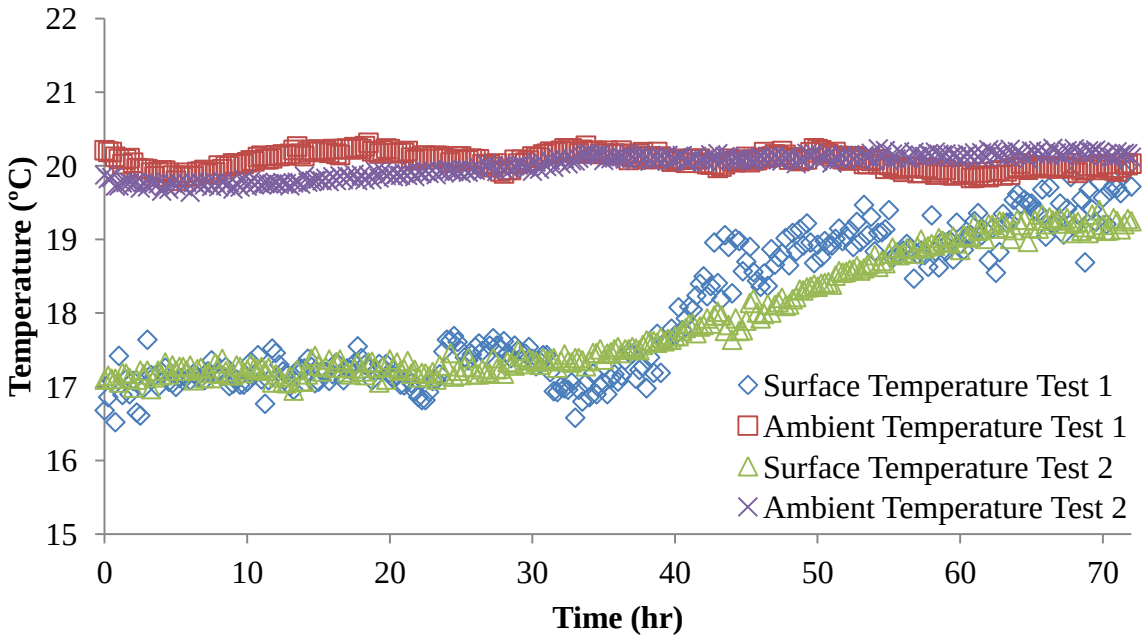

(a)

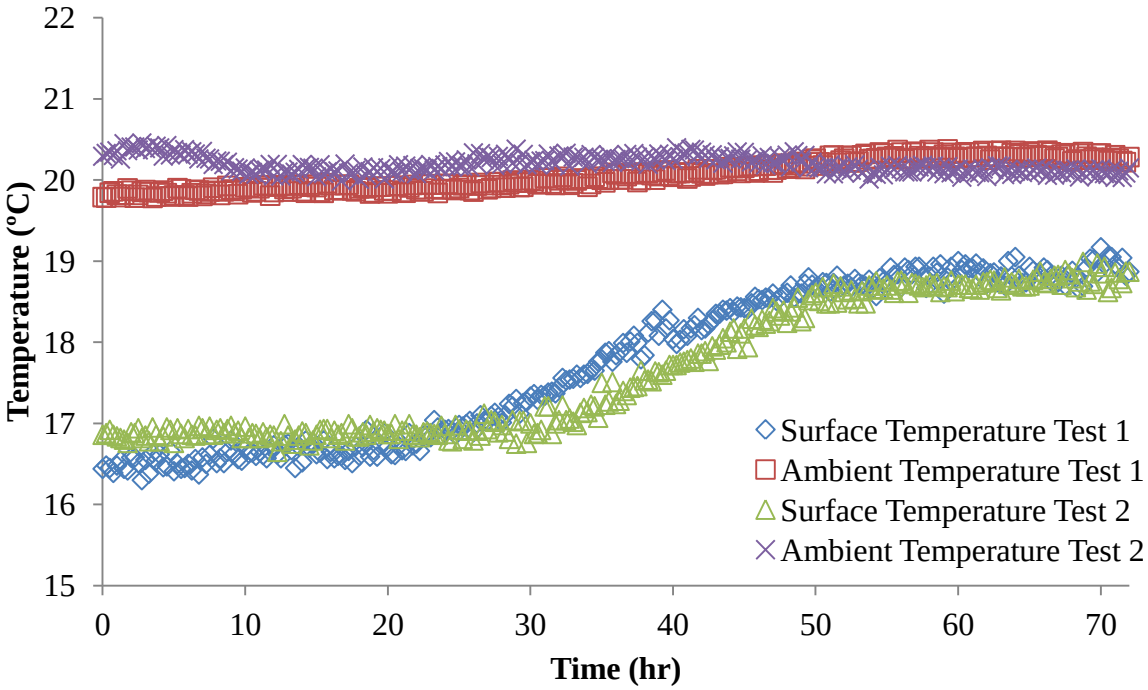
Temperature (ºC)
22
21
20
19
18
17
16
15
0
10
20
30
40
50
60
70
Time (hr)
Surface Temperature Test 1
Ambient Temperature Test 1
Surface Temperature Test 2
Ambient Temperature Test 2

(b)

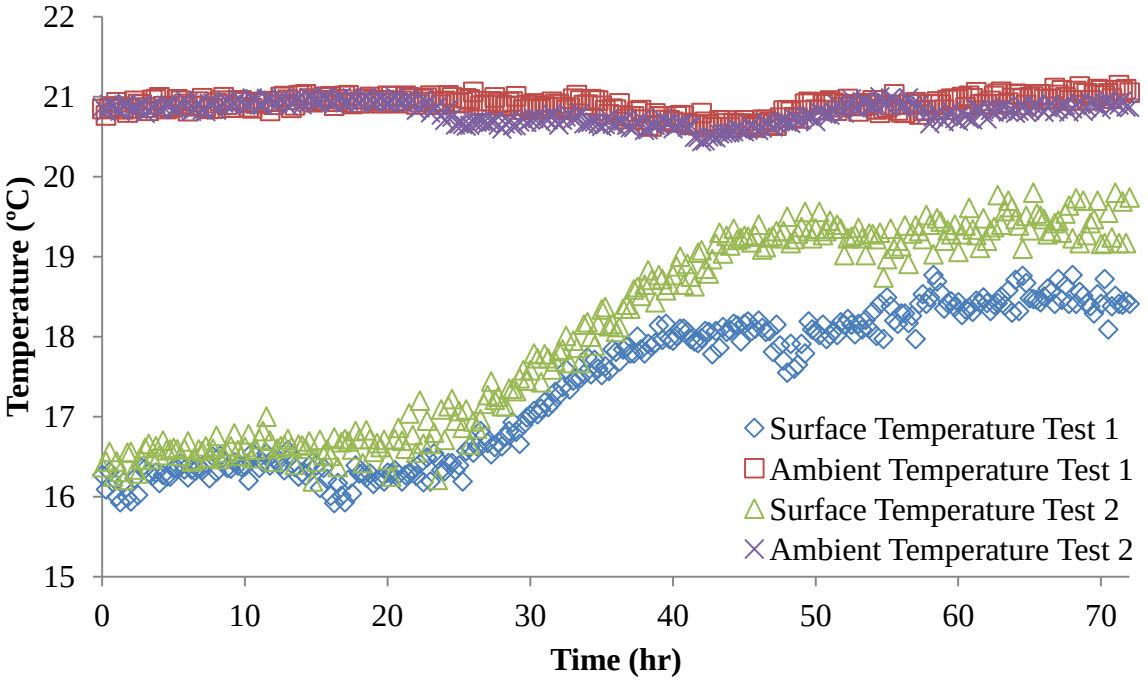
Temperature (ºC)
22
21
20
19
18
17
16
15
0
10
20
30
40
50
60
70
Time (hr)
Surface Temperature Test 1
Ambient Temperature Test 1
Surface Temperature Test 2
Ambient Temperature Test 2

(c)

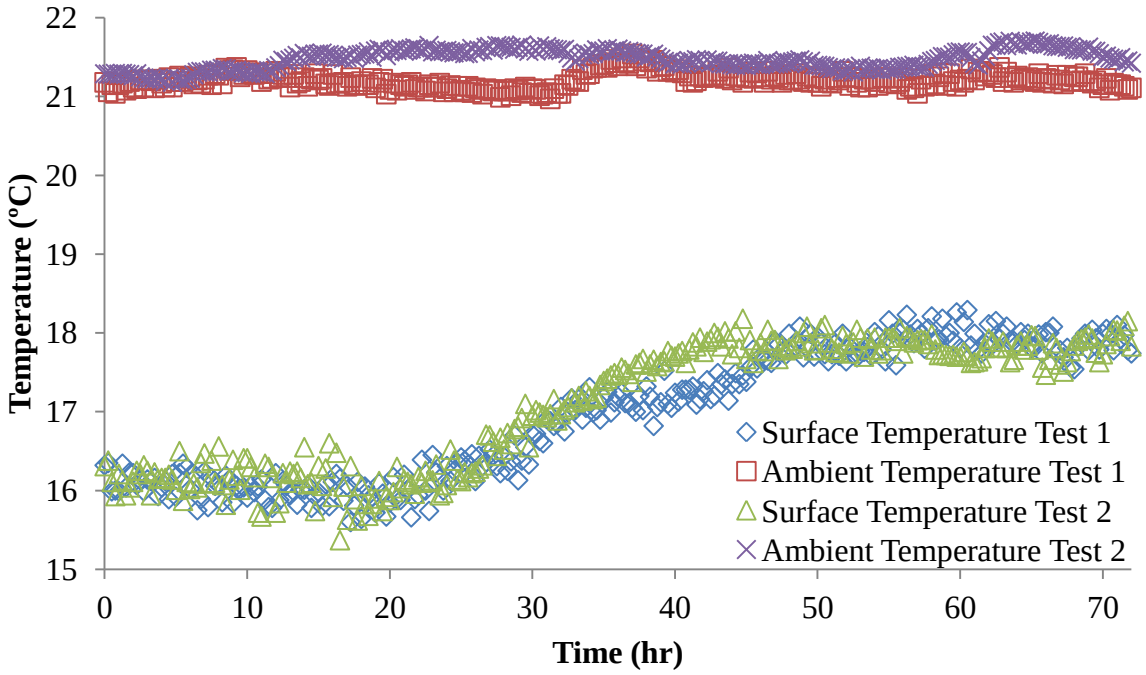

(d)

Figure 4.6 Infrared temperatures of the mixed sand surface in the large tunnel for air flow velocities of (a) 2.3 m/s, (b) 2.6 m/s, (c) 3.2 m/s and (d) 3.6 m/s

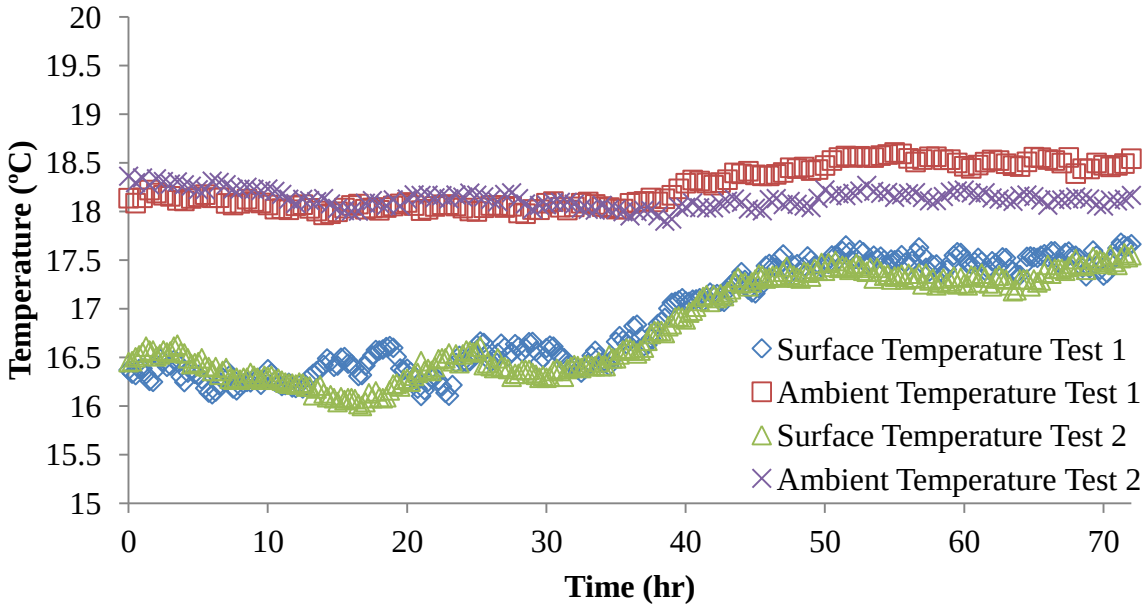

(a)

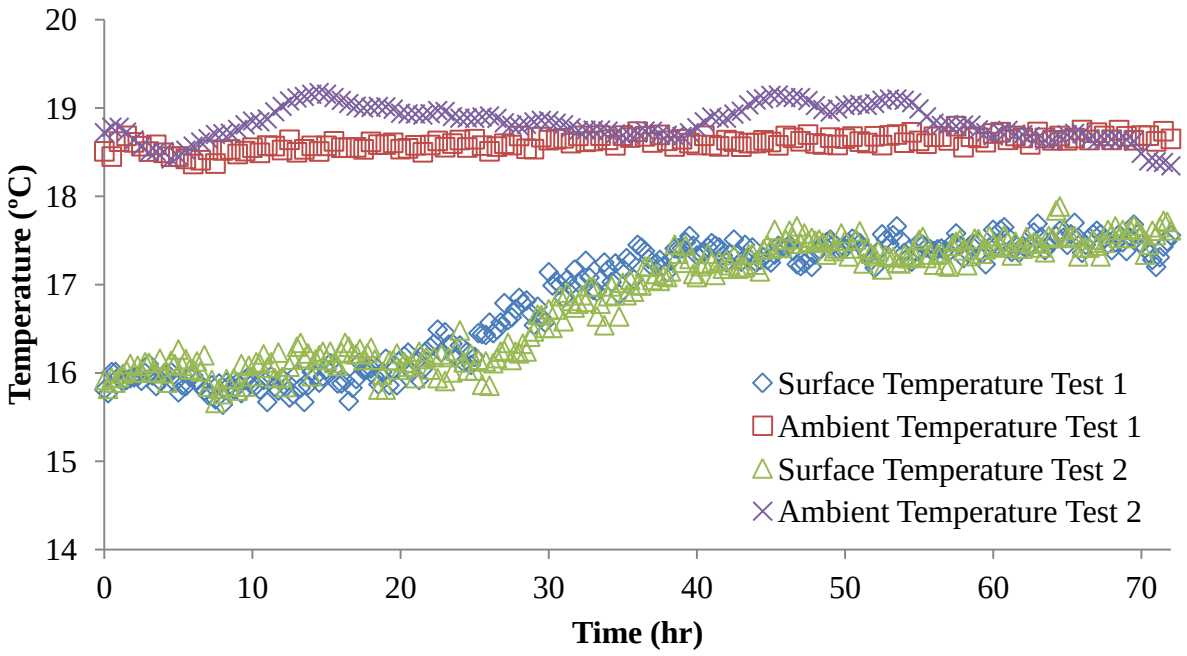

(b)

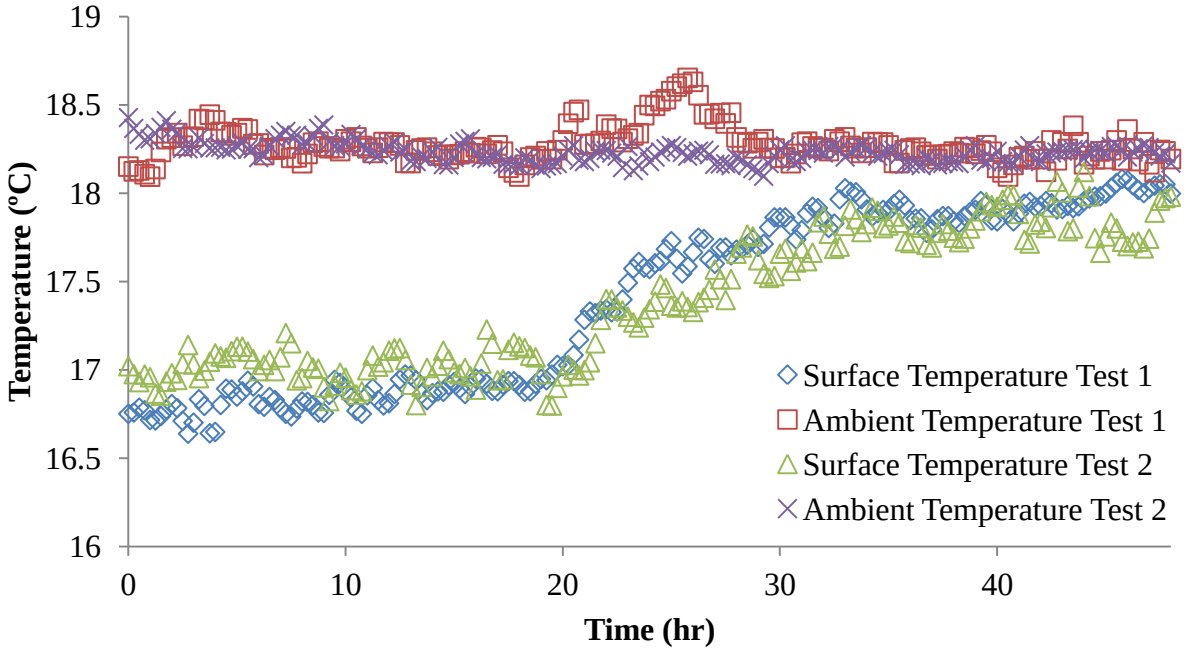

(c)

Figure 4.7 Infrared temperatures of the mixed sand surface in the small tunnel for air flow velocities of (a) 2.3 m/s, (b) 2.6 m/s and (c) 3.2 m/s

The use of the infrared imagery revealed the soil temperature behaviour during the drying process. From the use of infrared imagery we see that the surface temperatures of the soil samples tend to stay constant at the Stage 1 evaporation. From the infrared images we see that the Stage 1 evaporation is relatively short for the coarse sand whereas the tests have shown that for the fine and mixed samples of sand the temperature of the surface stayed constant for a much longer duration. This shows that water rehydrates the surface of the finer sand much easier than the larger coarse sand. Infrared imagery was also helpful in detecting the falling rate period at which the temperature of the surface of the sample increases indicating that the drying front is receding deeper into the soil. After the drying front moves deeper into the soil the temperatures of the surface stays constant at the ambient temperature.

4.3 Evaluation of Wind Velocity Effects on Various Soil Types

The effects of varying wind velocities were investigated in three different types of soil. The premise of this investigation is to find how the increase in velocity affects the drying process in different types of soils. The effects range with time variation and water loss. For the analysis three different types of sand were used: coarse (d_{50} = 2.6 mm), fine (d_{50} = 0.23 mm) and mixed (d_{50} = 0.57 mm). The experimentally determined water losses for the coarse sand are shown in **Figures 4.8** and **4.9** for the small and large tunnel; the measurements were taken at 30 min intervals. The observations show that the drying pattern for all of the coarse sand tests follow the parabolic pattern with high and almost linear water loss during the Stage 1 evaporation followed by the falling rate period (FRP). Falling rate period is the period where the water loss decreases nonlinearly which occurs approximately 10 hours after the Stage 1 evaporation. During that period the evaporation changes fall significantly ending at the Stage 2 evaporation. Looking at **Figures 4.8** and **4.9** we see that increase in air velocity does indeed increase the initial evaporation. Looking at the first 10-13 hours we see that there is a slight increase in evaporation for all of the three wind velocities. More pronounced increase in evaporation is shown in **Figure 4.9** of the large tunnel where the increase in wind velocity increased the evaporation.

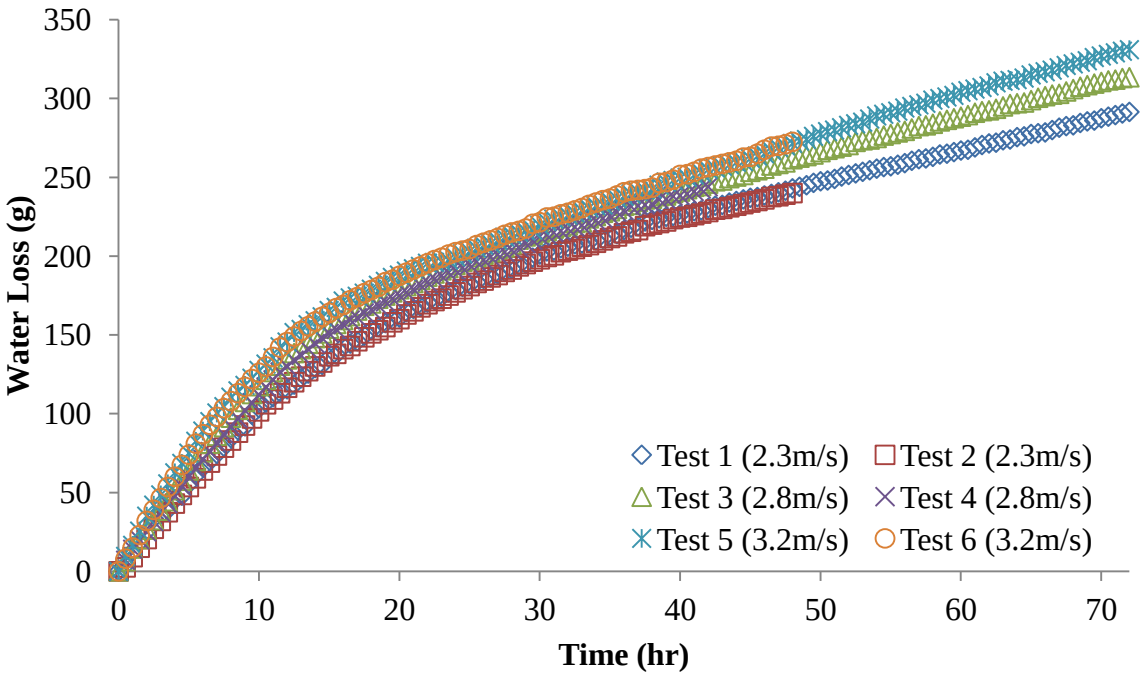

Figure 4.8 Comparison of water loss from coarse sand subjected to different air flow rates in small tunnel

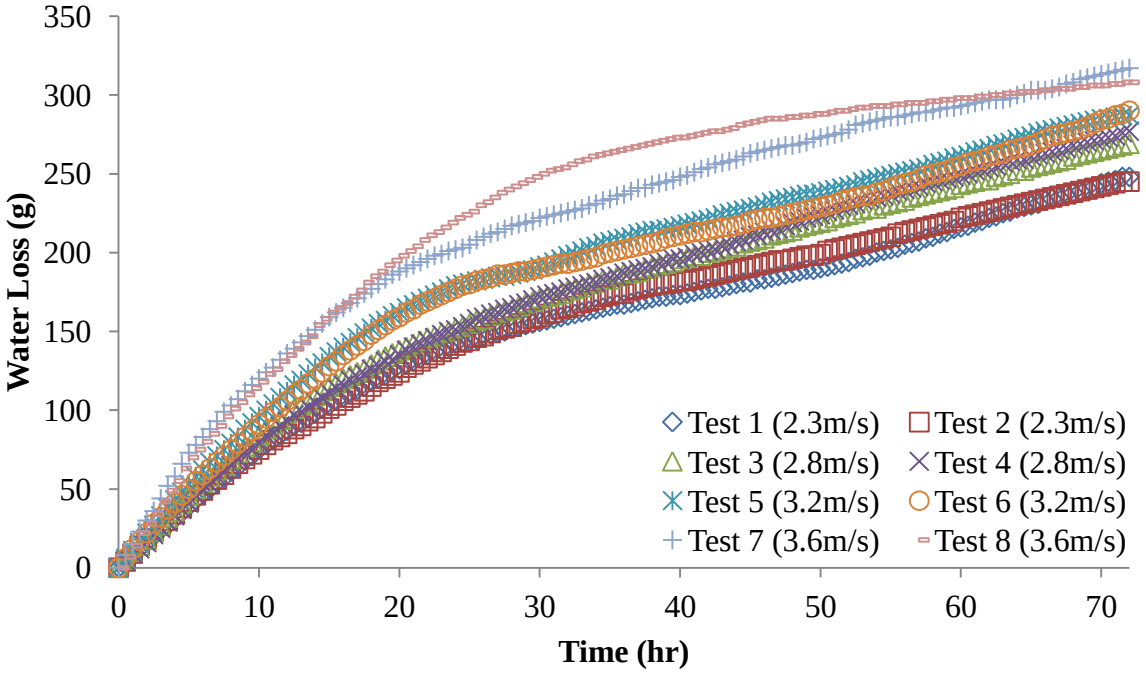

Figure 4.9 Comparison of water loss from coarse sand subjected to different air flow rates in large tunnel

There were substantial differences in water losses between the fine sand (**Figures 4.10** and **4.11**) and the coarse sand. The main difference is that the water loss comes from the Stage 1 evaporation where coarse sand had a significantly shorter duration than the fine sand. In the case of the fine sand the duration of the Stage 1 evaporation is about five times longer than the coarse sand. The increase in Stage 1 duration is mainly caused by the small particle size of the sand thus affecting the size of the pores in the sand. With the smaller pores in the fine sand the water from greater depths can easily reach the top of the evaporating surface, this is mainly due to the stronger surface tension between the water particles. As the water at the drying front vaporizes it gets replenished with the water that is being drawn from the bottom of the sample. From **Figures 4.10** and **4.11** we see that the increase in velocity affects the evaporation rate in the same manner as the coarse sand.

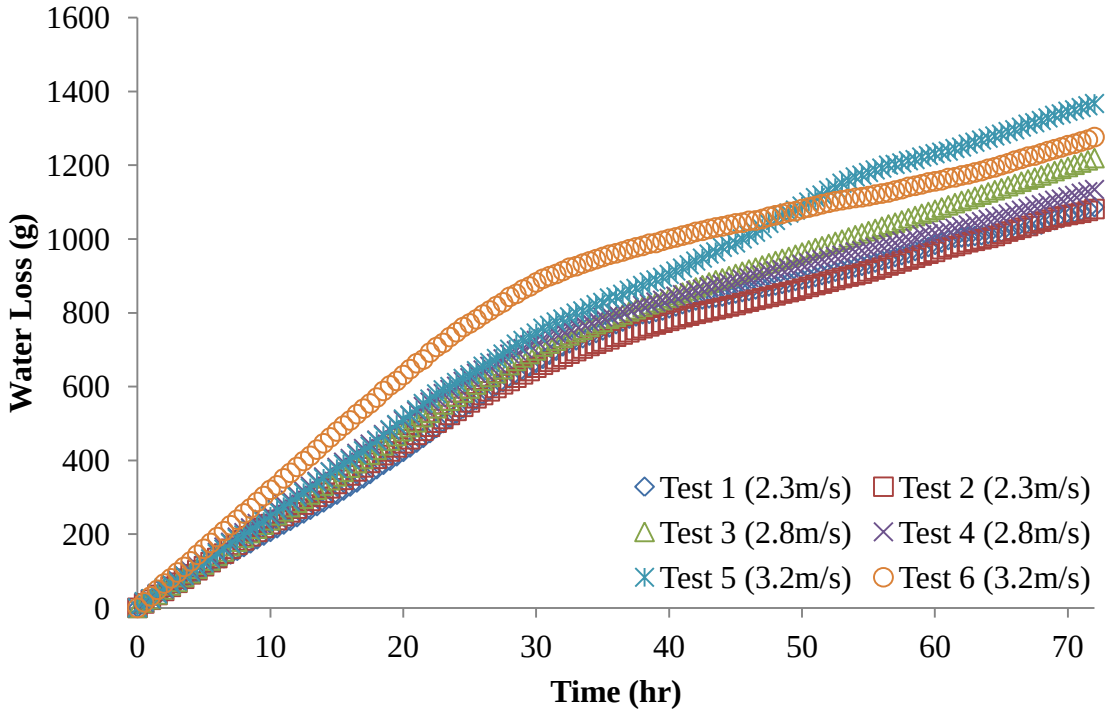

Figure 4.10 Comparison of water loss from fine sand subjected to different air flow rates in small tunnel

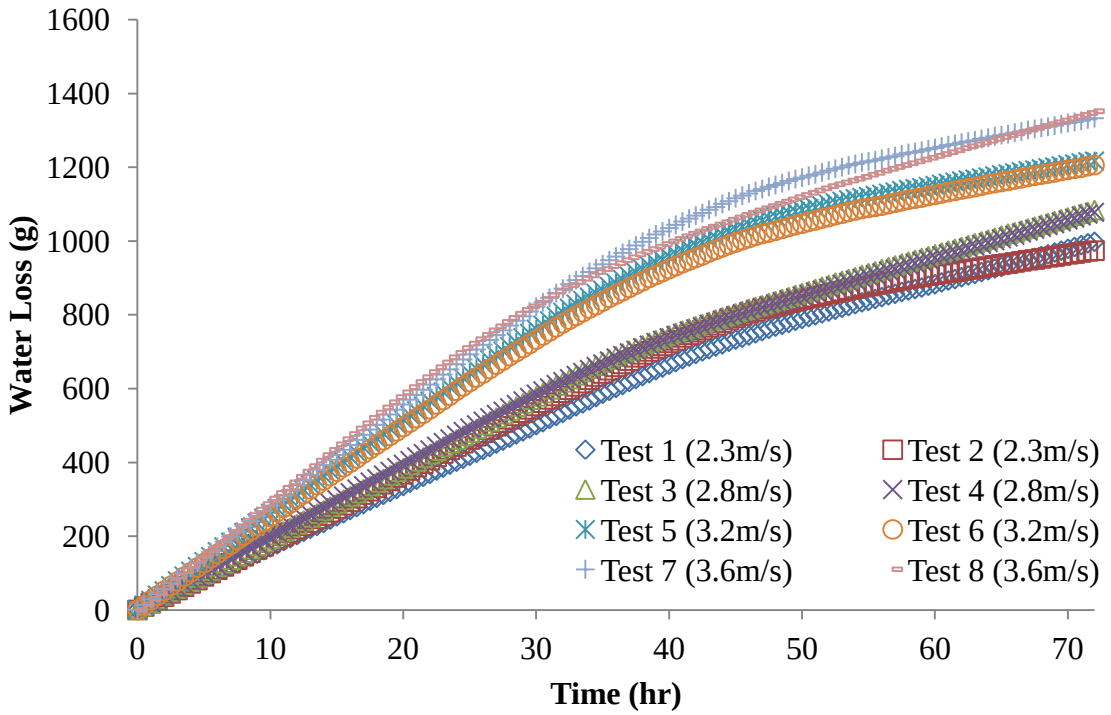

Figure 4.11 Comparison of water loss from fine sand subjected to different air flow rates in large tunnel

Evaporation behaviour of the mixed sand was observed to be similar to the fine sand evaporation. The evaporation occurred in the same parabolic fashion as the coarse and the fine sand and with increasing velocity the evaporation of water increased (see **Figures 4.12** and **4.13**). The water loss during the first 30 hours of the evaporation process remained constant in both the large and small tunnel and ending at the FRP. Similarly to the fine sand, the mixed sand has an increased falling rate period when compared to the coarse material. The increase in falling rate period duration is mostly due to the finer particles in the soil rehydrating the surface. The evaporation then slows down significantly which marks the beginning of Stage 2 evaporation. During Stage 2 evaporation, the effects of wind velocity are minimal for mixed sand mostly due to the fact that the drying front moved deep into the soil.

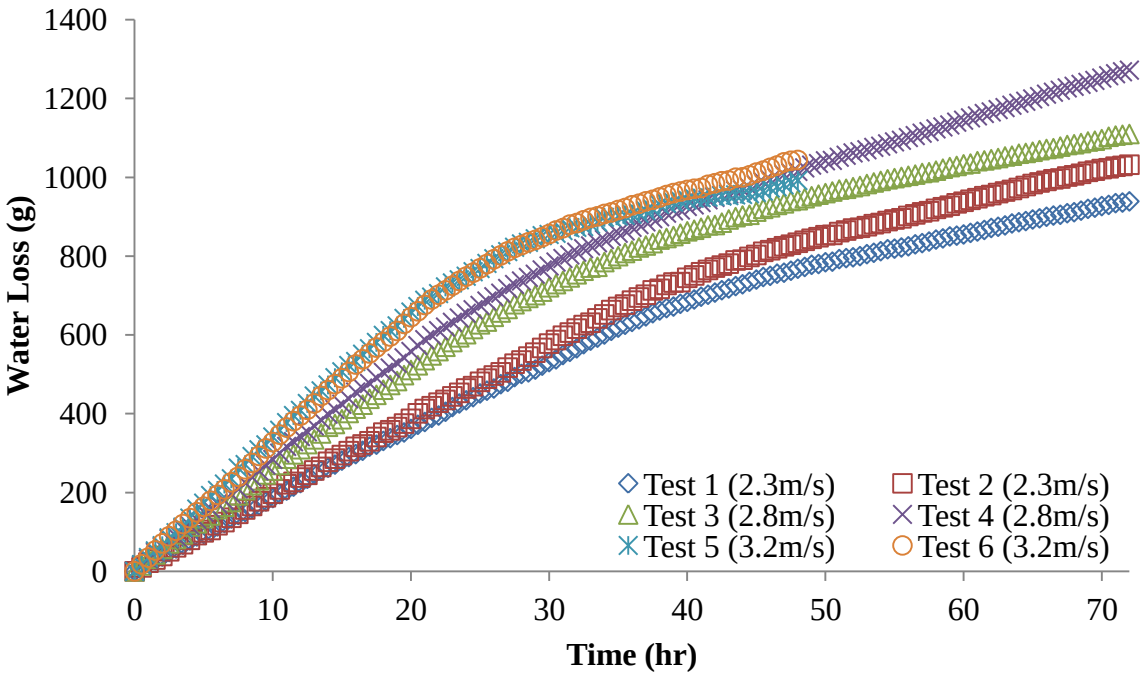

Figure 4.12 Comparison of water loss from mixed sand subjected to different air flow rates in small tunnel

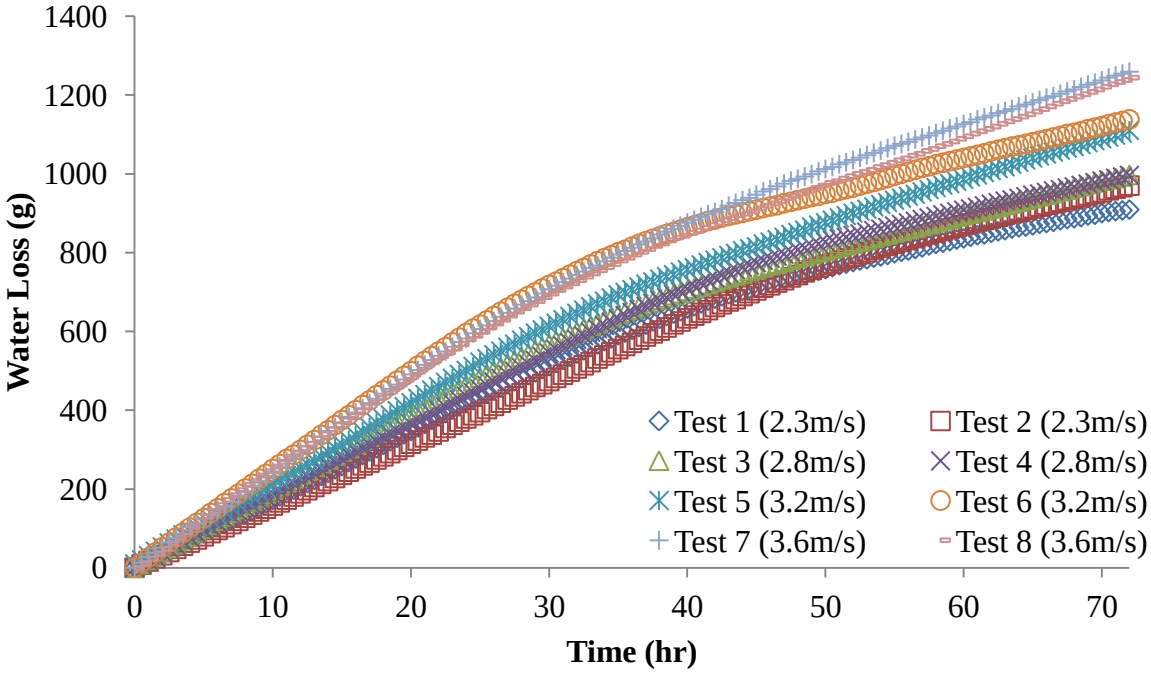

Figure 4.13 Comparison of water loss from mixed sand subjected to different air flow rates in large tunnel

These experiments have shown that with lower air velocity incoming into the tunnel resulted in a smaller evaporation rate than with the higher air velocities. Increasing the fan speed from 2.3 m/s to 3.6 m/s in the large tunnel increased water loss significantly. The same trend was shown in the smaller tunnel where the increase in velocity of 2.3 m/s to 3.2 m/s increased the water loss of each sand sample. This indicates that increasing the air velocity inside the tunnel increases the mass transfer across the interface between the soil surface and the ambient air. This has resulted in reduced Stage 1 evaporation rate period with increasing air flow.

A comparison of evaporation rates subjected to increasing air flow velocity for coarse sand is shown in **Figures 4.14** and **4.15**. From the figures we see that there is no significant impact on evaporation for the coarse sand with increasing velocity. This phenomenon can be associated with the large pore sizes that prohibit the capillary action to rehydrate the evaporating surface. Looking at the first few hours of the evaporating process we see that the evaporation is higher at the start of the drying cycle, this is also where the difference in evaporation is noticeable.

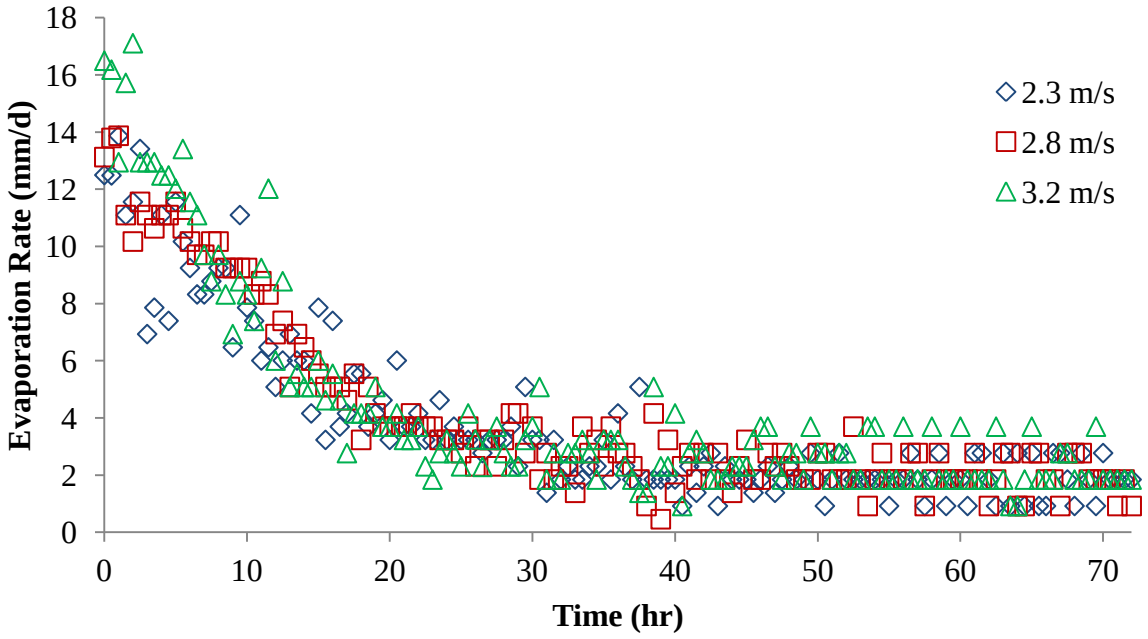

Figure 4.14 Comparison of evaporation rates from coarse sand subjected to increase in air flow rates in small tunnel

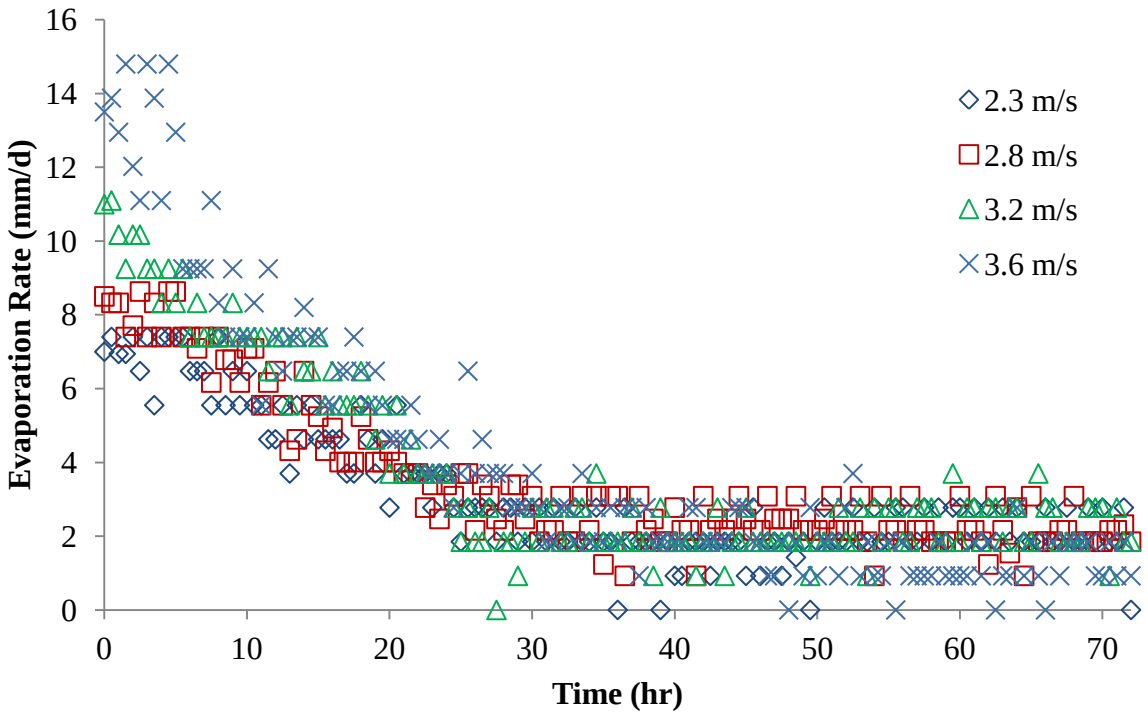

Figure 4.15 Comparison of evaporation rates from coarse sand subjected to increase in air flow rates in large tunnel

Fine and mixed sand had shown a more distinguishable difference during Stage 1 evaporation. **Figures 4.16** and **4.17** show the comparison of the increase of the evaporation rate with higher velocities. A difference in evaporation rate can be clearly seen for the duration of Stage 1 evaporation for the large tunnel we see that the evaporation rate is significantly more affected when the air flow increases from 2.8 m/s to 3.2 m/s. The same phenomenon can be seen for the small tunnel where the evaporation increases when the velocity is increased to 3.2 m/s. Looking at the **Figures 4.18** and **4.19** we see that the phenomenon of evaporation rate increase is the same as the mixed sand. With increased air flow velocity there is a substantial increases in evaporation. Mostly due to the stronger capillary action in the fine sand where the water molecules are brought up to the surface at much faster rate. With smaller pore sizes than coarse sand the Stage 1 evaporation rate of the fine sand is much more pronounced than the coarse sand.

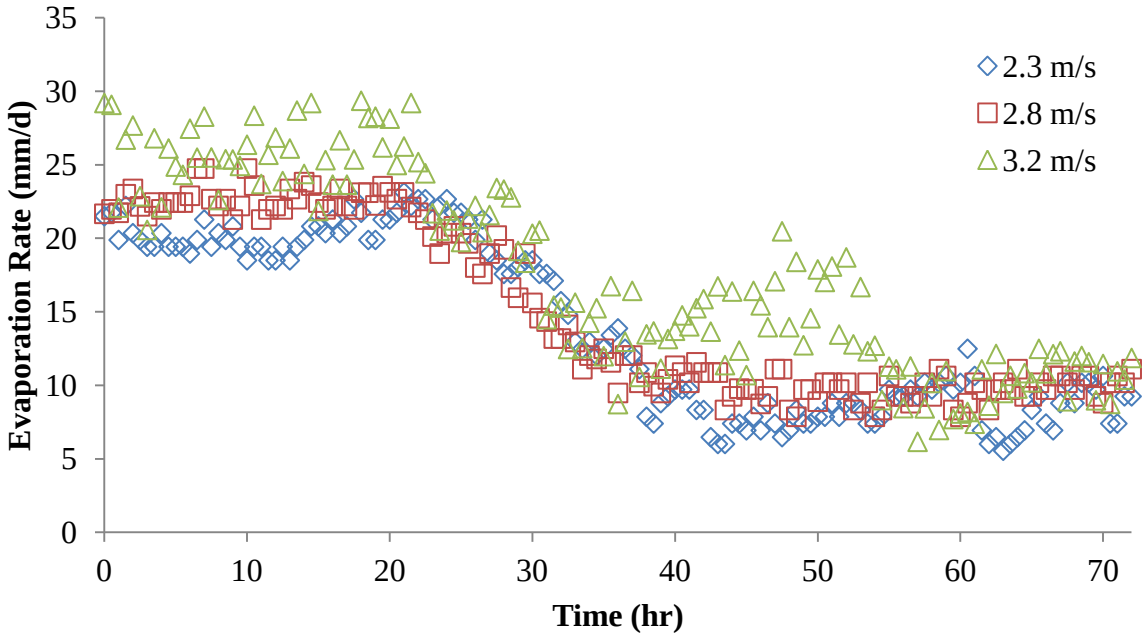

Figure 4.16 Comparison of evaporation rates from fine sand subjected to increase in air flow rates in small tunnel

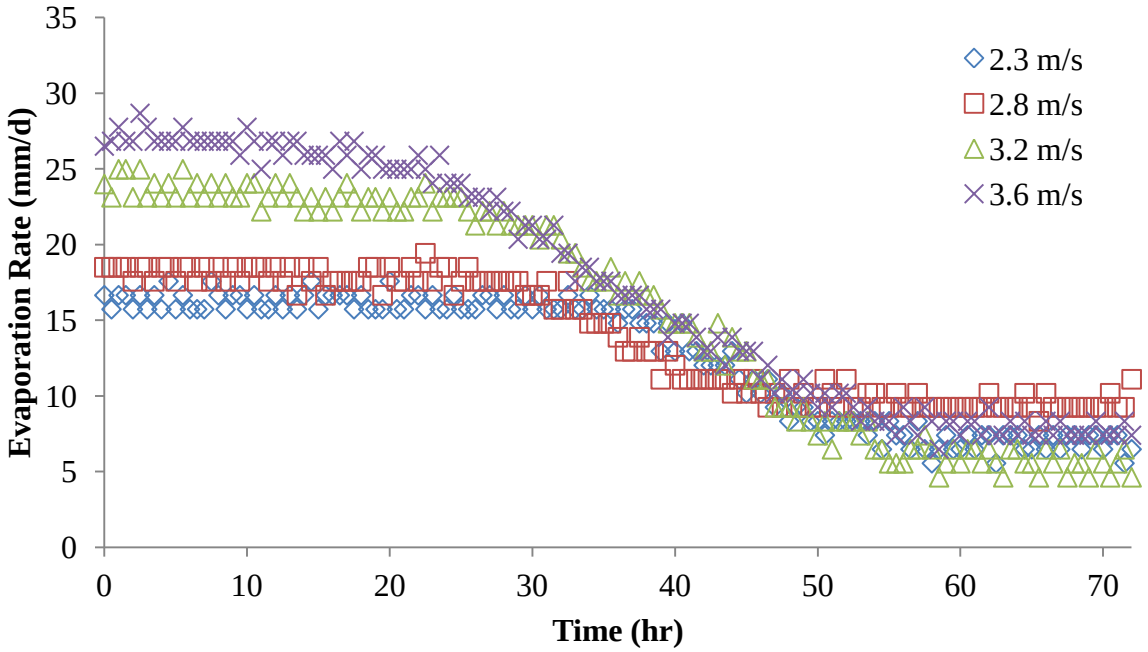

Figure 4.17 Comparison of evaporation rates from fine sand subjected to increase in air flow rates in large tunnel

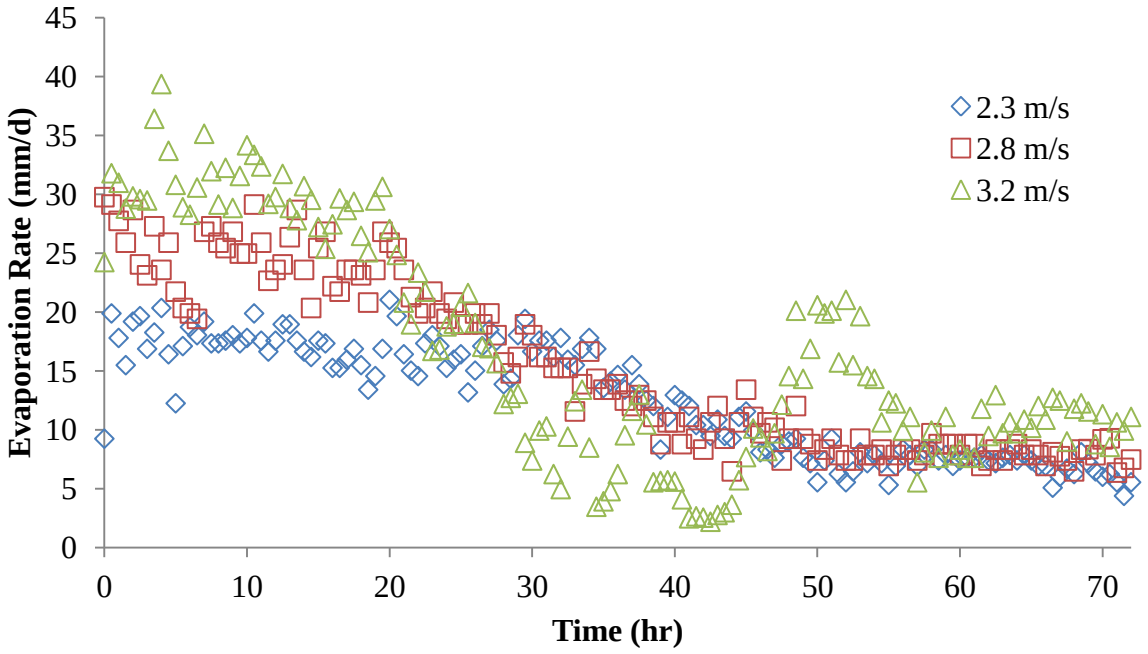

Figure 4.18 Comparison of evaporation rates from mixed sand subjected to increase in air flow rates in small tunnel

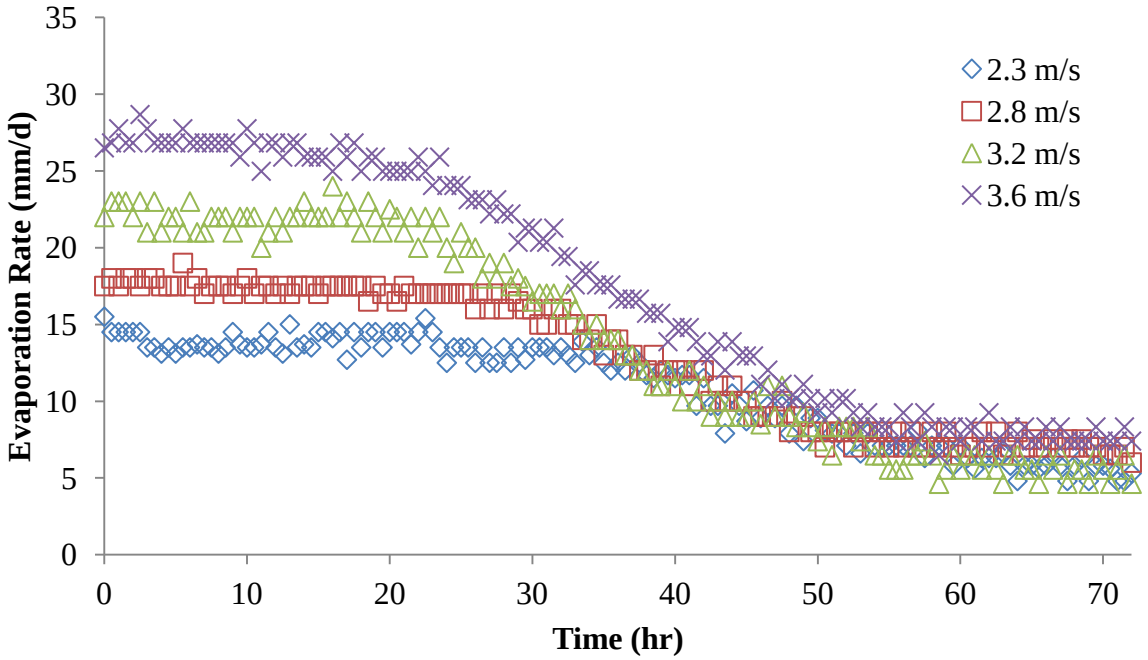

Figure 4.19 Comparison of evaporation rates from mixed sand subjected to increase in air flow rates in large tunnel

From the experiments we see that increases in air flow velocity had a significant impact on the total water losses as well as increases in evaporation rates. We noticed that coarse sand not significantly affected by the increase in air flow velocity but there were still some changes shown in the evaporation rates of the initial drying stages. The two sands that were most significantly affected by the changes in air flow velocity were mixed and fine sand, both showed increases in evaporation rates as well as total water losses.

4.4 Investigation of Tunnel Boundary Effects

4.4.1 Coarse Sand Boundary Effects

The investigation of the boundary effects for the coarse sand in the small and the large tunnel reveal that due to the thinner boundary layer in smaller tunnel, the evaporation is slightly higher than that of the large tunnel. Looking at the slopes of the Stage 1 evaporation in **Figure 4.20** for the coarse sand in the small tunnel it appears to be slightly higher than the large tunnel. The slope for the large tunnel appears slightly less steep signifying less evaporation during the Stage 1. As mentioned earlier the boundary layer thickness might be affecting the rate of initial evaporation of a fully saturated sample. The surface water in the small tunnel sample vaporizes much faster into the atmosphere than the large tunnel mostly due to the higher mass transfer rate from the passing air flow. With the thinner boundary layer the less humid air is much more likely to infiltrate the capillary voids and vaporise the surface water.

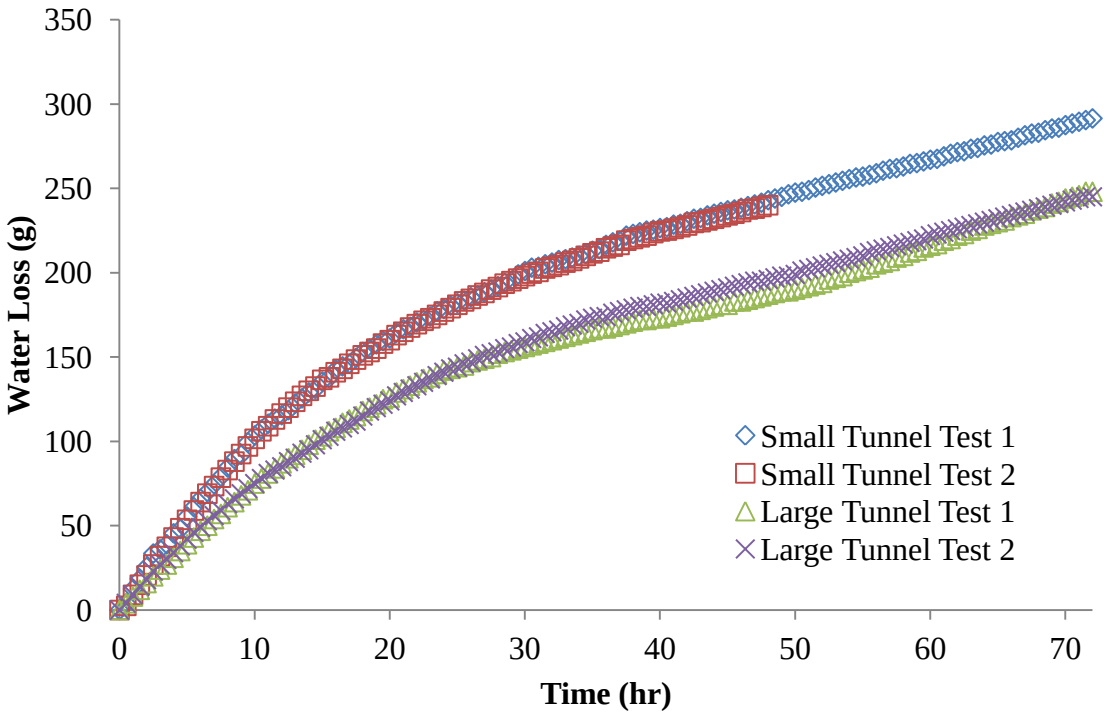
Water Loss (g)
350
300
250
200
150
100
50
0
0
10
20
30
40
50
60
70
Time (hr)
Small Tunnel Test 1
Small Tunnel Test 2
Large Tunnel Test 1
Large Tunnel Test 2

(a)

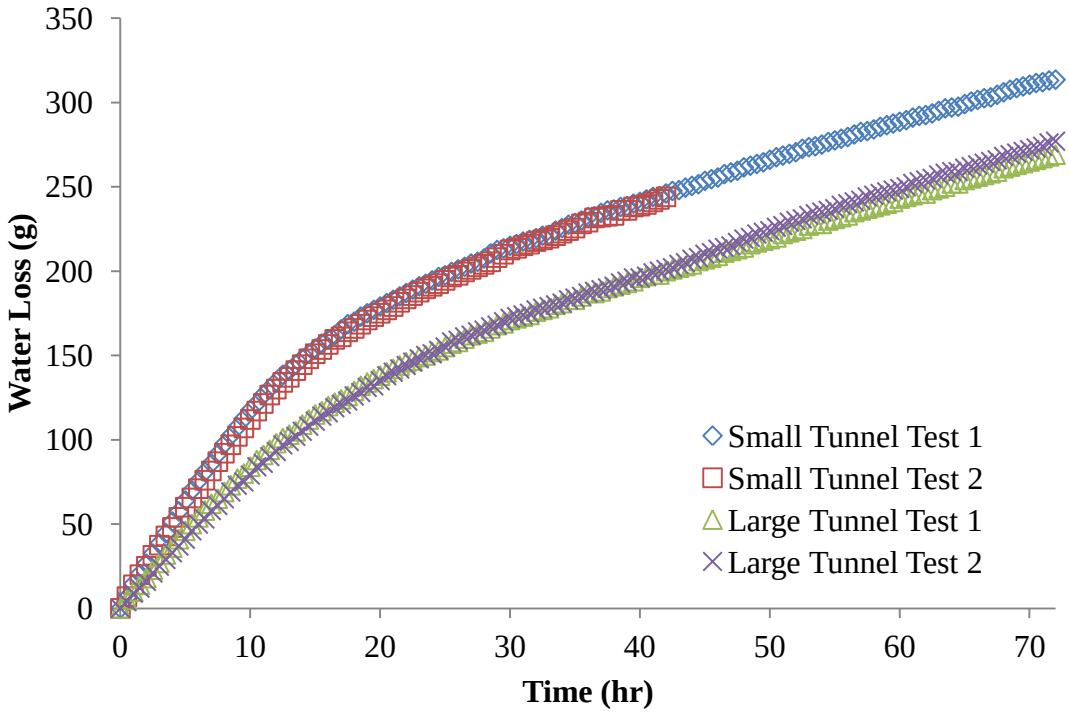
Water Loss (g)
350
300
250
200
150
100
50
0
0
10
20
30
40
50
60
70
Time (hr)
Small Tunnel Test 1
Small Tunnel Test 2
Large Tunnel Test 1
Large Tunnel Test 2

(b)

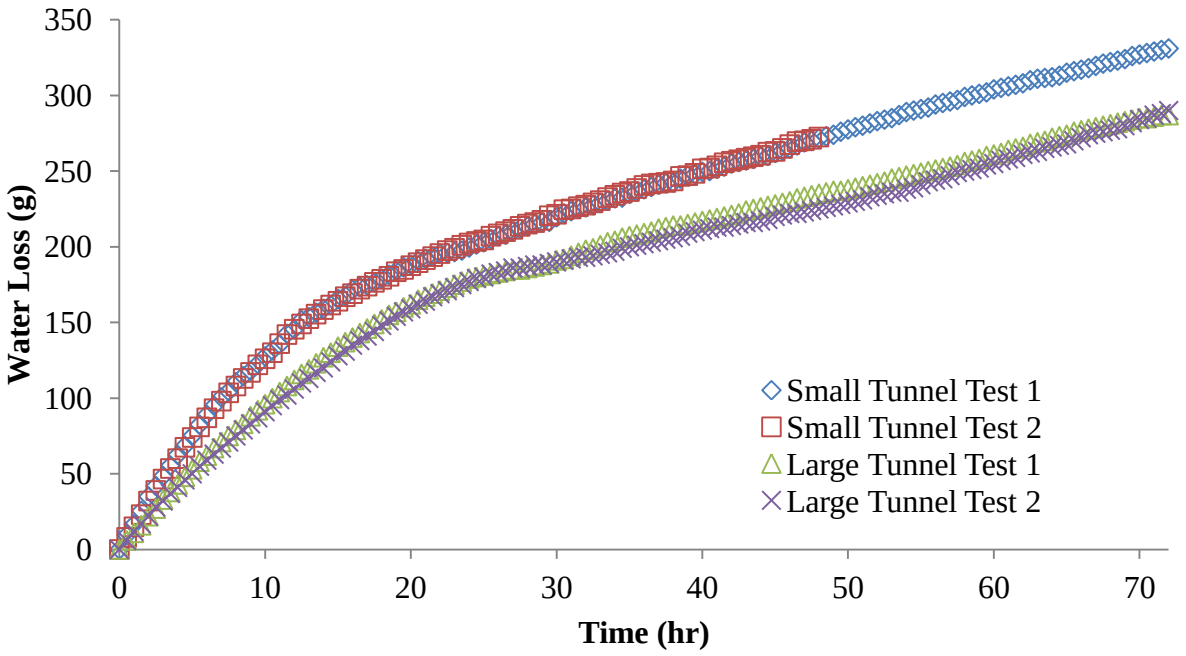

(c)

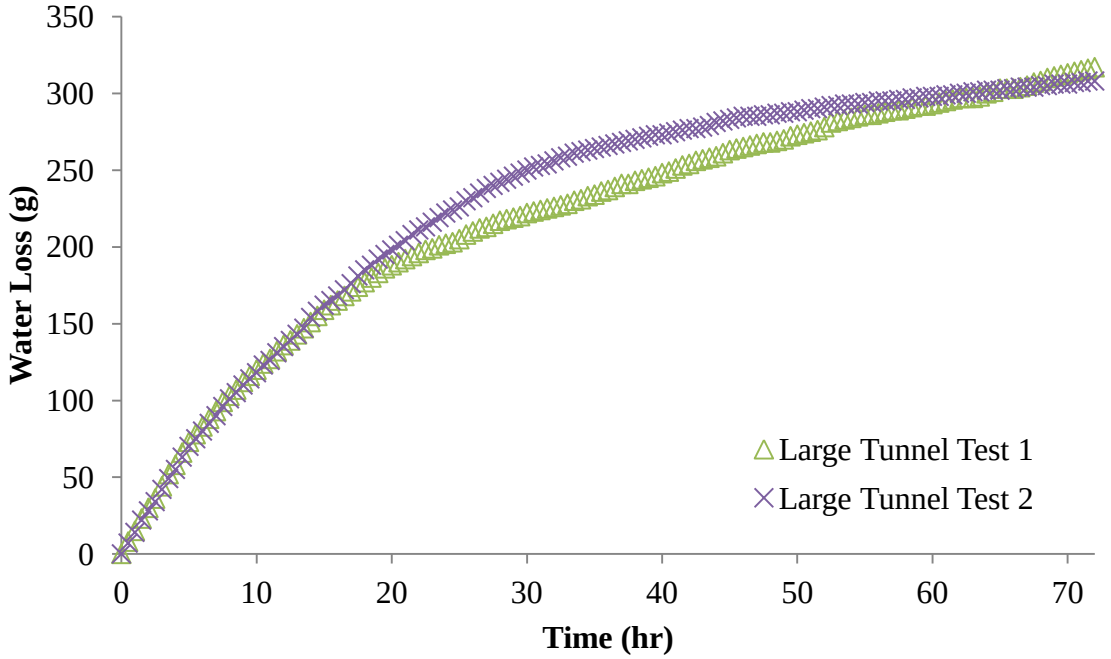

(d)

Figure 4.20 Comparison of water loss from coarse sand in small and the large tunnels with air flow velocities of (a) 2.3 m/s, (b) 2.8 m/s, (c) 3.2 m/s and (d) 3.6 m/s

Table 4.1 Total mass water loss for coarse sand

Velocity, (m/s)	Water Loss, (kg)	
Small Tunnel	Test 1	Test 2
2.3	0.291	0.240(48hr)
2.8	0.314	0.244(48hr)
3.2	0.331	0.273(48hr)
Large Tunnel	Test 1	Test 2
2.3	0.248	0.245
2.8	0.269	0.277
3.2	0.287	0.290
3.6	0.315	0.318

The experiment duration was 72 hours for all of the samples, in order to confirm validity a second test was ran. Since the coarse sand entered Stage 2 much quicker during small tunnel testing the test was only ran for 48 hours; however, for large tunnel testing the experiments were ran for 72 hours. **Table 4.1** shows the total water loss during the experiments. Since small tunnel had a longer Stage 1 evaporation in all of the cases of the wind velocity it lost the most water.

Experimental evaporation rate was found by the use of a simple empirical formula that converted the water mass loss into the evaporation rate. The equation used was as follows

$$e = \frac{\Delta m}{t \rho_w A} \qquad (4.1)$$

where the e is the experimental evaporation rate in mm/d, Δm is the change in mass (kg), ρ_w is the density of water in kg/m^3, A is the evaporating area m^2 and t is the time interval in days. **Figure 4.21** shows the experimental evaporation rates from the small and large tunnels at velocities of 2.3 m/s, 2.8 m/s and 3.2 m/s. From **Figure 4.21**, we can see that the Stage 1 evaporation is indeed higher in the small tunnel than the large tunnel, which was represented in the water mass loss figures.

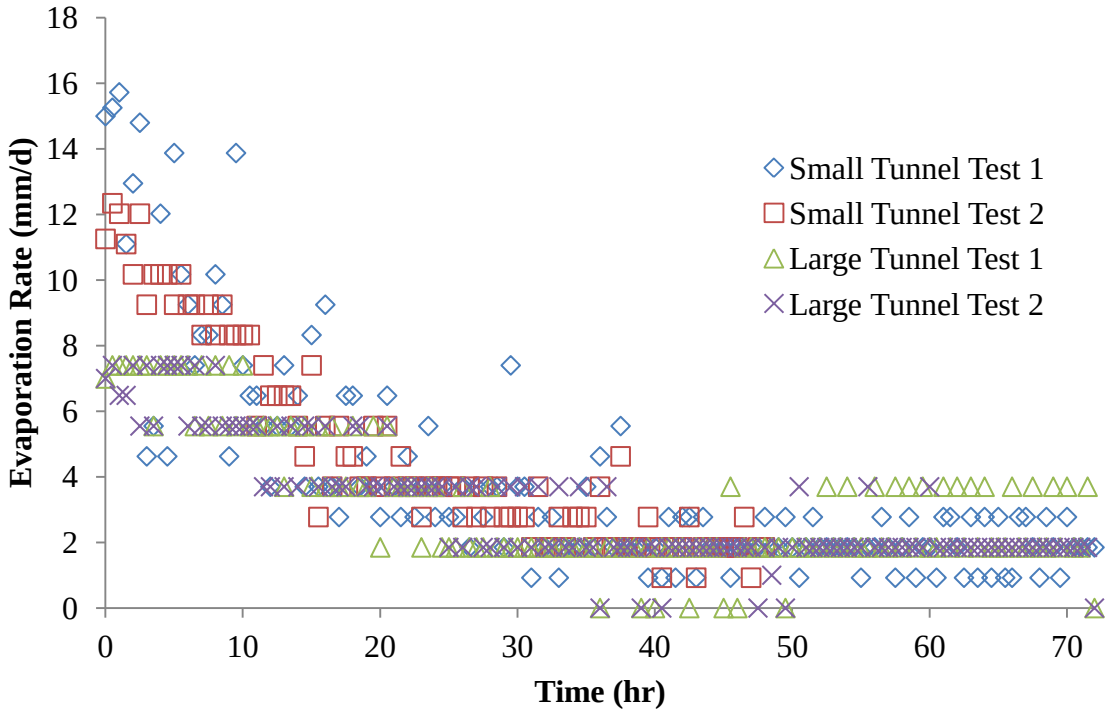
Evaporation Rate (mm/d)
Time (hr)
Small Tunnel Test 1
Small Tunnel Test 2
Large Tunnel Test 1
Large Tunnel Test 2

(a)

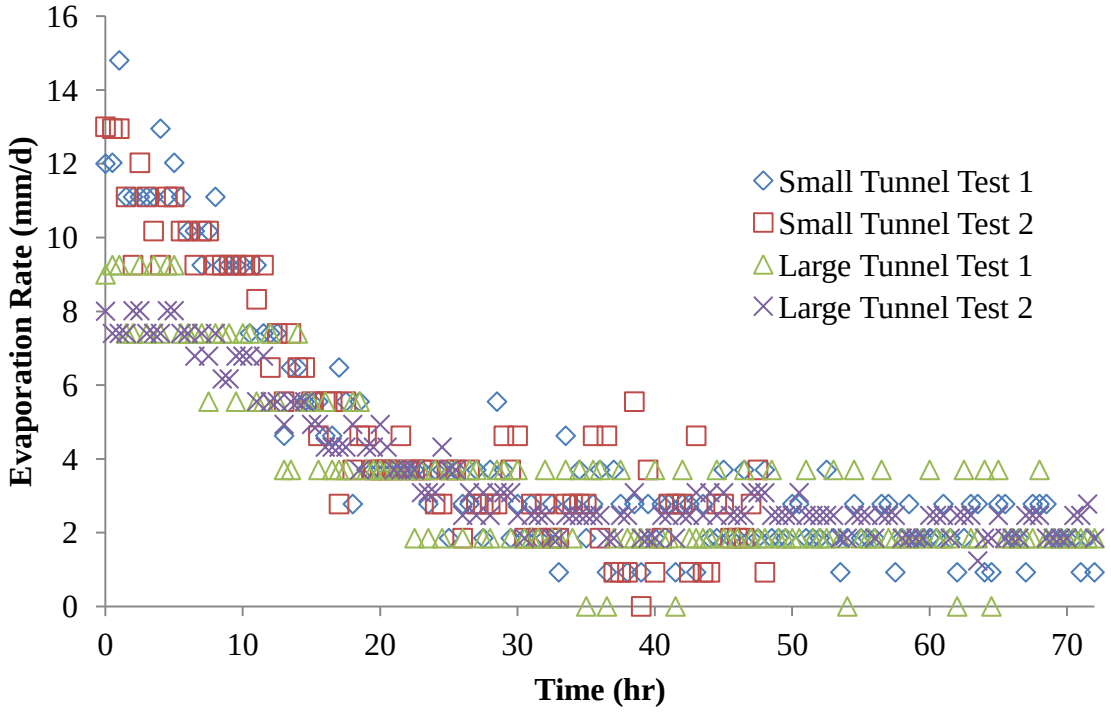
Evaporation Rate (mm/d)
Time (hr)
Small Tunnel Test 1
Small Tunnel Test 2
Large Tunnel Test 1
Large Tunnel Test 2

(b)

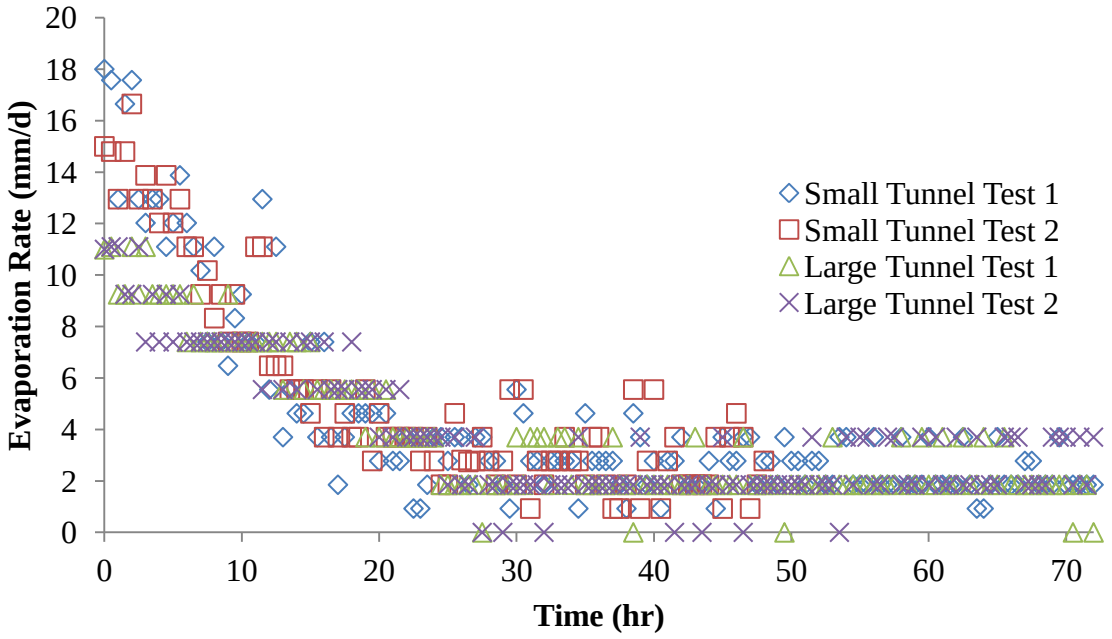

(c)

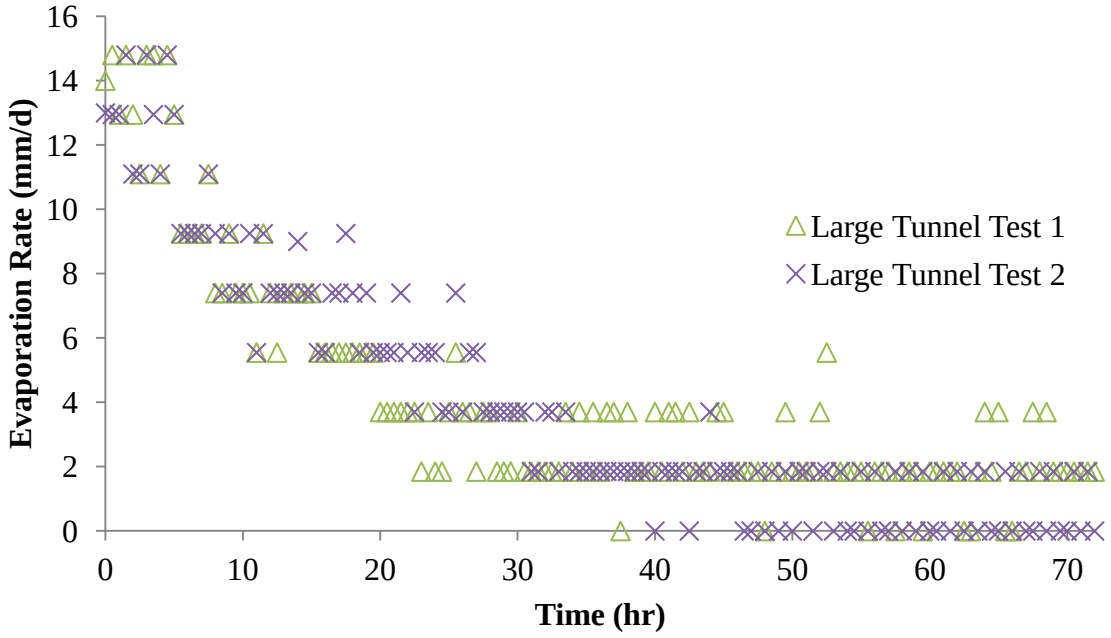

(d)

Figure 4.21 Comparison of experimental evaporation rates from coarse sand in small and the large tunnels with air flow velocities of (a) 2.3 m/s, (b) 2.8 m/s, (c) 3.2 m/s and (d) 3.6 m/s

The difference in evaporation between small tunnel and the large tunnel during the Stage 1 for velocity of 2.3 m/s is approximately 6.2-6.5 mm/d; for the velocity of 2.8 m/s the difference in evaporation is approximately 4.1-4.6 mm/d and for the velocity of 3.2 m/s the difference is 5.1-5.5 mm/d. The difference in evaporation between the small and the large tunnel seem to be affected by the amount of surface water on top of the soil. With the surface water present the small tunnel has higher capability to exchange mass transfer between the water particles and the air due to the thinner boundary layer.

After the Stage 1 the evaporation enters the falling rate period (FRP). From the graphs the initial transition period varies slightly with time when comparing the small and the large tunnel. With approximately 8-10 hours of the transition period in the small tunnel, the falling rate period is slightly longer than the large tunnel. After this transition the stage 2 evaporation rates in both tunnels match. With both falling rate periods matching the two rates have the same slope thus indicating that the influence of the flowing air is no longer the factor in the evaporation during stage 2. At that stage the capillary forces take over and give way to the penetrating air that slowly vaporises the water at the second drying front. During Stage 2 the evaporation rates of all of the experiments match which proves the hypothesis that the evaporation is controlled by the gravitational and capillary forces. With the large pores the water surface tension is not strong enough to raise the water to the surface thus slowing down the evaporation significantly. With the lower evaporation the average Stage 2 evaporation for velocities 2.3, 2.8 and 3.2 m/s are 2.31, 2.46 and 2.71 mm/d, respectively, for both tunnels.

4.4.2 Fine Sand Boundary Effects

The investigation of the boundary effects on fine sand with the d_{50} of 0.23 mm revealed that the results are similar to the ones obtained for the coarse sand. From the water loss figures shown in **Figure 4.22** we see that the fully saturated fine sand in the small tunnel experiences slightly more evaporation than the large tunnel. The cumulative water loss form fully saturated fine sand surface follows a linear pattern during the Stage 1 evaporation but at a higher rate than the coarse sand. When comparing the small and large tunnel, the mass of the water loss during Stage 1 evaporation is higher in the small tunnel than the large. The steepness of the slope during

Stage 1 in both tunnels is affected by the boundary layer; thus with the thinner boundary layer the small tunnel has much higher mass loss. The thicker boundary layer in the large tunnel produces slower mass transfer exchange of the less humid air in the large tunnel.

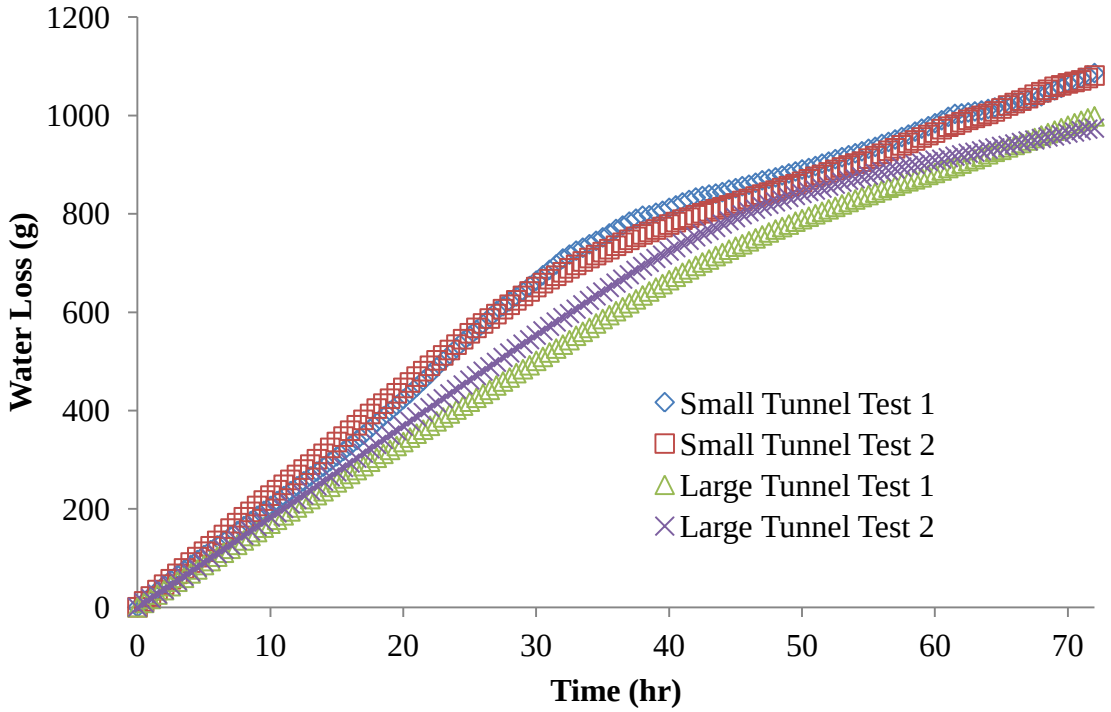

(a)

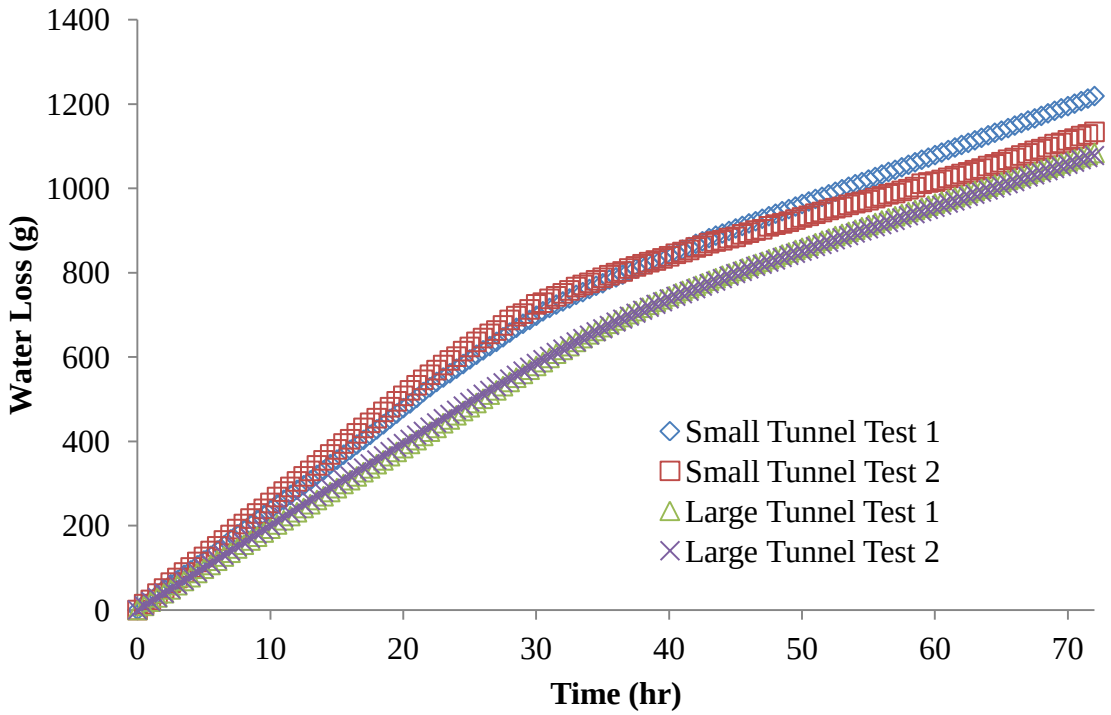
1400
1200
1000
800
600
400
200
0
Water Loss (g)
0
10
20
30
40
50
60
70
Time (hr)
Small Tunnel Test 1
Small Tunnel Test 2
Large Tunnel Test 1
Large Tunnel Test 2

(b)

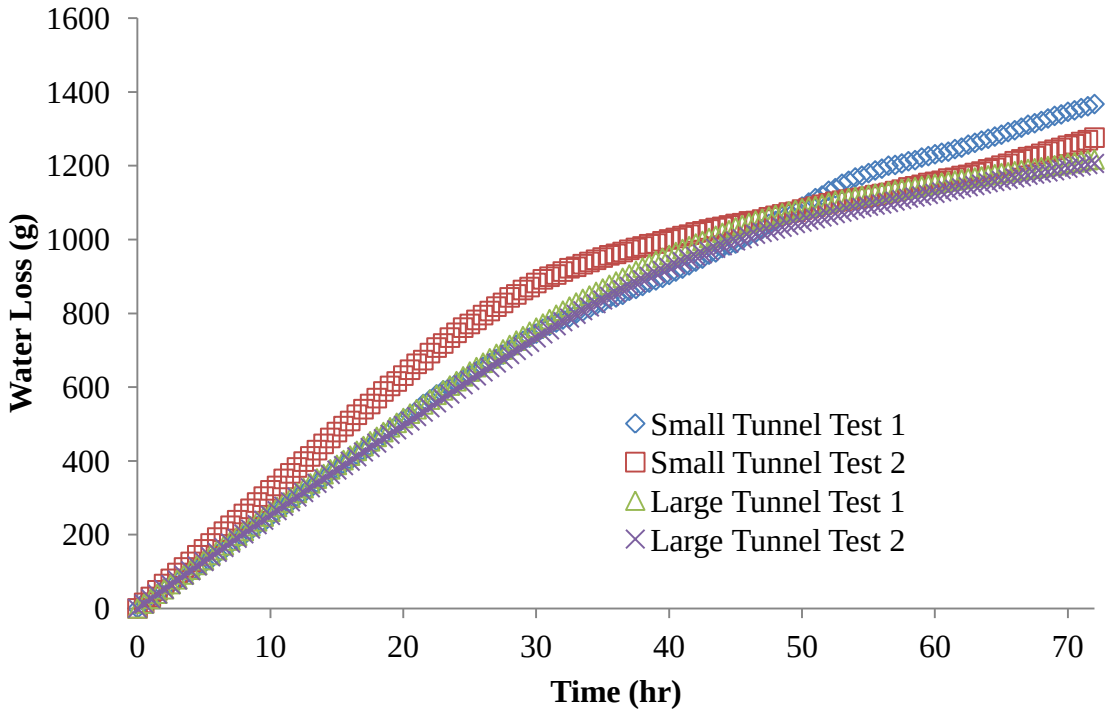
1600
1400
1200
1000
800
600
400
200
0
Water Loss (g)
0
10
20
30
40
50
60
70
Time (hr)
Small Tunnel Test 1
Small Tunnel Test 2
Large Tunnel Test 1
Large Tunnel Test 2

(c)

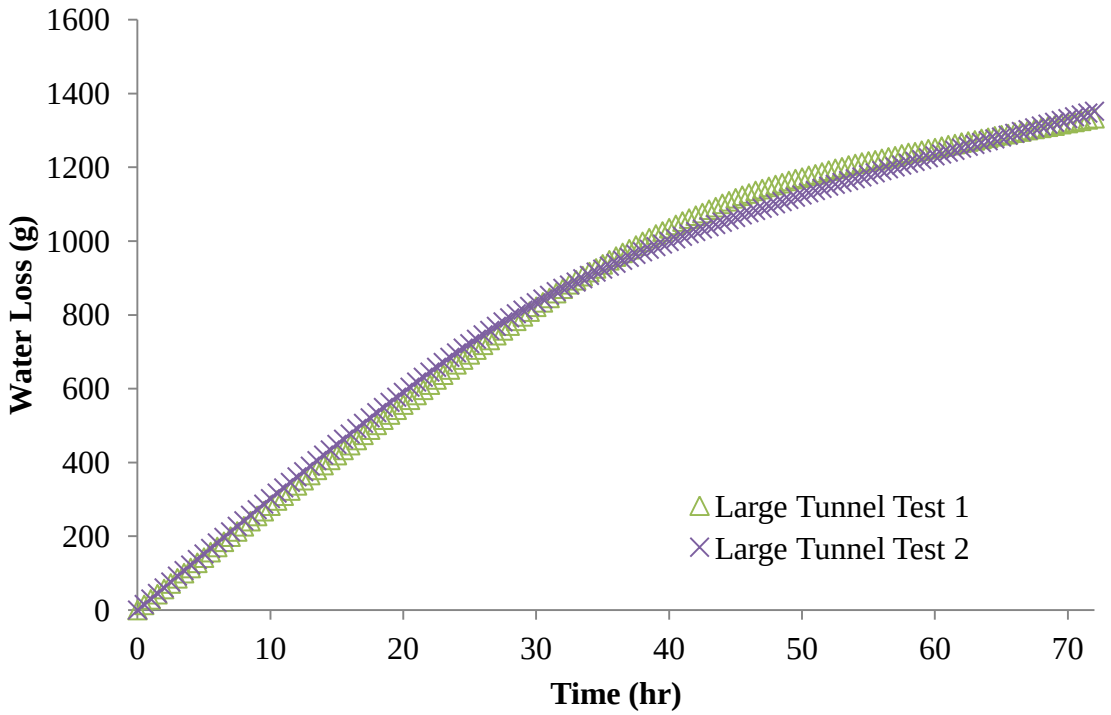

(d)

Figure 4.22 Comparison of water loss from fine sand in small and the large tunnels with air flow velocities of (a) 2.3 m/s, (b) 2.8 m/s, (c) 3.2 m/s and (d) 3.6 m/s

Table 4.2 Total mass water loss for fine sand

Velocity, (m/s)	Water Loss, (kg)	
Small Tunnel	Test 1	Test 2
2.3	1.086	1.081
2.8	1.219	1.134
3.2	1.367	1.415
Large Tunnel	Test 1	Test 2
2.3	0.998	0.974
2.8	1.084	1.078
3.2	1.217	1.206
3.6	1.375	1.384

The duration of the experiment for the fine soil was 72 hours, this was primarily due to the extensive water loss through the experiment. Reading **Table 4.2** the total water loss for the fine sand is approximately 1 - 1.4 kg for each test ran regardless if the test was ran in the small or the large tunnel.

The water mass loss was converted into evaporation rates using **Equation 4.1**. The evaporation results were then combined for comparison of the small and the large tunnel boundary conditions. **Figure 4.23** shows the results of the evaporation rates from fine sand. From the figures we see that there is an increase in evaporation rates in the small tunnel when comparing to the large tunnel evaporation rate. It is the same phenomenon as we observed in the case coarse sand. The difference of evaporation between the small and the large tunnel during Stage 1 evaporation for velocity 2.3 m/s is 2.23-4.62 mm/d, for 2.8 m/s is 3.48-5.78 mm/d and for the velocity of 3.2 m/s the difference of evaporation is 3.23-6.9 mm/d. The difference of evaporation is considerably less than that of the coarse sand mostly due to the fact that the coarse sand had significantly more surface water that was on top of the sand when the porous media was fully saturated. This allowed the thinner boundary layer of the small tunnel to have faster mass transfer than the thicker boundary layer of the large tunnel. Although the fine sand had some surface water on the surface it was significantly less than the coarse sand thus most of the water was drawn from the bottom depths of the porous media. Since the same type of fine sand was used for the small and the large tunnel testing the hydraulic properties were the same, thus the water was supplied at the same rate in both cases. Now since the small tunnel had thinner boundary layer it dried the soil slightly quicker than the large tunnel. Another observation when comparing the two cases of coarse and fine sand is the Stage 1 duration, looking at the graph of fine sand evaporation the Stage 1 length is significantly longer than the coarse sand. This is mostly due to the capillary forces being stronger due the smaller pore sizes in comparison to the larger coarse sand. After the falling rate period of approximately 23-30 hours, the fine sand enters Stage 2 evaporation where the rate of drying slows down significantly at that stage. The water in the soil sample is almost completely gone with only some residual moisture left. During Stage 2 the residual moisture slowly creeps up to the surface due to the capillary forces. The average Stage 2 evaporation rates are approximately 8.32, 8.78 and 8.55 mm/d for velocities of 2.3, 2.8 and 3.2 m/s, respectively.

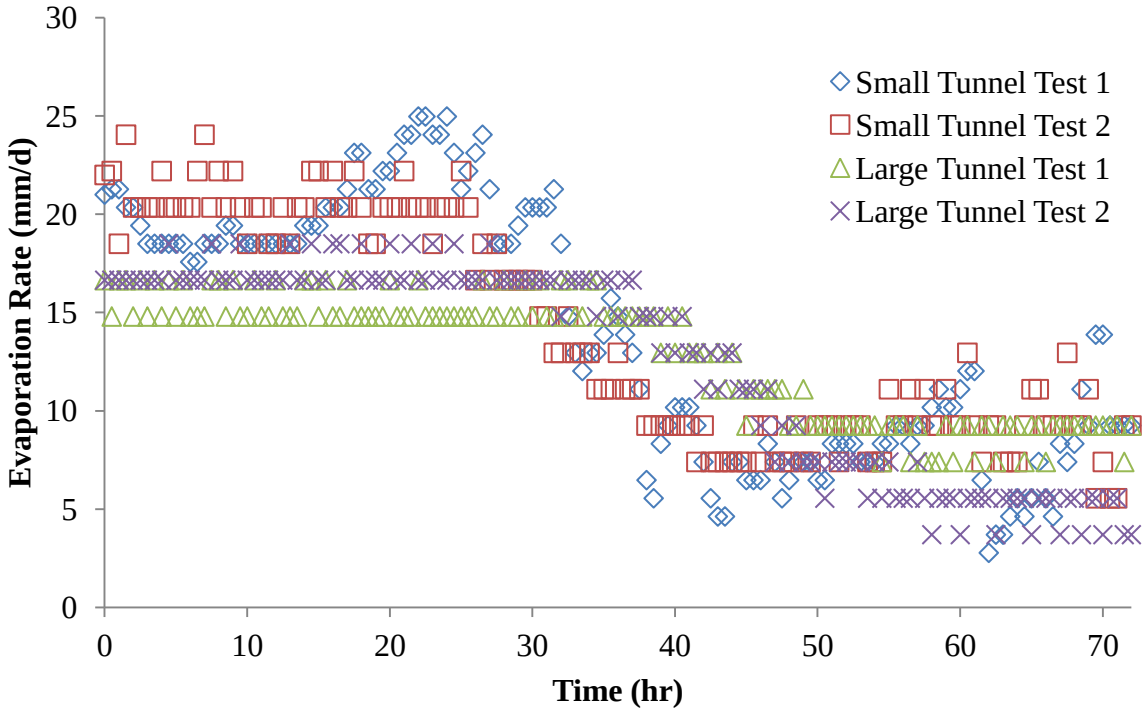
Evaporation Rate (mm/d)
Time (hr)
Small Tunnel Test 1
Small Tunnel Test 2
Large Tunnel Test 1
Large Tunnel Test 2
0
5
10
15
20
25
30
0
10
20
30
40
50
60
70

(a)

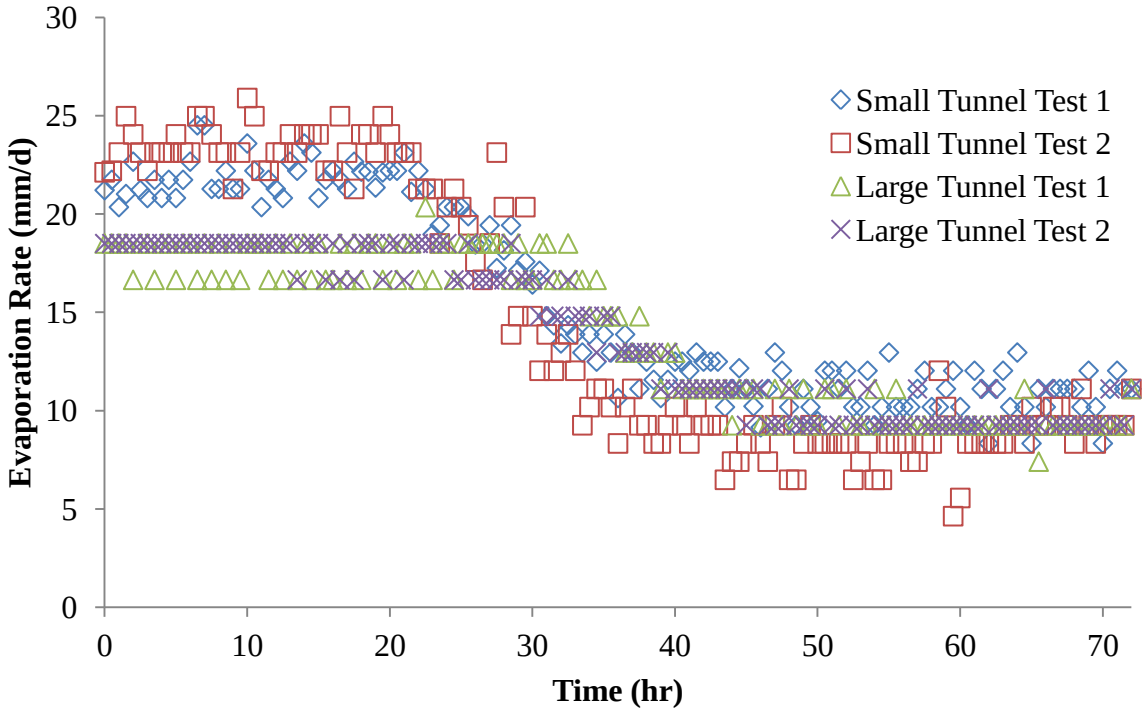
Evaporation Rate (mm/d)
Time (hr)
Small Tunnel Test 1
Small Tunnel Test 2
Large Tunnel Test 1
Large Tunnel Test 2
0
5
10
15
20
25
30
0
10
20
30
40
50
60
70

(b)

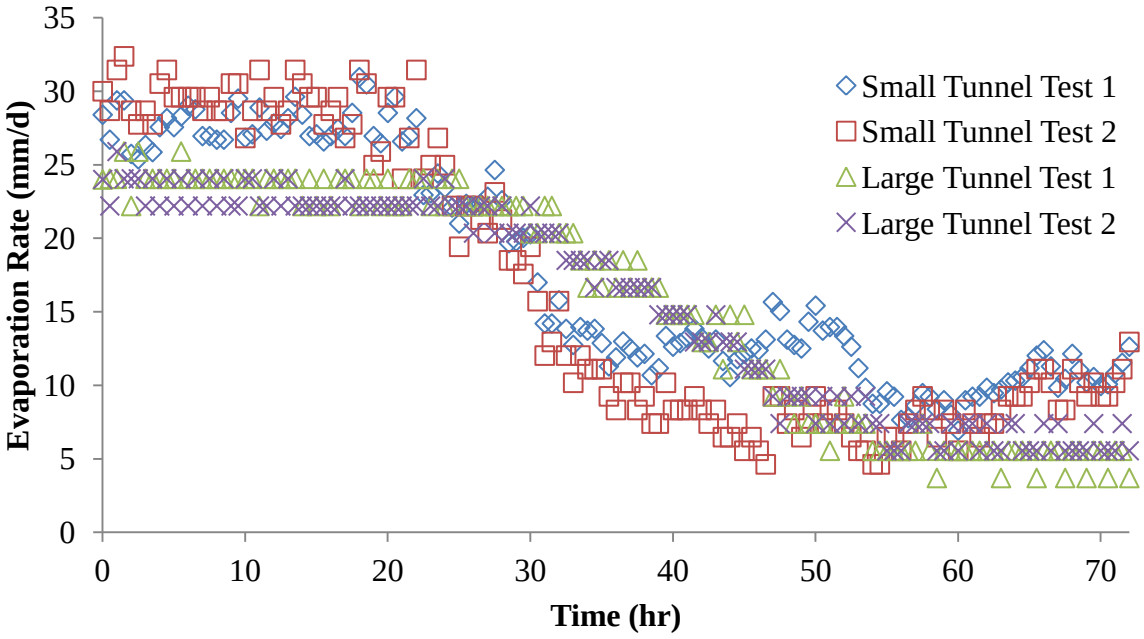

(c)

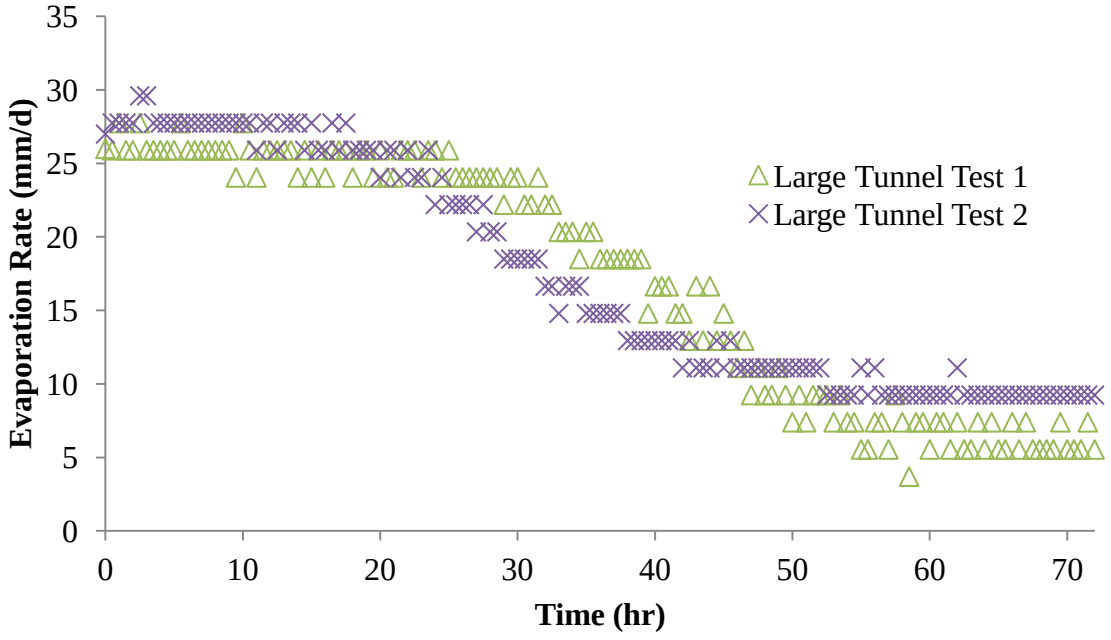

(d)

Figure 4.23 Comparison of experimental evaporation rates from fine sand in small and the large tunnels with air flow velocities of (a) 2.3 m/s, (b) 2.8 m/s, (c) 3.2 m/s and (d) 3.6 m/s

4.4.3 Mixed Sand Boundary Effects

Investigation of the boundary effects on the mixed sand (d_{50} = 0.57 mm) evaporation yielded results similar to the ones obtained for the fine sand. The mass of water loss from the mixed sand experiment are shown in **Figure 4.24**. The comparison shows the difference between the small and the large tunnel. From these graphs we can see that the water loss curve exhibits a parabolic shape as presented in the previous two porous media samples. During the initial drying cycle the sand exhibits linear style water loss. The comparison of the drying between the small and the large tunnel show that the large tunnel has less water loss during the Stage 1 evaporation, similar to the fine sand. Looking at the graphs, the water loss from mixed sand exhibits Stage 1 evaporation for over 35-45 hours after which it enters into the FRP for over 10-15 hours. The evaporation then enters the stage 2 evaporation which is seen as the linear slope after the FRP (curved line). The Stage 2 evaporation slope is significantly lesser than the Stage 1 as the evaporation rate drops mostly due to the smaller capillary forces acting upon water molecules.

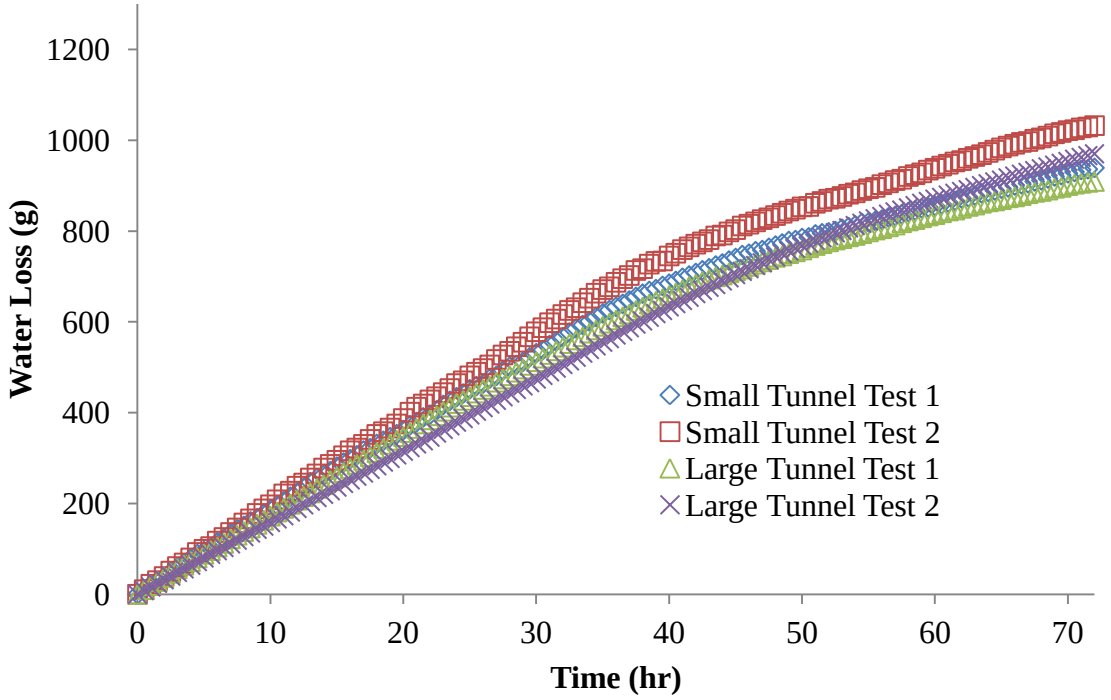

(a)

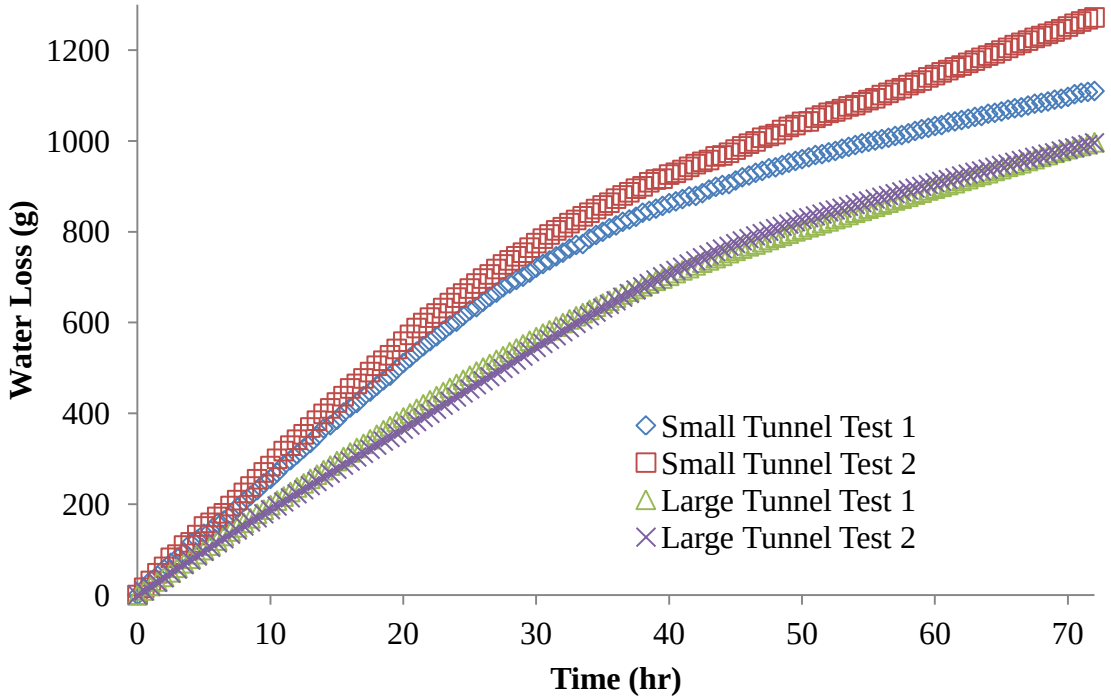
Water Loss (g)
1200
1000
800
600
400
200
0
0
10
20
30
40
50
60
70
Time (hr)
Small Tunnel Test 1
Small Tunnel Test 2
Large Tunnel Test 1
Large Tunnel Test 2

(b)

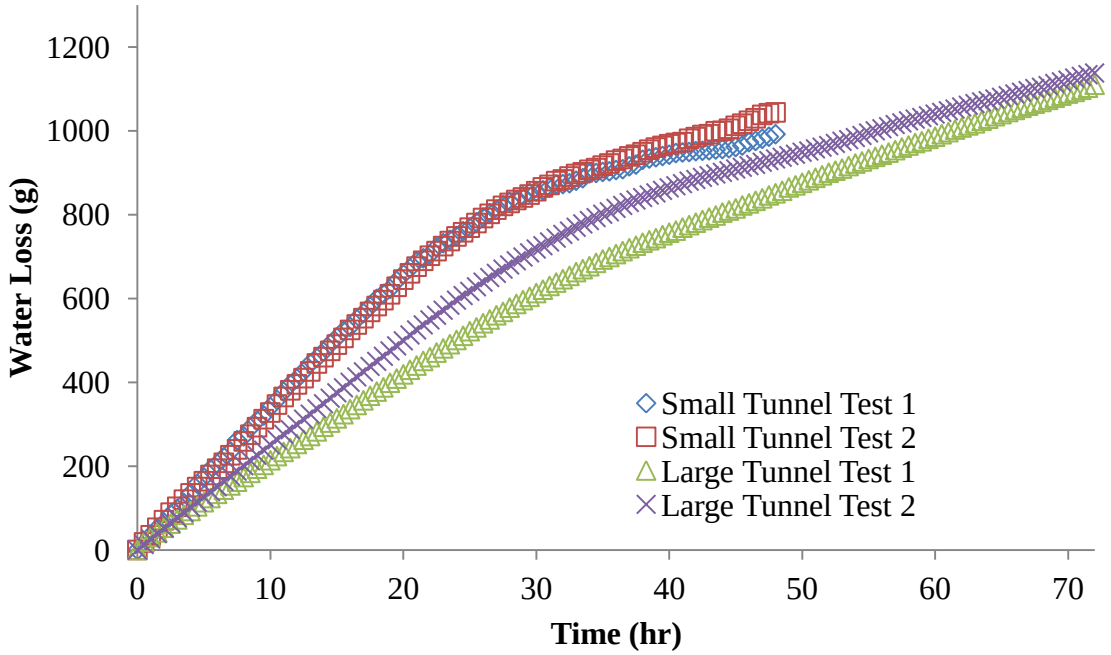
Water Loss (g)
1200
1000
800
600
400
200
0
0
10
20
30
40
50
60
70
Time (hr)
Small Tunnel Test 1
Small Tunnel Test 2
Large Tunnel Test 1
Large Tunnel Test 2

(c)

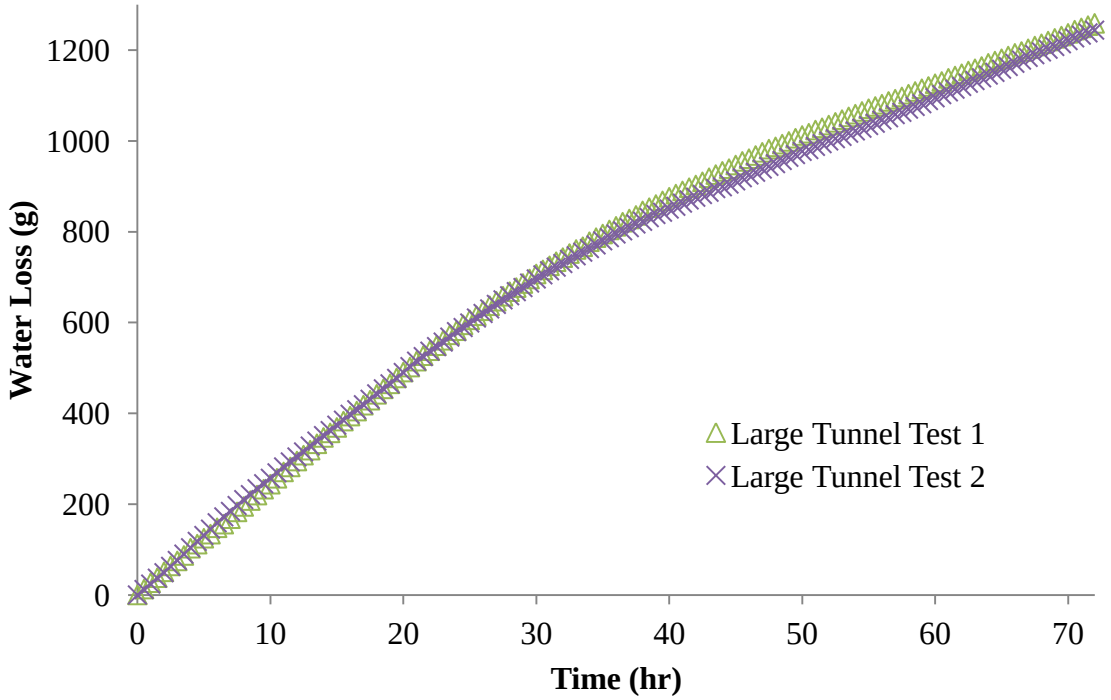

(d)

Figure 4.24 Comparison of water loss from mixed sand in small and the large tunnels with air flow velocities of (a) 2.3 m/s, (b) 2.8 m/s, (c) 3.2 m/s and (d) 3.6 m/s

Table 4.3 Total mass water loss for mixed sand

Velocity, (m/s)	Water Loss, (kg)	
Small Tunnel	Test 1	Test 2
2.3	0.939	1.032
2.8	1.110	1.272
3.2	0.992(48hr)	1.044(48hr)
Large Tunnel	Test 1	Test 2
2.3	0.909	0.970
2.8	0.997	0.996
3.2	1.110	1.138
3.6	1.214	1.224

Table 4.3 shows the water loss over the 72 hour period. Comparing the mass loss of the mixed and the fine sand we can see that both samples lost approximately 1 - 1.2 kg of water over the course of the experiments. It is seen that the soil particle size does affect the capillary action. Due to smaller pores in the sample of the mixed soil compared to coarse sand the water easily reaches the top of the drying front due to the stronger capillary action.

The mass water loss was converted to the experimental evaporation by the use of the **Equation 4.1**. **Figure 4.25** shows the experimental evaporation rates from the mixed sand based on the mass measurements at 30 min interval. From these graphs we can see the difference in evaporation rates in the small and large tunnels during Stage 1 evaporation. The average difference in the evaporation rates for the 2.3 m/s velocity is 4.14 mm/d, for the velocity of 2.8 m/s the difference is 5.61 mm/d and for the velocity of 3.2 m/s the difference is 8.44 mm/d. With slightly more coarse sand in the sample the mixed sand had more water on top of the surface than the fine sand which explains the higher evaporation difference of the tunnel models. The larger pore sizes in the soil sample cause the increased difference of evaporation between the small and the large tunnel. Stage 2 has a low and constant evaporation rates mostly due to the water slowly rising to the secondary drying front. Whereas, the infiltrating low humid air vaporizes the remaining water. From the graph it is seen that the differences in evaporation between the small and the large tunnel are 5.21-8.14 mm/d for 2.3 m/s velocity, 6.51-9.85 mm/d for 2.8 m/s and 4.82-9.81 mm/d for the 3.2 m/s.

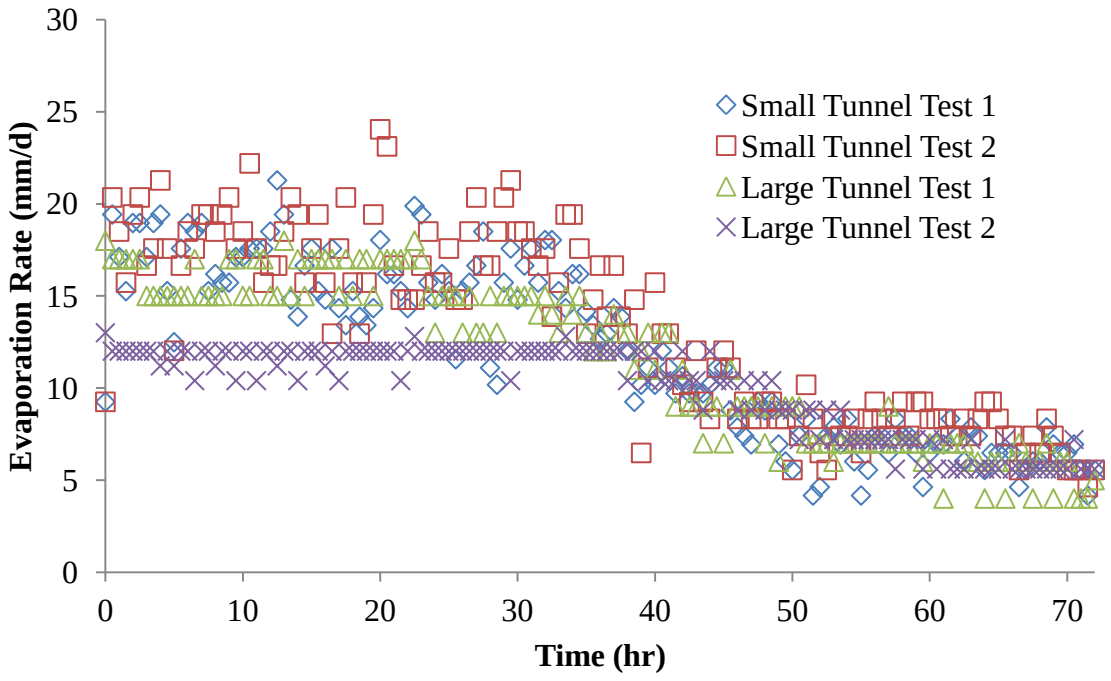
Evaporation Rate (mm/d)
Time (hr)
Small Tunnel Test 1
Small Tunnel Test 2
Large Tunnel Test 1
Large Tunnel Test 2
0
5
10
15
20
25
30
0
10
20
30
40
50
60
70

(a)

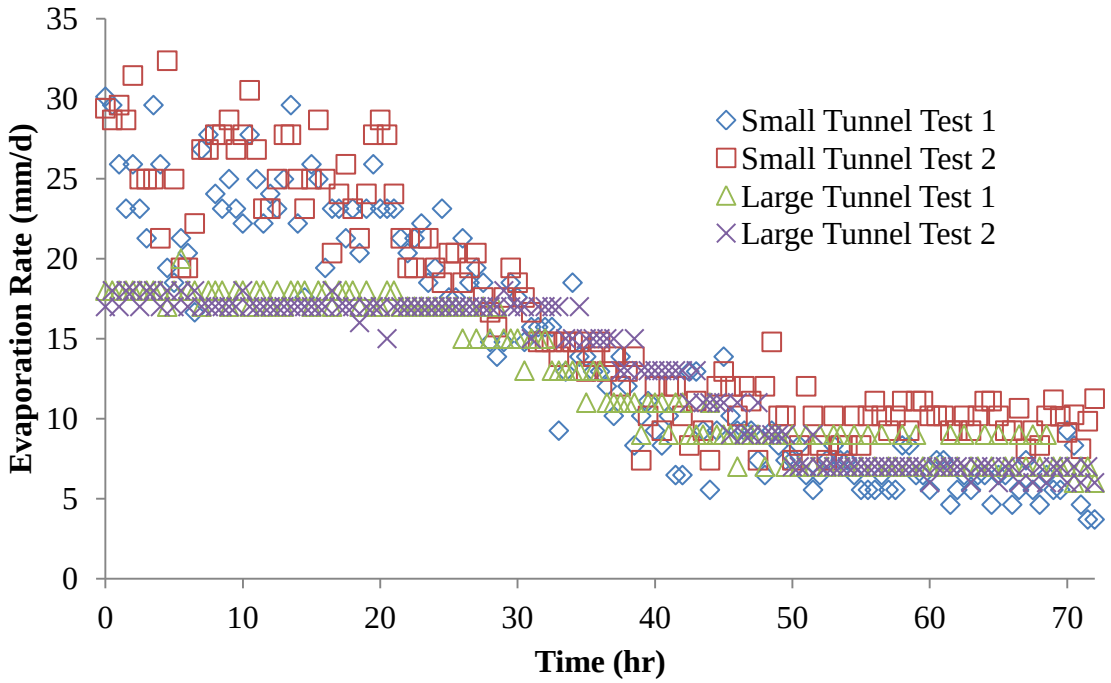
Evaporation Rate (mm/d)
Time (hr)
Small Tunnel Test 1
Small Tunnel Test 2
Large Tunnel Test 1
Large Tunnel Test 2
0
5
10
15
20
25
30
35
0
10
20
30
40
50
60
70

(b)

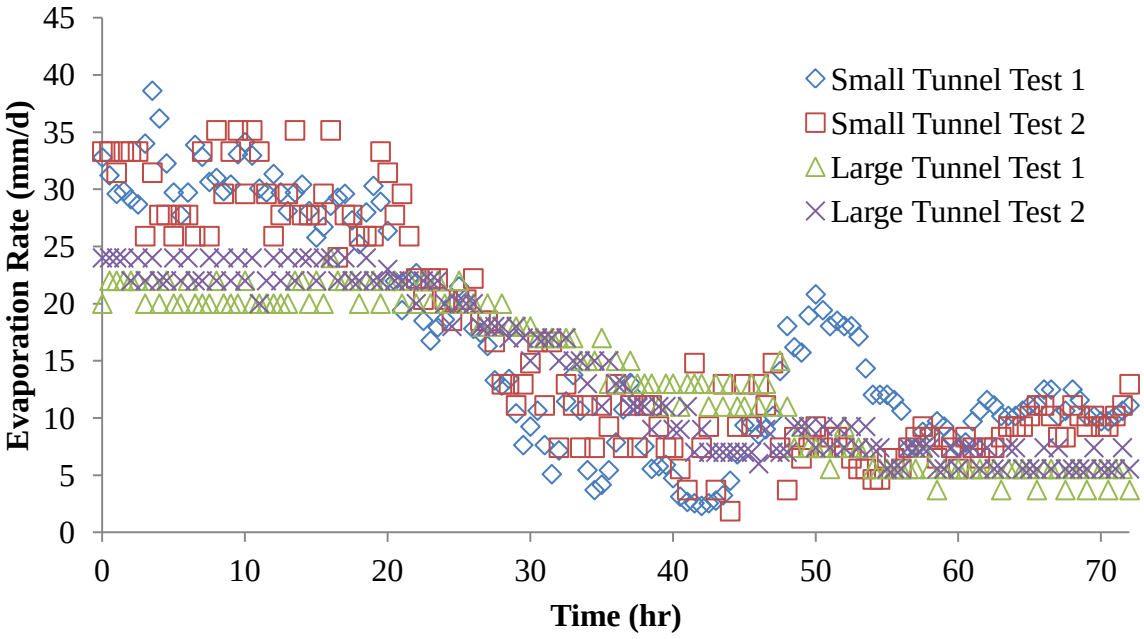

(c)

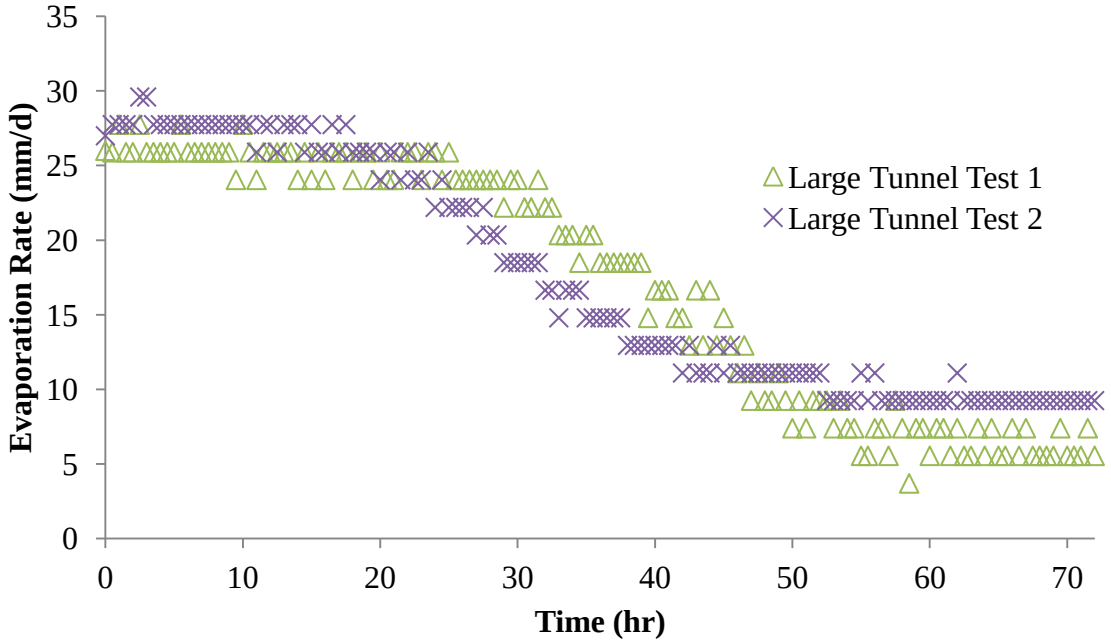

(d)

Figure 4.25 Comparison of experimental evaporation rates from mixed sand in small and the large tunnels with air flow velocities of (a) 2.3 m/s, (b) 2.8 m/s, (c) 3.2 m/s and (d) 3.6 m/s

The investigations of the boundary effects of the two different tunnels have revealed that the thickness of the boundary layer of the same air velocities has an effect on the drying behaviour of the soil. With the thinner boundary layer of the small tunnel the water has a tendency of evaporating at much higher rate than the thicker boundary layer of the large tunnel. As stated previously, the tests have been repeated in order to confirm the validity of the drying pattern in both tunnels.

4.5 Uncertainty Analysis

Uncertainty analysis performed is presented in the procedure following the root sum square method (RSS) based on the work of Figliola and Beasley 2011. The following uncertainties are based on the pressure transducer (P), digital scale (m), relative humidity (RH), ambient temperature (T_a) and thermocouple temperature (T_s). The measured uncertainties are grouped in two different error uncertainties instrument error and data acquisition. Each of the groups has its own source of error. The manufacturers of the instruments used provided plenty of information used to calculate the instrument uncertainty. Some of the information provided was the resolution, accuracy, hysteresis and repeatability. The source of bias is due to zero-order uncertainty u_0 and instrument uncertainty u_a. The design-state uncertainties are summarized in the **Table 4.4**. The design-state uncertainties were obtained by the use of equation below

$$u_d = \sqrt{u_0^2 + u_a^2} \qquad (4.2)$$

Table 4.4 Design-stage uncertainty of the instruments

Measurement	u_0	u_a	u_d
Pressure Transducer (Pa)	0.005	0.023	0.023
Digital Scale (g)	0.015	1.150	1.152
Humidity (%)	0.0015	0.35	0.35
Thermocouple (°C)	0.005	0.81	0.81
Infrared Camera (°C)	0.001	1	1

A simple uncertainty analysis was then performed on the data collected using the formula

$$UN = \pm\sqrt{(Bias)^2 + (t_{95}S_x)^2} \quad (95\%) \qquad (4.3)$$

where the *Bias* is the uncertainty of the instrument, t_{95} is the Student's t variable and σ is the standard deviation of the data from the fit.

4.5.1 Uncertainty Estimation for the Relative Humidity

A humidity probe was used to obtain the relative humidity of the air inside of the tunnel; the mean and the standard deviation of the measurements was calculated. The average of the measurements was computed as:

$$\overline{RH} = \frac{1}{N}\sum_n^N RH \qquad (4.4)$$

Standard deviation was calculated using the standard formula:

$$S_{RH} = \sqrt{\frac{1}{n-1}\sum_n^N (RH - \overline{RH})^2} \qquad (4.5)$$

Uncertainty of the instrument was found by the use of the manufacturers specifications, with the resolution of the instrument 0.003 % and the accuracy of ±0.35 %.

$Bias = \sqrt{(0.0015)^2 + (0.35)^2}$

$Bias = \pm 0.35\ \%$

The total uncertainty (UN) was then found using **Equation 4.3** with the results of the uncertainty measurement summarized in **Table 4.5**.

Table 4.5 Uncertainty measurement of the relative humidity

	Uncertainty Measurement	
Relative Humidity (Coarse Sand)	Large Tunnel	Small Tunnel
2.3 m/s	4.76 %	2.79 %
2.8 m/s	2.83 %	3.48 %
3. 2m/s	3.37 %	2.88 %
Relative Humidity (Fine Sand)	Large Tunnel	Small Tunnel
2.3 m/s	2.31 %	3.20 %
2.8 m/s	2.63 %	3.50 %
3. 2m/s	2.67 %	4.81 %
Relative Humidity (Mixed Sand)	Large Tunnel	Small Tunnel
2.3 m/s	3.81 %	2.62 %
2.8 m/s	2.67 %	1.88 %
3. 2 m/s	2.46 %	3.34 %

4.5.2 Uncertainty Estimation for the Thermocouple Temperature Measurements

Thermocouple uncertainty was found for the temperature measurements taken inside the tunnels. The uncertainty was found by the use of the mean of the temperatures and standard deviation of data from the fit. The mean of the temperatures was found using the equation below.

$$\overline{T} = \frac{1}{N}\sum_{n}^{N} T \qquad (4.6)$$

Standard deviation was calculated using the standard formula:

$$S_T = \sqrt{\frac{1}{n-1}\sum_{n}^{N}(T-\overline{T})^2} \qquad (4.7)$$

The instrument bias was found by the use of the **Equation 4.2** with the data provided by the manufacturer of the thermocouple data acquisition device. The data provided included the resolution and the accuracy of the device, with the resolution of 0.01°C and accuracy of ±0.81°C.

$$Bias = \pm\sqrt{(0.005)^2 + (0.81)^2}$$

$$Bias = \pm 0.81\ ^{\circ}C$$

The total uncertainty of the measurements was then analyzed by the use of **Equation 4.3** with the results summarized in **Table 4.6**.

Table 4.6 Uncertainty measurement of the thermocouple temperature

	Uncertainty Measurement	
Temperature (Coarse Sand)	Large Tunnel	Small Tunnel
2.3 m/s	1.42 °C	1.53 °C
2.8 m/s	1.31 °C	1.28 °C
3. 2m/s	1.49 °C	1.32 °C
Temperature (Fine Sand)	Large Tunnel	Small Tunnel
2.3 m/s	1.18 °C	1.22 °C
2.8 m/s	1.15 °C	1.32 °C
3. 2m/s	1.18 °C	1.53 °C
Temperature (Mixed Sand)	Large Tunnel	Small Tunnel
2.3 m/s	1.17 °C	1.18 °C
2.8 m/s	1.17 °C	1.19 °C
3. 2 m/s	1.15 °C	1.16 °C

4.5.3 Uncertainty Estimation for the Wind Velocity

Uncertainty of the air flow velocity was found using the procedure described by the (Figliola and Beasley 2011).The pressure transducer was connected to the voltmeter which had a resolution of 10 μV and accuracy of 1.5 %. The transducer data based on the manufacturer's specifications gives the range of 0 - 125 Pa, sensitivity of 1.5 V/Pa, input voltage of 10 VDC ±1%, output of ±5 V, linearity of 2.5 mV/Pa, repeatability if 3 mV/Pa and resolution of 0.01 Pa. The uncertainty was found for the pressure of 4 Pa. The uncertainty of the voltmeter is expressed as:

$U_0 = 5\ \mu V$

$Bias_{cv} = 6V\ x\ 0.00002 = 120\ \mu V$

Pressure transducer uncertainty is expressed as:

$U_0 = 0.005\ Pa$

$$Bias_{ct} = \pm\sqrt{(\frac{2.5mV}{Pa}x\ 4Pa)^2 + (\frac{3mV}{Pa}x\ 4Pa)} = \pm 15.62\ mV$$

Total instrument uncertainty is expressed as:

$$Bias = \pm\sqrt{(15.62mV)^2 + (0.12mV)^2} = \pm 15.62mV \sim \pm\ 0.02343\ Pa$$

The analysis was performed for the entire velocity profile curves with the results summarized in the **Table 4.7**.

Table 4.7 Uncertainty measurement of the wind velocity

	Uncertainty Measurement	
Wind Velocity	Large Tunnel	Small Tunnel
2.3 m/s	0.057 Pa	0.073 Pa
2.8 m/s	0.092 Pa	0.112 Pa
3.2 m/s	0.142 Pa	0.139 Pa
3.6 m/s	0.168 Pa	0.145 Pa

4.5.4 Uncertainty Estimation for the Water Loss Analysis

Water loss uncertainty was established based on the digital scale uncertainty found from the calibration. The uncertainty of the digital scale was found based on the eccentricity, accuracy and resolution. Accuracy of ±1.5 g and resolution of 0.03 g was found from the manufacturer's manual where the rest of the uncertainties had to be established manually. Eccentricity uncertainty was found manually by placing a calibration mass around the perimeter of the scale and recording the displayed mass.

The total uncertainty was found by using the standard uncertainty equation:

$$Bias = \pm\sqrt{(0.015)^2 + (1.5)^2}$$

$$Bias = \pm 1.52\ g$$

The uncertainties of all of the measurements are summarized in **Table 4.8**.

Table 4.8 Uncertainty measurement of the water loss

	Uncertainty Measurement	
Mass Loss (Coarse Sand)	Large Tunnel	Small Tunnel
2.3 m/s	4.99 g	5.34 g
2.8 m/s	4.26 g	3.78 g
3. 2m/s	5.46 g	2.32 g
Mass Loss (Fine Sand)	Large Tunnel	Small Tunnel
2.3 m/s	5.82 g	5.04 g
2.8 m/s	2.26 g	4.29 g
3. 2m/s	6.01 g	6.89 g
Mass Loss (Mixed Sand)	Large Tunnel	Small Tunnel
2.3 m/s	4.76 g	3.35 g
2.8 m/s	2.71 g	4.54 g
3. 2m/s	7.71 g	4.42 g

4.5.5 Uncertainty Estimation for the Infrared Camera

The information for the uncertainty analysis was provided by the manufacturer of the infrared camera. The information provided the resolution and the accuracy of the camera with 0.02 °C resolution and ±1 °C for the accuracy. The bias of the instrument accuracy was calculated.

$$Bias = \pm\sqrt{(0.01)^2 + (1)^2}$$

$$Bias = \pm 1\ ^{o}C$$

Table 4.9 Uncertainty measurement of the infrared temperature

	Uncertainty Measurement	
Coarse Sand	Large Tunnel	Small Tunnel
2.3 m/s	1.173 °C	1.302 °C
2.8 m/s	1.037 °C	1.994 °C
3.2 m/s	1.260 °C	1.042 °C
3.6 m/s	1.912 °C	-
Mixed Sand	Large Tunnel	Small Tunnel
2.3 m/s	1.834 °C	1.849 °C
2.8 m/s	1.856 °C	1.867 °C
3.2 m/s	1.823 °C	1.822 °C
3.6 m/s	1.870 °C	-
Fine Sand	Large Tunnel	Small Tunnel
2.3 m/s	1.865 °C	1.913 °C
2.8 m/s	1.824 °C	1.046 °C
3.2 m/s	1.861 °C	1.294 °C
3.6 m/s	1.954 °C	-

CHAPTER 5

ANALYSIS

5.1 General

This section covers the modelling of the Stage 1 and Stage 2 evaporation. Modelling was done based on the ambient conditions recorded during the experimentation. The results from the model are then compared to the experimental data.

5.2 Stage 1 and Stage 2 evaporation

When considering drying of a fully saturated porous medium, the evaporation is categorized into two stages. During the initial evaporation of a fully saturated soil sample, the soil exhibits a constant evaporation. At this stage the surface water is removed from the porous medium and is referred to as Stage 1 (Shahraeeni et al., 2012); it can be estimated by the simple equation:

$$e_{s1} = \frac{(Pv_s - Pv_a)}{r_{s1}} \qquad (5.1)$$

where, e_{s1} is the evaporation during stage 1, Pv_s is the saturated vapour pressure, Pv_a is the air vapour pressure. With the r_{s1} being a combination of the surface resistance and boundary layer thickness defined from the **Equation 2.12** which is dependent on the velocity of the moving air. At the end of stage 1, the evaporation enters into a transition stage, where the rate of drying slows down non-linearly as the rate of evaporation reaches stage 2. At this stage the evaporating front recedes deep into the soil (also called secondary drying front) (Shokri et al., 2011). Stage 2 evaporation rate is described as

$$e_{s2} = \frac{(Pv_s - Pv_a)}{r_{s2}} \qquad (5.2)$$

where, e_{s2} is the evaporation rate of stage 2 evaporation and r_{s2} is the resistance of the combination of the stage 1 and viscous resistance. At stage 2 the evaporation rate is significantly reduced in comparison to the stage 1 evaporation. With water evaporating from the second drying front the drying process depends minimally on the atmospheric conditions (Davarzani et al., 2014), such as wind or temperature. The evaporation predominantly focuses on the

characteristics of the porous medium (porosity, angularity and size). One of the main similarities that stage 1 and stage 2 exhibits is the constant evaporation aside from the falling rate period. **Figure 5.1** shows the different stages of evaporation rate over the 72 hour period of a fully saturated sample of mixed sand subject to 2.8 m/s from preliminary data of the experiment in the small tunnel. For this particular velocity the stage 1 evaporation occurs at 20.4-20.6 hour period after the end of stage 1 (20.5 hr) the evaporation enters the falling rate period for approximately 20 hour period after which stage 2 occurs.

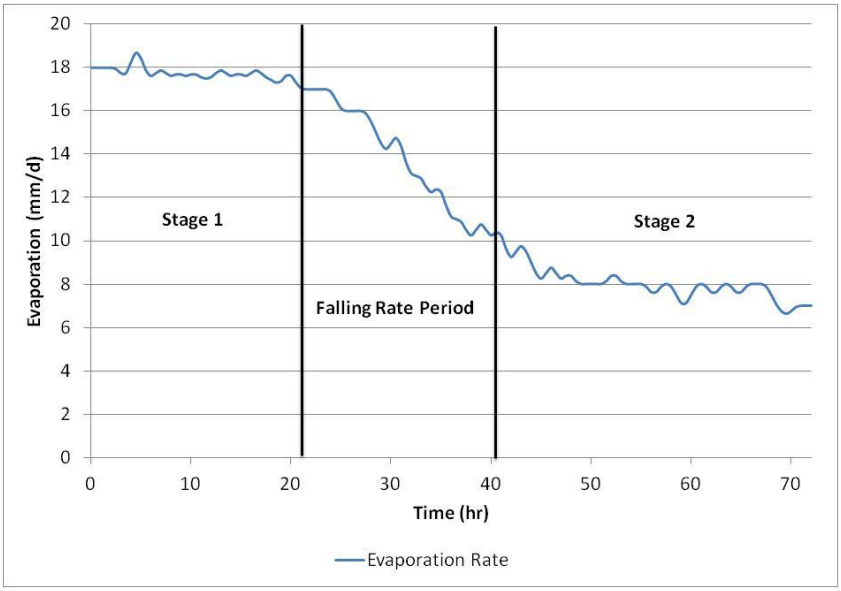

Figure 5.1 Schematic of evaporation rate over 72 hours

One of the most influencing parameters for evaporation is the saturation of the porous media and the humidity of the air. The saturation and humidity govern the evaporation rate in the initial stages of the drying process, especially in the case of soil strata when the groundwater is located close to the surface of the porous media. When the water is located close to the surface dry or less humid air is more likely to increase the rate of evaporation as it picks up more water particles when the air passes over the moist surface. As discussed previously the highest evaporation rate occurs at the beginning of evaporation from a fully saturated porous medium. The vast amount of moisture on top of the surface allows the mass transfer to occur swiftly. This is mainly due to the difference between the vapour pressure between the top of the soil surface and the ambient air (Smits et al., 2011).

5.3 Characteristic Lengths and Determination of Stage 1 Length

Constant rate of evaporation or stage 1 evaporation is subject to a force balance among gravitational, capillary and viscous forces. Capillary forces induce the liquid from the bottom of the porous medium to flow towards the surface of the drying front. This takes place due to the pressure difference between the significantly larger pores at the drying surface and the finer pores below the drying front. As the water evaporates from the surface of the soil sample the drying front recedes deeper into the porous medium. Over a certain period of time the rate of evaporation drops significantly. With the receding evaporation front and low evaporation rates it is assumed that the capillary and the gravitational forces are in equilibrium. This force balance is also defined as gravitational characteristic length (Lehmann et al., 2008) L_G which is found by the equation:

$$L_G = \frac{\sigma}{\rho g r_2}\left(\frac{2}{\gamma} - 2\right) \quad (5.3)$$

where, ρ is the density of water (kg/m3), σ surface tension (N/m) and r_2 large pore size (mm). The gravitational characteristic length describes the maximum capillary head at which the force of capillary flow is almost nonexistent. Another variable that slows down the evaporation is the viscous dissipation which is expressed as viscous characteristic length L_V. Viscous characteristic length is given by equation:

$$L_V = \frac{\sigma\kappa}{\eta e_p r_2}\left(\frac{2}{\gamma} - 2\right) \quad (5.4)$$

where, κ is the permeability of the porous medium, η is dynamic viscosity (Pa-s) and e_p is the potential evaporation (mm/d). Combining both, the gravitational and viscous length, the characteristic length (L_C) can be found (Lehmann et al., 2008). Characteristic length marks the end of stage 1 and the beginning of the falling rate period and it is expressed as:

$$L_C = \frac{L_G}{\frac{L_G}{L_V}+1} \quad (5.5)$$

Given the length L_C, we can easily find the length of time in days for the stage 1 of evaporation (τ). Equation for calculating τ is given as (Neriah et al., 2014)

$$\tau = \frac{L_C(\theta_s - \theta_r)}{e_{s1}} \quad (5.6)$$

where, θ_s is the saturated water content, θ_r is the residual water content and e_{s1} is the stage 1 evaporation.

5.4 Evaporation Model Based on Experimental Results

This section shows the evaporation model based on the ambient and soil conditions taken through the experiment. The evaporation model covers the evaporation rates of the Stage 1 and the duration of the Stage 1 evaporation. The model also shows the evaporation Stage 2 and its starting point.

5.4.1 Coarse Sand Evaporation Model

The evaporation rates were estimated using **Equations 5.4** and **5.5** corresponding to the experimental conditions such as: ambient temperature, humidity and air flow velocity. As discussed earlier, the equations for predicting evaporation rates are available only for Stage 1 and Stage 2. **Figures 5.2** and **5.3** show the results of the Stage 1 and Stage 2 evaporation based on the ambient conditions of the coarse sand material in the small and large tunnels, respectively.

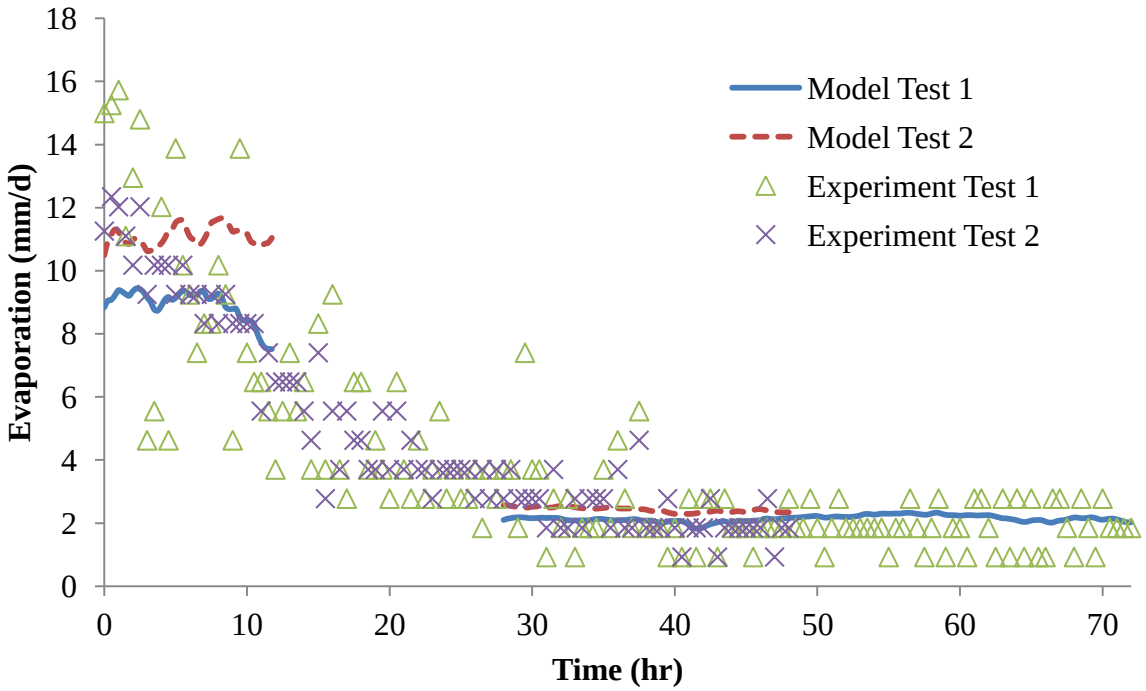

(a)

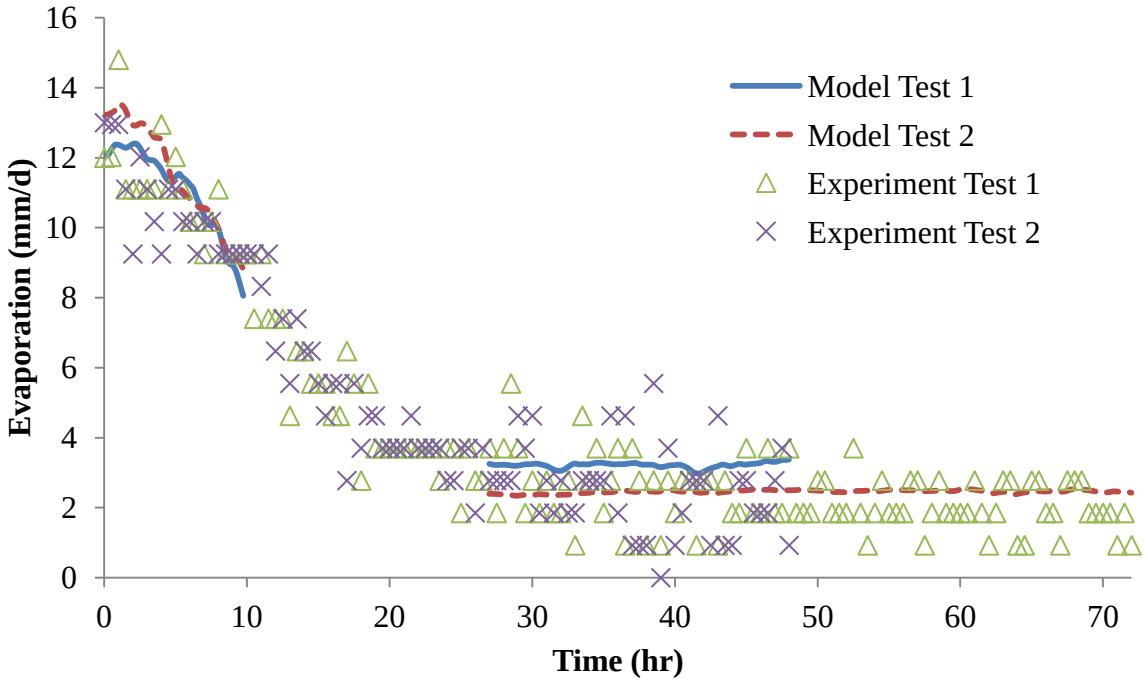

(b)

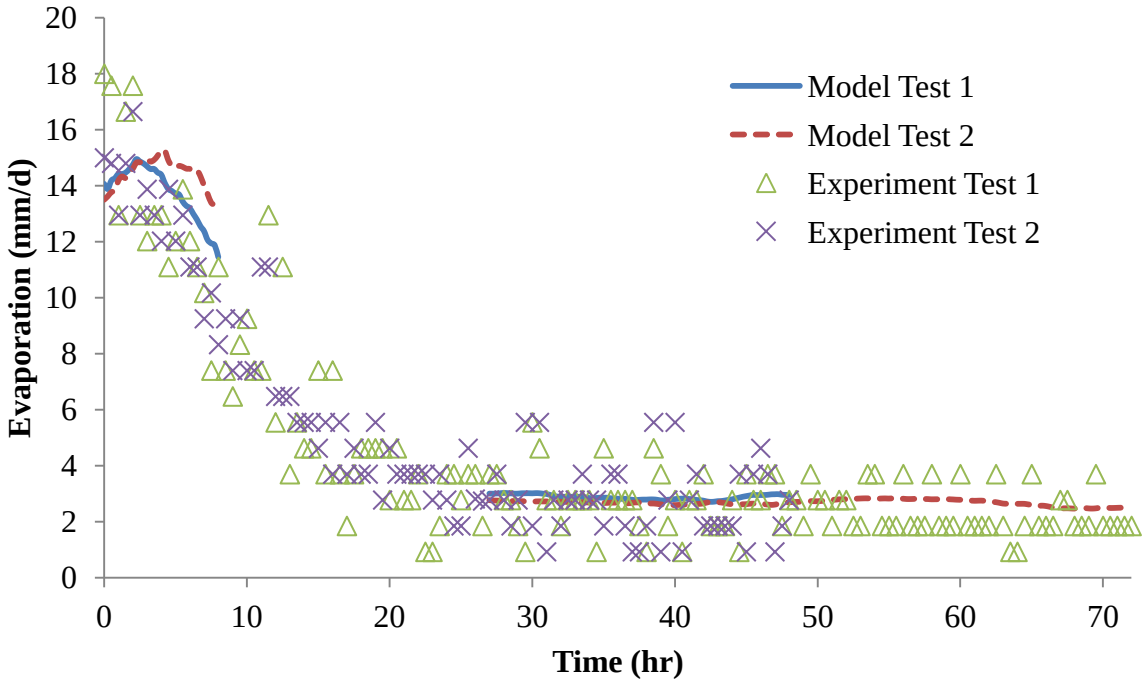

(c)

Figure 5.2 Comparison of the evaporation model results and experimental data of coarse sand for small tunnel with air flow velocity of (a) 2.3 m/s, (b) 2.8 m/s, (c) 3.2 m/s

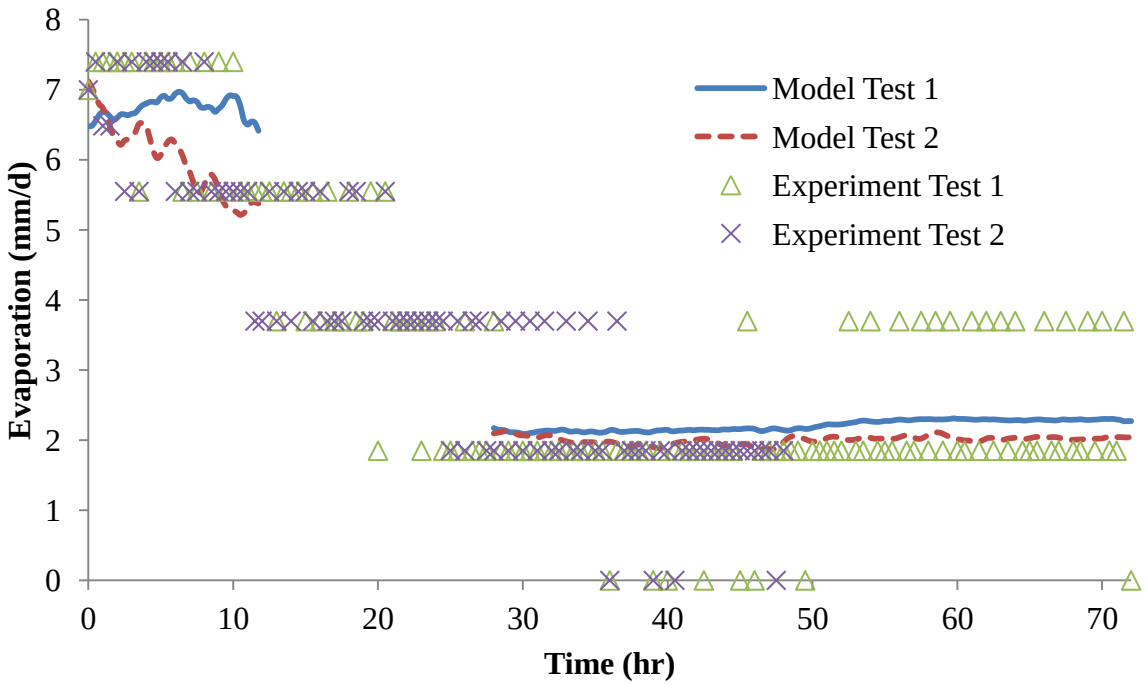
Evaporation (mm/d)
Time (hr)
Model Test 1
Model Test 2
Experiment Test 1
Experiment Test 2
0
1
2
3
4
5
6
7
8
0
10
20
30
40
50
60
70

(a)

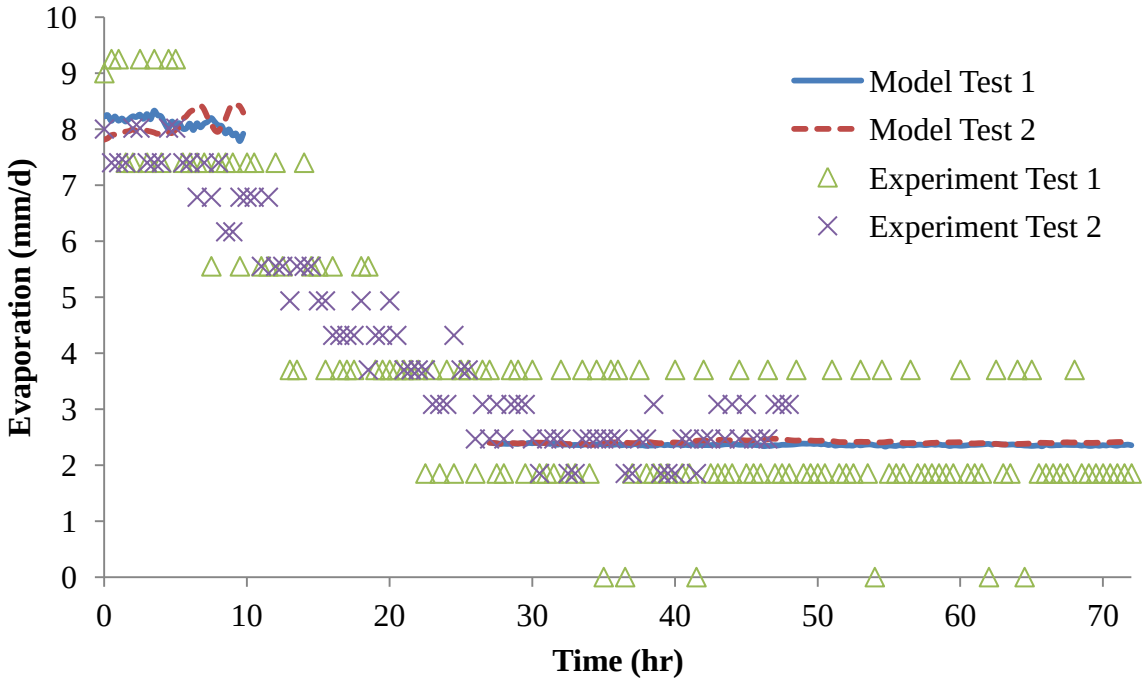
Evaporation (mm/d)
Time (hr)
Model Test 1
Model Test 2
Experiment Test 1
Experiment Test 2
0
1
2
3
4
5
6
7
8
9
10
0
10
20
30
40
50
60
70

(b)

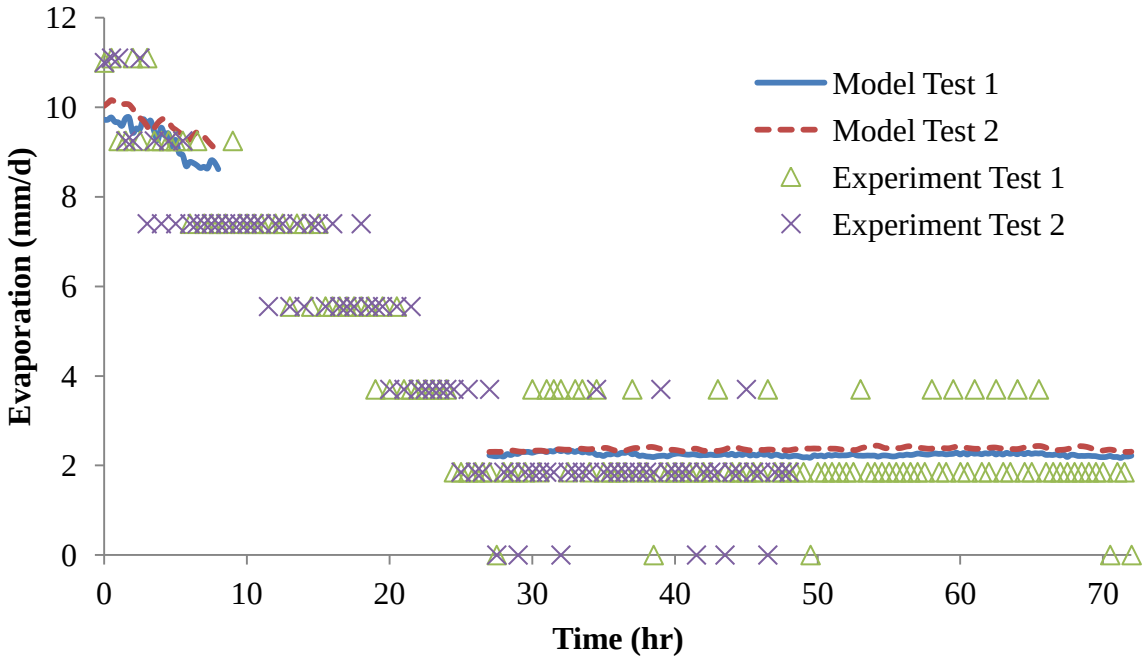

(c)

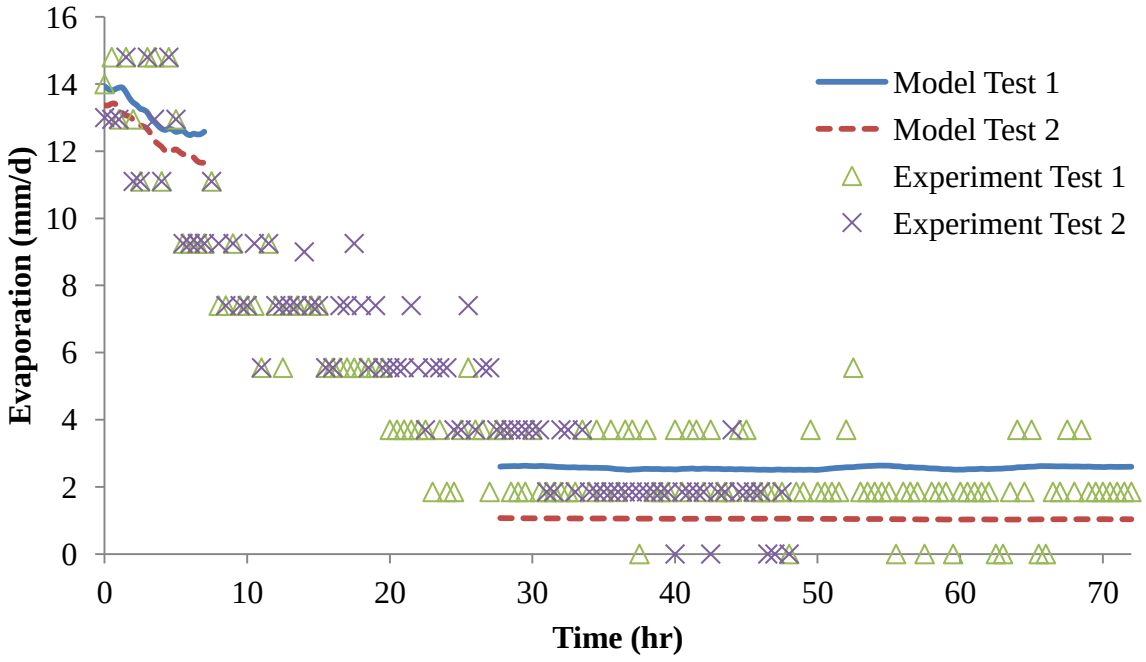

(d)

Figure 5.3 Comparison of the evaporation model results and experimental data of coarse sand for large tunnel with air flow velocity of (a) 2.3 m/s, (b) 2.8 m/s, (c) 3.2 m/s and (d) 3.6 m/s

From these figures we find that the analytical models for predicting the stage 1 and stage 2 evaporation are able to reproduce the evaporation rates similar to the experimental evaporation rates. We see that the evaporation in the small tunnel is also higher than the large tunnels as previously indicated by the water loss due to evaporation. The factor that affects the evaporation in the model aside from the environmental conditions is the boundary layer thickness. With the thinner boundary layer in the **Equation 5.4** the rate of evaporation that will be produced is going to be increased unlike the large tunnel where the boundary layer is almost twice as thick the evaporation rate will be much lower. From the graphs it is seen that the duration of Stage 1 evaporation is relatively short for both large and the small tunnels. The duration of Stage 1 evaporation was found by obtaining characteristic length L_c, the characteristic length for coarse sand was found to be 29.4 mm. The duration of Stage 1 was found by using the **Equation 5.6** where the coarse sand exposed to wind velocity of 2.3 m/s was found to be 11.9 hr, coarse sand with wind velocity of 2.8 m/s was 9.8 hr and with wind velocity of 3.2 m/s was 8.0 hr. At the end of Stage 1 the evaporation goes though the falling rate period of evaporation, the mass loss goes through a non linear transition where the evaporation begins to slow down. After the falling rate period the evaporation enters Stage 2 evaporation where it exhibits a linear pattern of water loss. In Stage 2 the evaporation rates are significantly lower than the Stage 1 rates. From **Figure 5.2** and **5.3** it is seen that the water loss does indeed slow down at the beginning of Stage 2. When Stage 2 is reached the evaporation becomes almost linear as seen in the figures; this is mostly due to the second drying front retreating deep into the sample at which point the vaporisation of water is significantly lower. The average Stage 2 evaporation for the coarse sand is 2.2 mm/d for 2.3 m/s, 2.9 mm/d for 2.8 m/s, 2.4 mm/d for 3.2 m/s and 1.9 mm/d for 3.6 m/s

5.4.2 Fine Sand Evaporation Model

An evaporation model was also used to estimate the evaporation from the fine sand using **Equations 5.4** and **5.5**. The evaporation model results are shown in **Figure 5.4** and **5.5** they represent the 72 hour experiment of the Stage 1 and Stage 2 evaporation of the fine sand. We can see from these figures that the Stage 1 evaporation rates in fine sand are higher than the coarse sand in most of the cases. Also it is significantly longer than the Stage 1 in the coarse sand.

Another factor that differs from the small and the large tunnel is the Stage 1 duration due to the high evaporation rate. The length of Stage 1 is much shorter, this means that the sample in the small tunnels reaches the falling rate period much quicker than the large tunnel. After the transition period both tunnels reach the Stage 2 evaporation where the evaporation is the same in all of the cases.

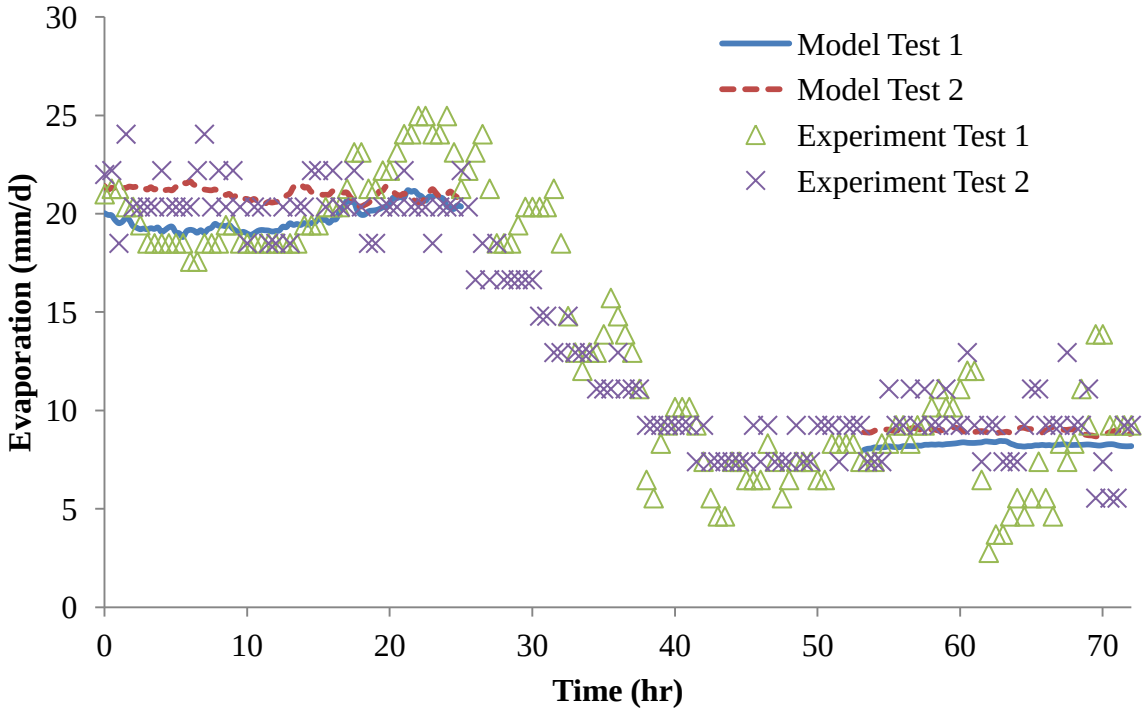

(a)

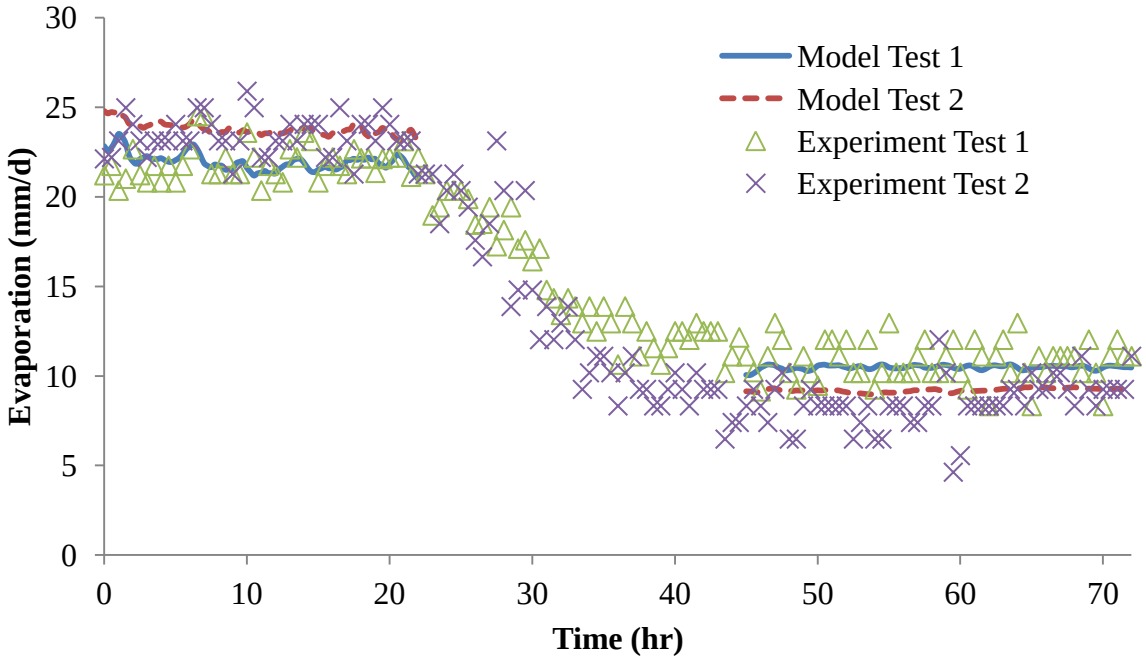

(b)

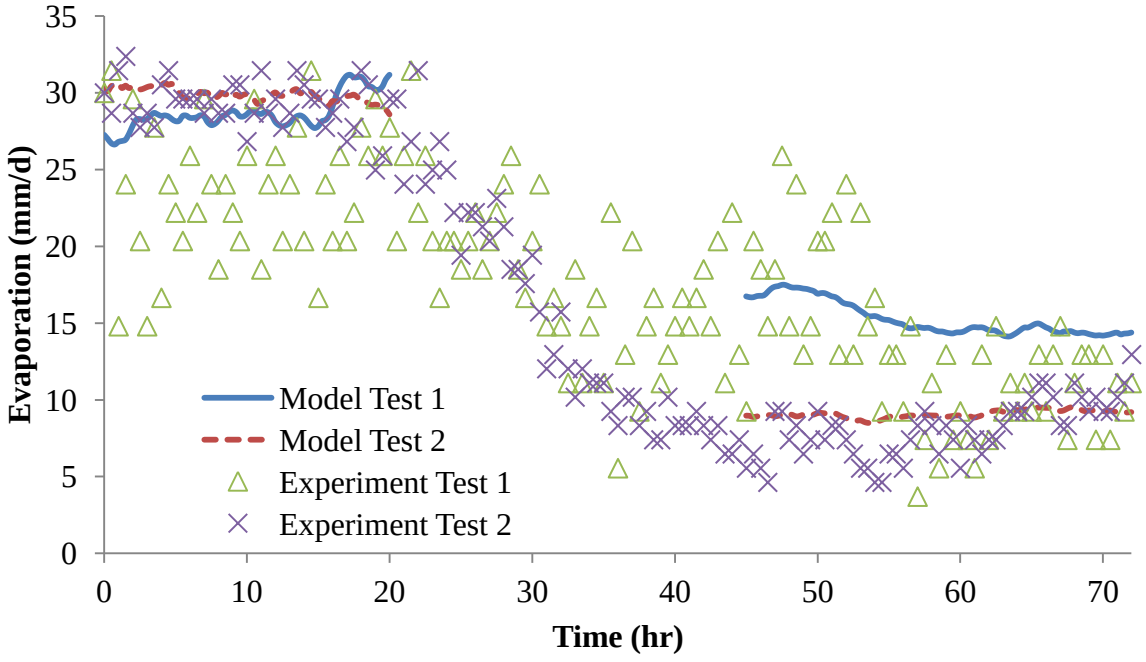

(c)

Figure 5.4 Comparison of the evaporation model results and experimental data of fine sand for small tunnel with air flow velocity of (a) 2.3 m/s, (b) 2.8 m/s, (c) 3.2 m/s

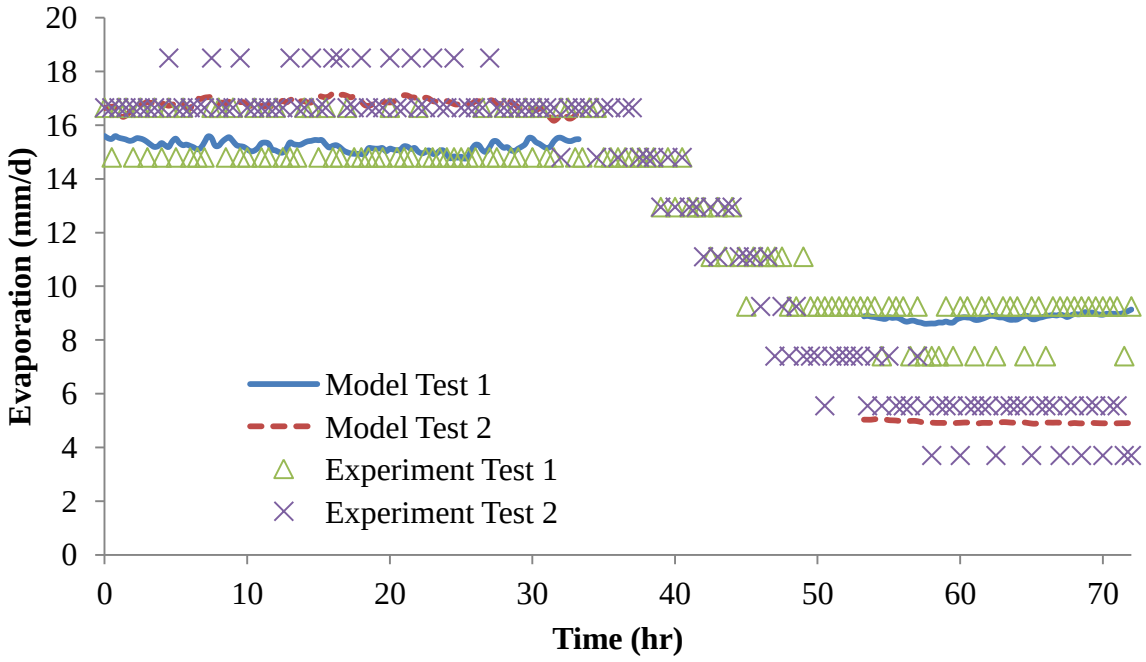
Evaporation (mm/d)
Time (hr)
Model Test 1
Model Test 2
Experiment Test 1
Experiment Test 2

(a)

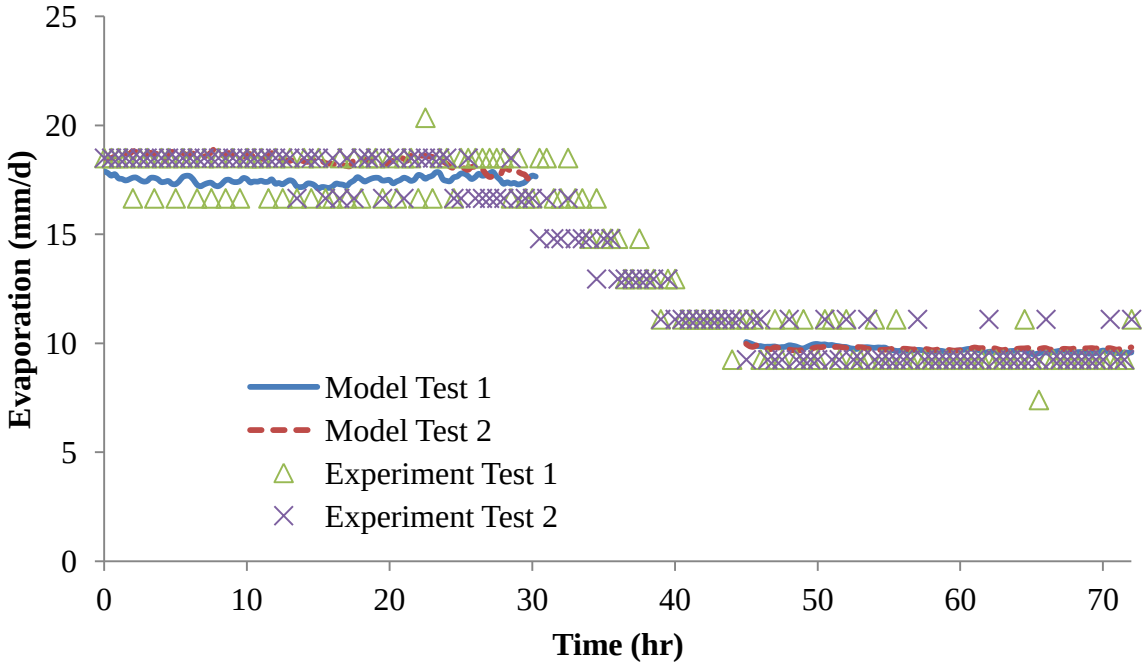
Evaporation (mm/d)
Time (hr)
Model Test 1
Model Test 2
Experiment Test 1
Experiment Test 2

(b)

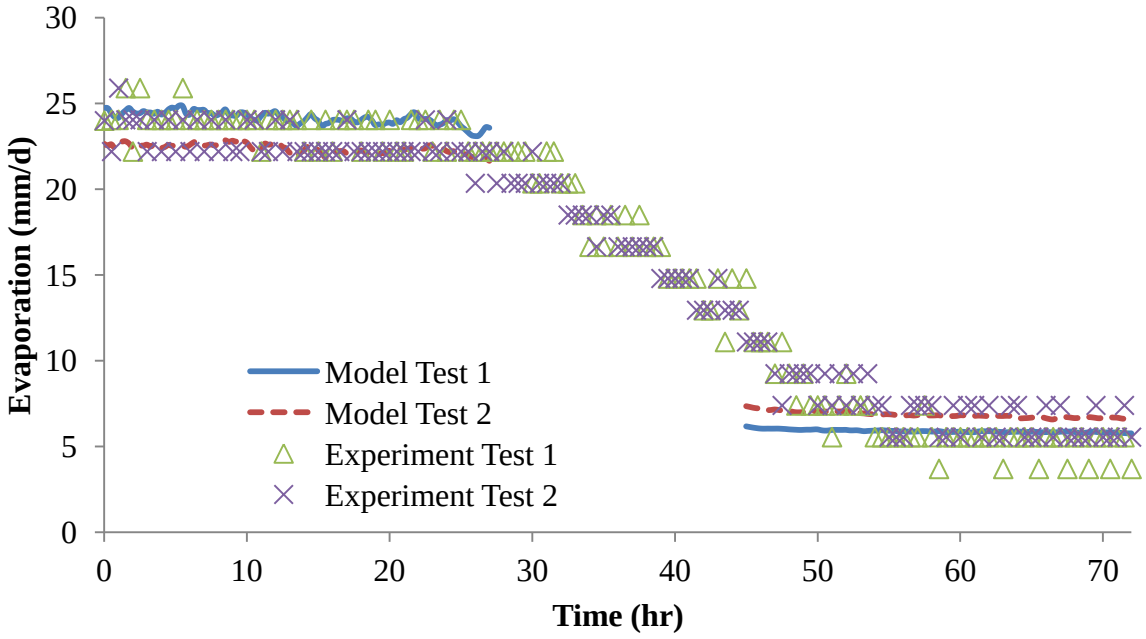

(c)

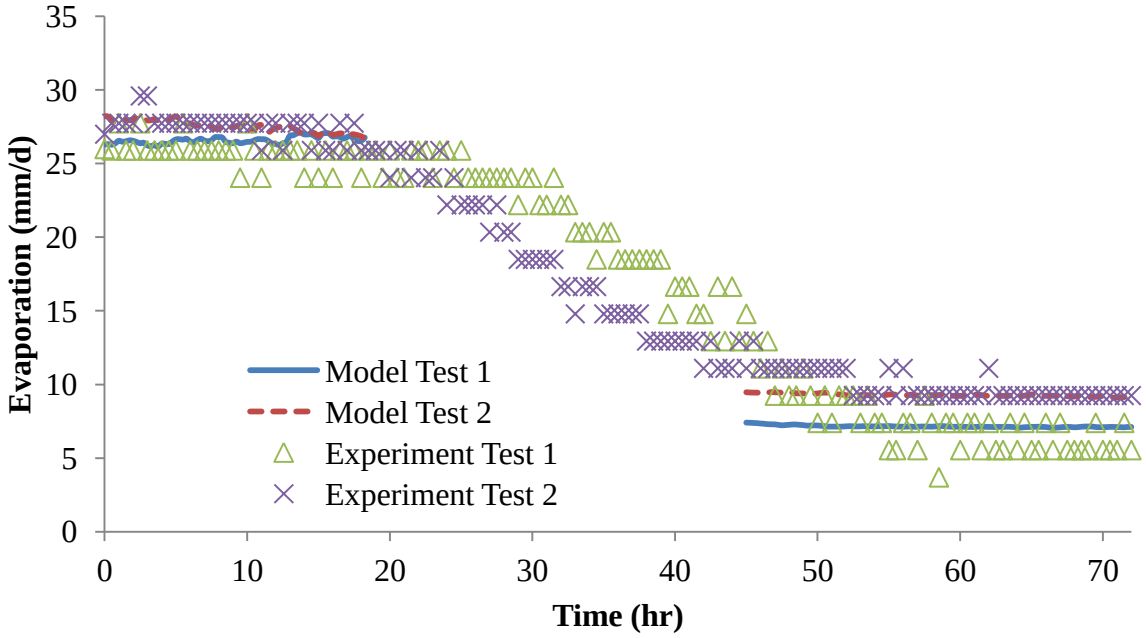

(d)

Figure 5.5 Comparison of the evaporation model results and experimental data of fine sand for large tunnel with air flow velocity of (a) 2.3 m/s, (b) 2.8 m/s, (c) 3.2 m/s and (d) 3.6 m/s

With capillary action limiting the evaporation rate during stage 2 the maximum evaporation rates recorded are 8.23, 8.57 and 9.21 mm/d for the corresponding velocities of 2.3, 2.8 and 3.2 m/s. The duration length of Stage 1 evaporation was found using the L_c, characteristic length calculation where it was found to be 247.3 mm. With the L_c length of 24.73 cm the duration was found to be 35.4, 30.2 and 27.7 hours for the velocities of 2.3, 2.8 and 3.2 m/s for the large tunnel. The duration of the Stage 1 evaporation is 25.3 hr, 22.4 hr and 20.1 hr for 2.3 m/s, 2.8 m /s and 3.2 m/s velocities for the small tunnel. With this information it is known approximately how much time it will take for Stage 1 evaporation to reach the transition stage which is significantly longer comparing to the coarse sand. Since the coarse sand has much larger pore sizes Stage 1 ends much sooner than the fine sand and enters the falling rate period. During Stage 2 evaporation the fine sand reaches almost linear state looking at **Figure 5.4** and **5.5** we can see that the average Stage 2 evaporation is approximately 8.77, 9.27, 9.31 and 9.45 mm/d for the velocities of 2.3, 2.8, 3.2 and 3.6 m/s.

5.4.3 Mixed Sand Evaporation Model

The results of the evaporation model developed using **Equations 5.4** and **5.5** are shown in **Figure 5.6** and **5.7** for the mixed sand. Form the figures it is seen that the evaporation rates during the Stage 1 evaporation for all of the cases are lower in the large tunnel than those in the small tunnel. Another factor to consider is the duration of the Stage 1 evaporation which is longer than the coarse sand but shorter than the fine sand. The duration of the Stage 1 evaporation mainly depends on the amount of the coarse particles in the sample where the water evaporates faster but decreases the duration of the Stage 1 evaporation. Mostly due to the amount of the surface water in the soil and the capillary action present.

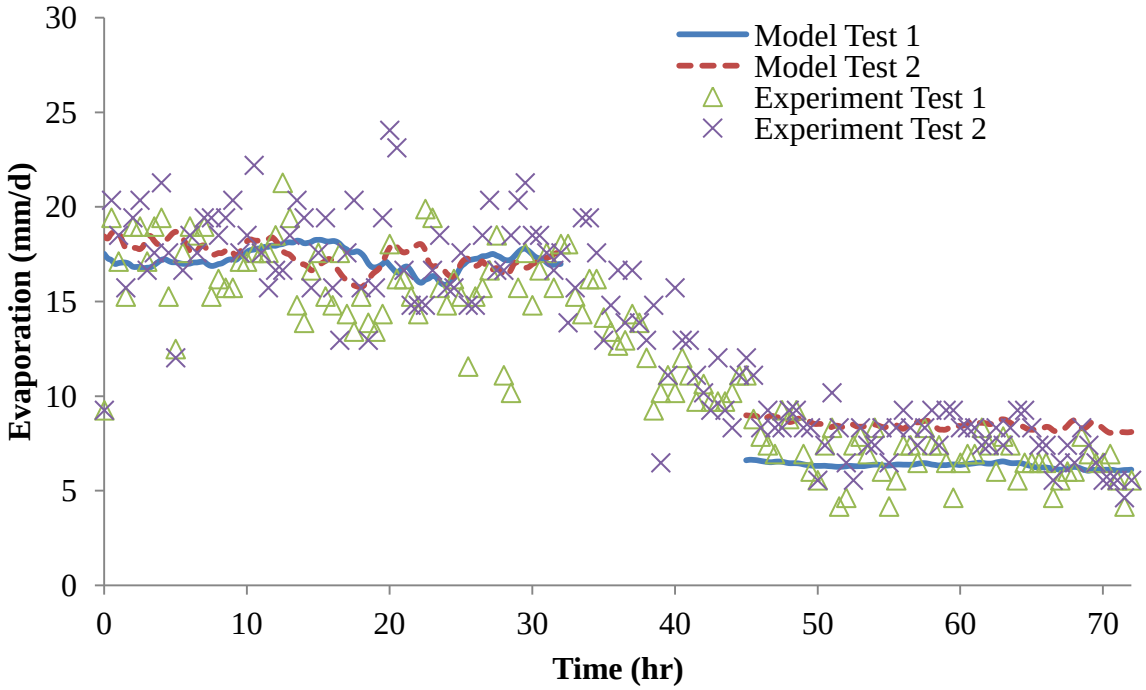
Model Test 1
Model Test 2
Experiment Test 1
Experiment Test 2
Evaporation (mm/d)
Time (hr)
0
5
10
15
20
25
30
0
10
20
30
40
50
60
70

(a)

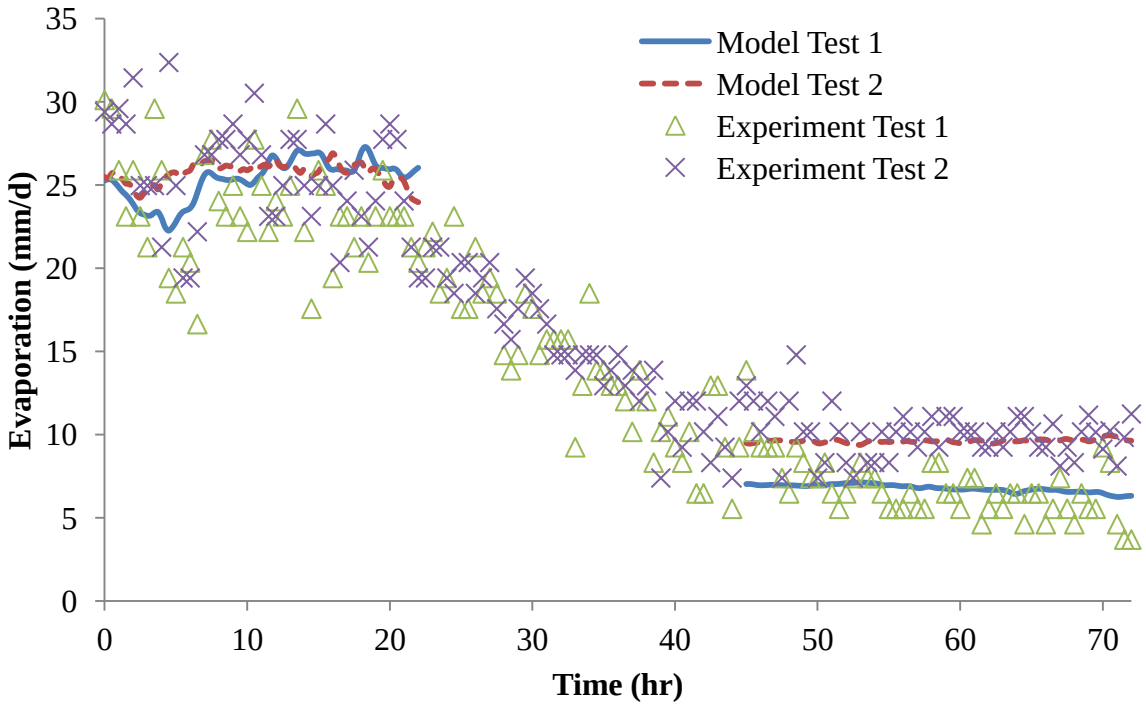
Model Test 1
Model Test 2
Experiment Test 1
Experiment Test 2
Evaporation (mm/d)
Time (hr)
0
5
10
15
20
25
30
35
0
10
20
30
40
50
60
70

(b)

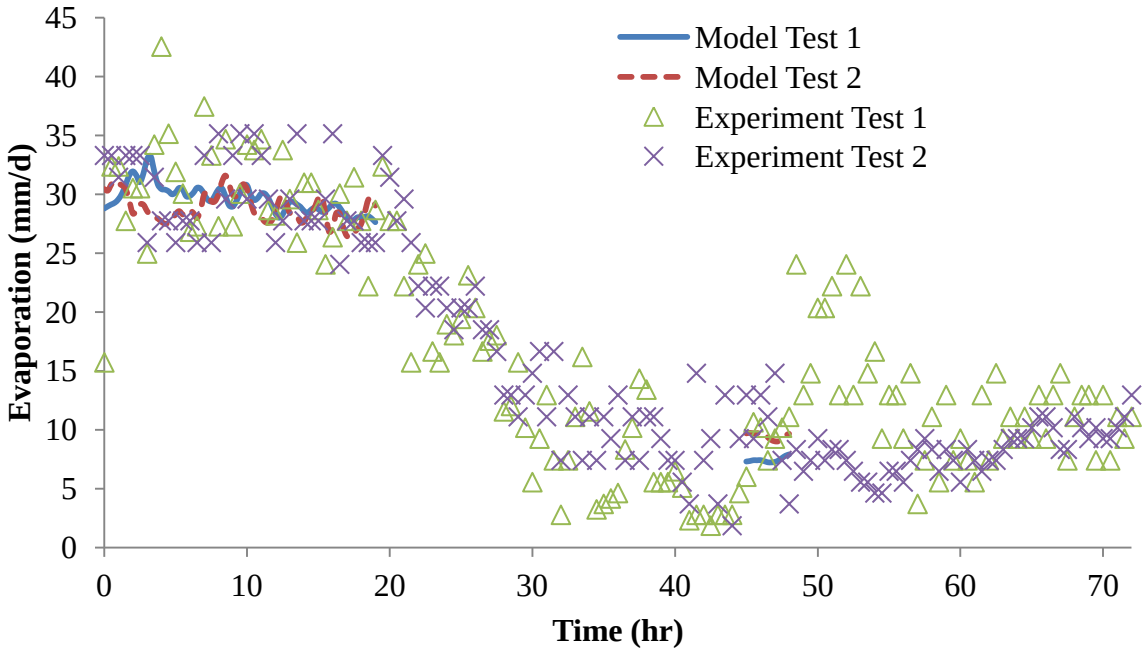

(c)

Figure 5.6 Comparison of evaporation model results and experimental data of mixed sand for small tunnel with air flow velocity of (a) 2.3 m/s, (b) 2.8 m/s, (c) 3.2 m/s

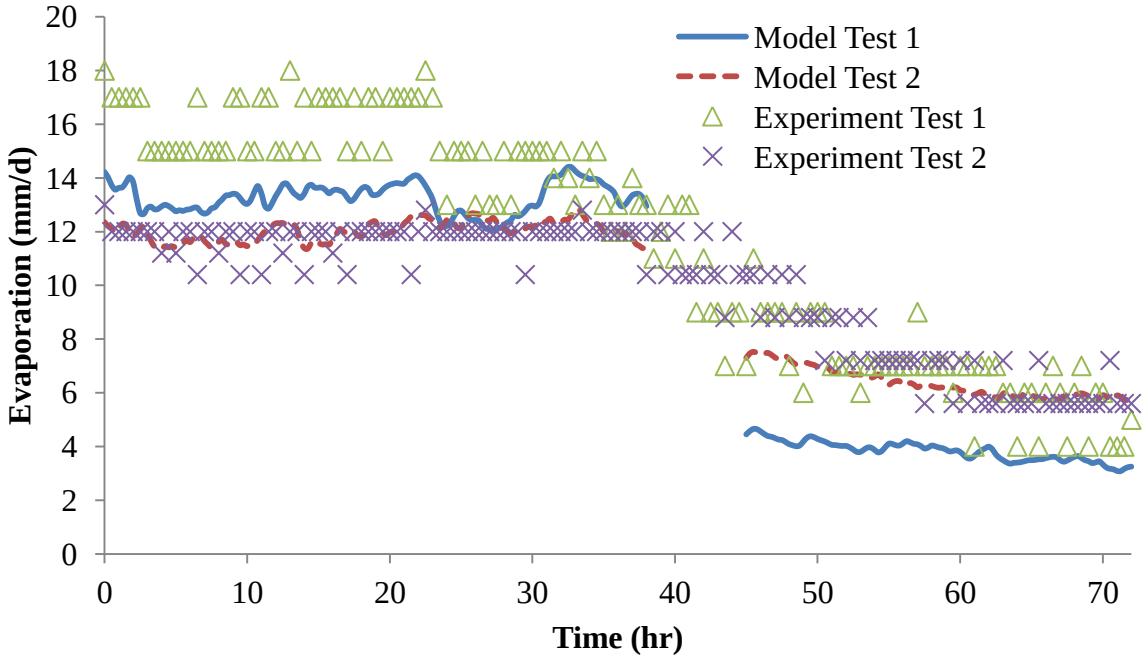

(a)

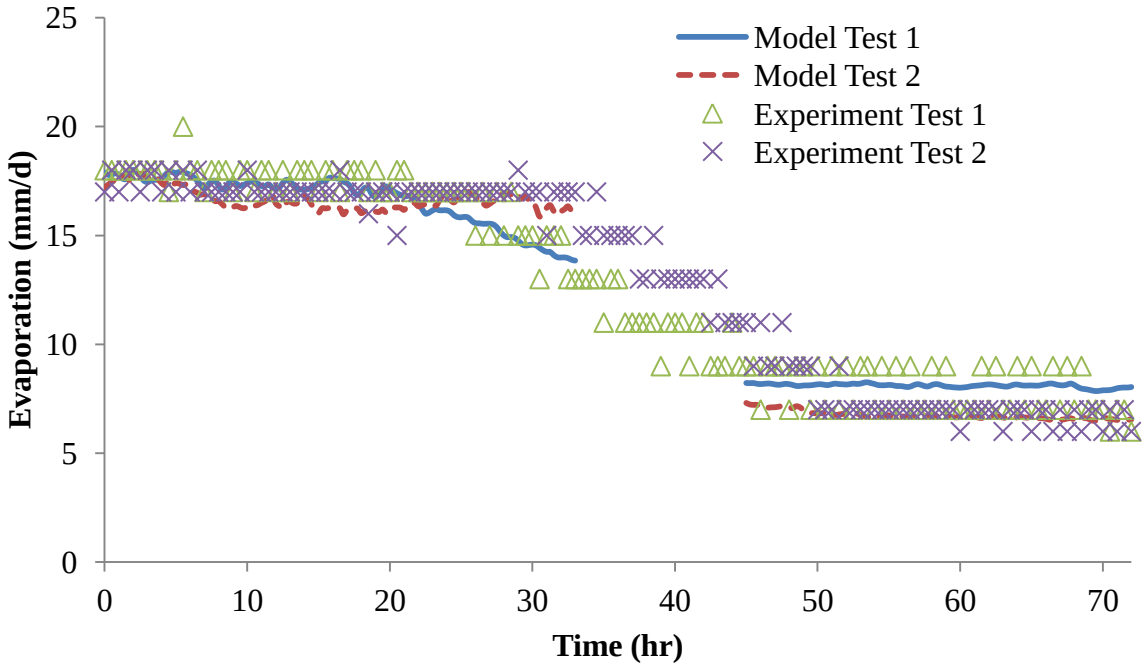
Model Test 1
Model Test 2
Experiment Test 1
Experiment Test 2
Evaporation (mm/d)
Time (hr)
0
5
10
15
20
25
0
10
20
30
40
50
60
70

(b)

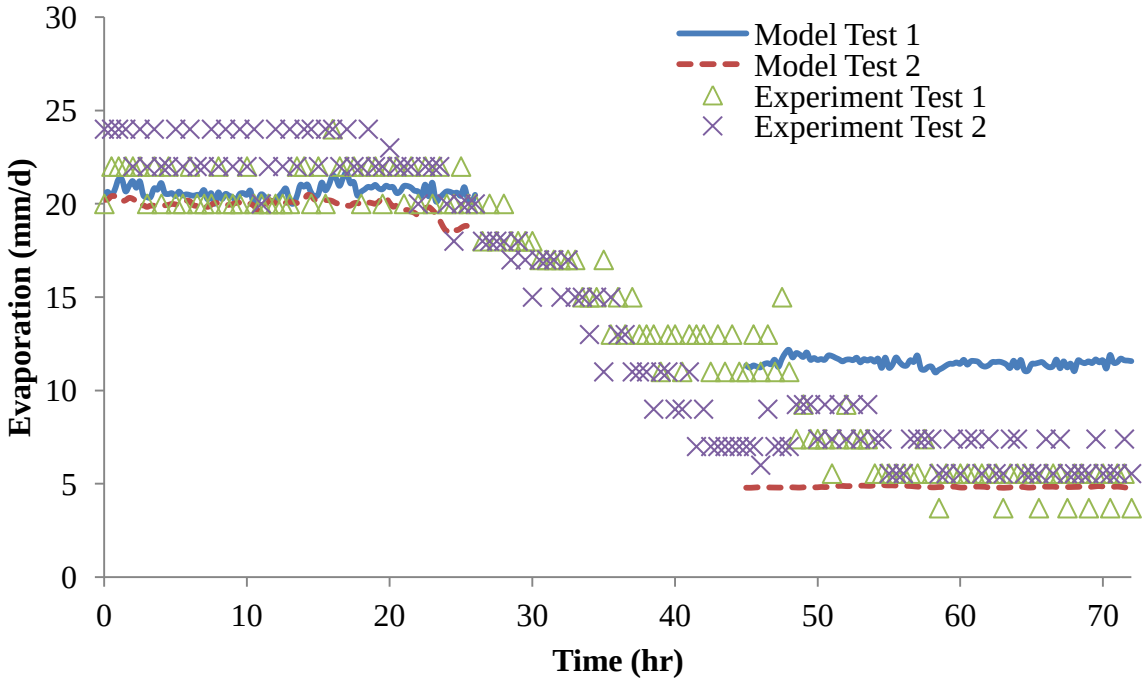
Model Test 1
Model Test 2
Experiment Test 1
Experiment Test 2
Evaporation (mm/d)
Time (hr)
0
5
10
15
20
25
30
0
10
20
30
40
50
60
70

(c)

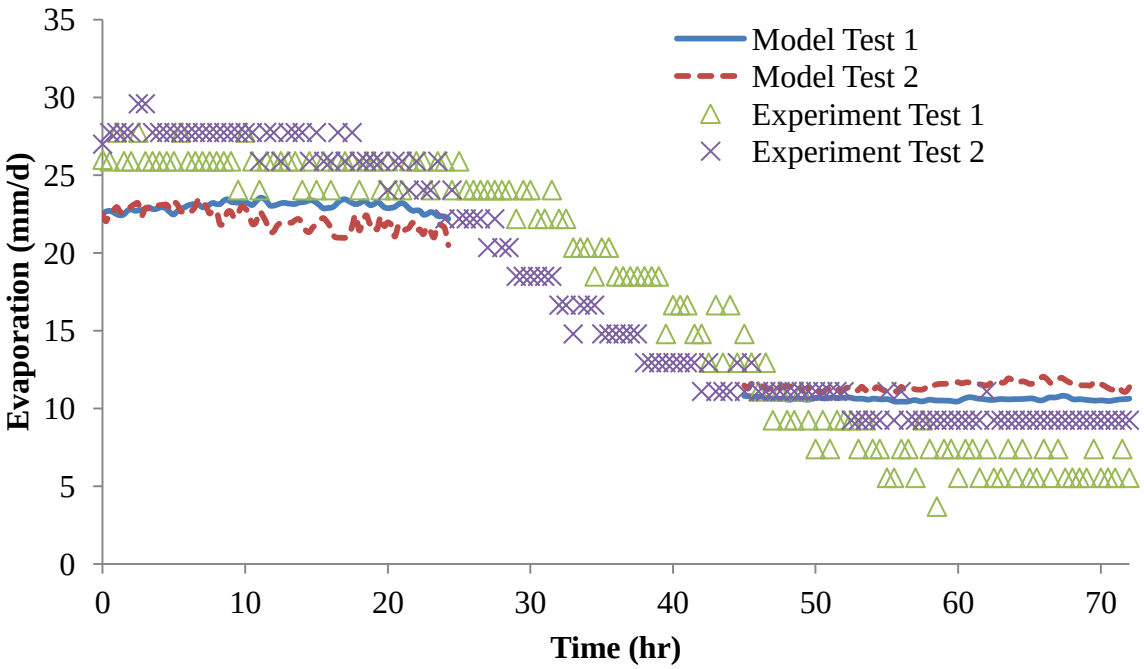

(d)

Figure 5.7 Comparison of evaporation model results and experimental data of mixed sand for large tunnel with air flow velocity of (a) 2.3 m/s, (b) 2.8 m/s, (c) 3.2 m/s and (d) 3.6 m/s

From the figures the average evaporation rate of the Stage 1 evaporation is 4.23, 5.72 and 8.34 mm/d for the velocities of 2.3 m/s, 2.8 m/s and 3.2 m/s. The duration of the Stage 1 evaporation was found to be 33.21, 24.38 and 20.95 hours for the 2.3 m/s, 2.8 m/s and 3.2 m/s velocities for the small tunnel. Duration of the Stage 1 evaporation for the large tunnel was found to be 38.5, 33.4 and 26.7 hours for the velocities of 2.3, 2.8 and 3.2 m/s. The duration was found using the characteristic length L_c calculation where the length found was 148.4 mm. After Stage 1 and the transition stage the evaporation enters Stage 2 evaporation where the rate of drying slows down significantly. From the figures we can read that the average evaporation is 6.84 mm/d for 2.3 m/s, 8.21 mm/d for 2.8 m/s, 6.47 mm/d for the 3.2 m/s and 10.21 mm/d for the 3.6 m/s velocity.

The evaporation model based on the soil and ambient conditions closely resembled the experimental evaporation captured using the electronic scale. From the evaporation model we can see the duration of Stage 1 evaporation of the coarse, fine and mixed sand based on the

characteristic length calculations. We can also see the representation of the evaporation rate in the model is comparable to the experimental data. From the model we can also see the start of Stage 2 evaporation and its rate of drying is which is represented well by the model. The model helps in predicting the evaporation rates for various types of soils under different ambient environmental conditions.

CHAPTER 6

CONCLUSIONS AND RECOMMENDATIONS

6.1 Conclusions

In this investigation, the effects that various parameters have on evaporation of water were explored in order to develop a better understanding of the rates and behaviour of saturated porous media subject to evaporation. The tests were carried out to investigate the effects of forced convection on various soil types and their effects, determine the tunnel boundary conditions and their effects, investigate the evaporation model based on the experimental results and investigate the soil conditions via infrared imagery. The following conclusions were drawn from this investigation:

- Infrared images captured in this investigation revealed that the mixed and fine soils have constant temperatures during the Stage 1 of evaporation for prolonged period of time whereas the coarse sand has really short Stage 1 evaporation, meaning the surface temperature of the porous coarse media stayed constant for a short amount of time. The FRP was easily detected due to the constant increasing temperatures of the surface of all of the samples as the water was released.
- The comparison of the infrared imagery and the experimental data had shown that the surface temperatures are dependent on the capillary action within the sand. These capillary actions help rehydrate the evaporating surface thus keeping the evaporating temperatures constant during Stage 1. When the capillary action is broken we see that the surface temperatures increases as the sample dries.
- Changes in velocity affect the initial drying process (Stage 1) of the soil evaporation regardless of the sand type. This includes coarse, fine and mixed sand. From the results we see that it takes less time for the soil to reach the FRP when the velocity of the air is increased.
- Although the changes in velocity affected all of the sand samples, coarse sand had only slight changes in evaporation rate when the velocities were increased. Fine and mixed sands had significantly larger differentiations in evaporation mostly due to stronger capillaries.

- Although the increase in evaporation shortened the Stage 1 with increased air flow, during the falling rate period the evaporation rates in most of the samples behaved the same regardless of the air flow velocity.
- Air flow velocities were found to have minimal effect on the Stage 2 drying process.
- Different boundary layer conditions affect the drying process of the soil. Thinner boundary layer of the small tunnel increased the evaporation of the soil depending on the surface water present on top of the soil.
- Obtained the experimental data sets from 42 experiments for different soils, different velocities and two different tunnels. These sets are helpful in developing physically based numerical models to simulate the evaporation at the interface between the porous media and the free surface
- The evaporation model developed based on the ambient and soil conditions simulated the results of the experimental results. The evaporation model clearly showed the Stage 1 and Stage 2 evaporation as well as the time duration of the Stage 1 evaporation and beginning of Stage 2 evaporation based on the calculations of the characteristic length.

6.2 Recommendation for Future Research

Recommendations for the future exploration of the evaporation rates include:

- Understanding of the falling rate period of the transition between the Stage 1 and Stage 2 of the evaporation model.
- Investigate the porous media drying based on the side profile using the infrared imagery.
- Develop analytical models for estimating the evaporation during the falling rate period of the transition
- Develop numerical models to simulate the water flow through the porous media and in the free surface and investigate the process of evaporation at the interface between the soil surface and the free surface.

REFERENCES

Aksel, N., and M. Schmidtchen. 1996. “Analysis of the overall accuracy in LDV measurement of film flow in an inclined channel.” *Measurement Science and Technology* 7 (8): 1140.

Aluwihare, S., and K. Watanabe. 2003. “Measurement of evaporation on bare soil and estimating surface resistance.” *Journal of Environmental Engineering* 129 (12): 1157–1168.

Aoki, I. 2000. “Analysis of characteristics of water flash evaporation under low-pressure conditions,” Heat Transfer—Asian Research Heat Trans. Asian Res. 22–33.

Avdelidis, N.P., A. Moropoulou, and P. Theoulakis. 2003. “Detection of water deposits and movement in porous materials by infrared imaging.” *Infrared Physics & Technology* 44 (3): 183–90. doi:10.1016/S1350-4495(02)00212-8.

Bittelli, M., F. Ventura, S. Campbell, L. Snyder, and P. Pissa. 2008. “Coupling of heat, water vapor, and liquid water fluxes to compute evaporation in bare Soils.” *Journal of Hydrology* 362 (3–4): 191–205.

Boast, C., and T. Robertson. 1982. “A ‘micro-lysimeter’ method for determining evaporation from bare soil: description and laboratory evaluation.” *Soil Sci. Soc. Am. J.*, no. 46: 689–696.

Bouriga, M., J. Lemyre-Baron, F. Morency, and J. Weiss. 2014. “Preliminary experimental and numerical investigations of the flow in the contraction of a boundary layer wind tunnel.” *Transactions of the Canadian Society for Mechanical Engineering* 38 (4): 517.

Brutsaert, W. 2005. “Hydrology: An Introduction.” *Cambridge Univ. Press, Cambridge, U. K.*

Budyko, I. 1955. “On the determination of evaporation from land surface.” *Meteorol. Gidrol.*, 52–58.

Cengel, Y., and J. Cimbala. 2011. *Fluid Mechanics Fundamentals and Applications*. New York: McGraw Hill.

Chauvet, F., S. Cazin, P. Duru, and M. Prat. 2010. “Use of infrared thermography for the study of evaporation in a square capillary tube.” *International Journal of Heat and Mass Transfer* 53 (9–10): 1808–18. doi:10.1016/j.ijheatmasstransfer.2010.01.008.

Daamen, C., and L. Simmonds. 1996. “Measurement of evaporation from bare soil and its estimation using surface resistance.” *Water Resources Research* 32 (5): 1393–1402.

Davarzani, H., K. Smits, R. M. Tolene, and T. Illangasekare. 2014. “Study of the effect of wind speed on evaporation from soil through integrated modeling of the atmospheric boundary layer and shallow subsurface: effect of wind speed on evaporation from soil.” *Water Resources Research* 50 (1): 661–80. doi:10.1002/2013WR013952.

Figliola, R., and D. Beasley. 2011. *Theory and Design for Mechanical Measurements*. Fifth Edition. New Jersey: John Wiley & Sons, Inc.

Ghosh, S., K. M. Keener, and Y. Pan. 2008. “A simulation based method to assess inversion algorithms for transverse relaxation data.” *Journal of Magnetic Resonance* 191 (2): 226–230.

Gupta, R. 1989. *Hydrology & Hydraulic Systems*. New Jersey: Prentice-Hall.

Haghighi, E., E. Shahraeeni, P. Lehmann, and D. Or. 2013. “Evaporation rates across a convective air boundary layer are dominated by diffusion: diffusion-dominant evaporation rates.” *Water Resources Research* 49 (3): 1602–10. doi:10.1002/wrcr.20166.

Hottner, T. 1995. “Theoretical tunnel and experimental investigations of wall hybrid wind tunnel testing.” *Experiments in Fluids* 19: 233–40.

Innocenzi, P., L. Malfatti, M. Piccinini, A. Marcelli, and D. Grosso. 2009. “Water evaporation studied by in situ time-resolved infrared spectroscopy.” *The Journal of Physical Chemistry A* 113 (12): 2745–49. doi:10.1021/jp806608d.

Jackson, R., B Kimball, R Reginato, and F Nakayama. 1974. “Diurnal soil water evaporation time-depth-flux patterns,” 505–9.

Jassal, S., M. Novak, and T. Black. 2003. “Effect of surface layer thickness on simultaneous transport of heat and water in a bare soil and its implications for land surface schemes.” *Atmosphere-Ocean* 41 (4): 259–72. doi:10.3137/ao.410401.

Kohsiek, W. 1980. “Rapid circulation chamber for measuring bulk stomatal resistance.” *Royal Netherland Meterological Institute*, 42–52.

Kondo, J., Sato, T and N. Saigusa. 1989. “A parameterization of evaporation from bare soil surfaces,” *Shinjo Branch of Snow and Ice Studies, National Research Center for Disaster Prevention, Shinjo, Japan* 385–89.

Laurindo, J., and M. Prat. 1996. “Numerical and experimental network study of evaporation in capillary porous media. phase distributions.” *Chemical Engineering Science* 51 (23): 5171–85.

Lehmann, P., S. Assouline, and D. Or. 2008. “Characteristic lengths affecting evaporative drying of porous media.” *Physical Review E* 77 (5). doi:10.1103/PhysRevE.77.056309.

Lehmann, P., and D. Or. 2009. “Evaporation and capillary coupling across vertical textural contrasts in porous media.” *Physical Review E* 80 (4). doi:10.1103/PhysRevE.80.046318.

Leuning, R., and I. Foster. 1981. “Estimation of transpiration by single trees: comparison of a ventilated chamber, leaf energy budgets and combination equation.” *Agric. Forest Meteorol.*, no. 20: 42–52.

Libii, J. 2013. “A method of evaluating the presence of fan-blade-rotation induced unsteadiness in wind tunnel experiments.”

Linsley, R., K. Max, and P. Joseph. 1982. *Hydrology for Engineers*. McGraw-Hill Book Company.

Mahfouf, J, and J Moilhan. 1991. “Comparative study of various formulations of bare soil using in situ data,” *Journal of Applied Meteorology* 1354–65.

Mokhtari, S, and P Bradshaw. 2016. “Longitudinal Vortices in Wind Tunnel Wall Boundary Layers.” *The Aeronautical Journal* 87 (866): 233–36. doi:10.1017/S0001924000019540.

Nachshon, U., E. Shahraeeni, D. Or, M. Dragila, and N. Weisbrod. 2011. “Infrared thermography of evaporative fluxes and dynamics of salt deposition on heterogeneous porous surfaces: irt of evaporation and salt precipitation.” *Water Resources Research* 47 (12): doi:10.1029/2011WR010776.

Neriah, B., S. Assouline, U. Shavit, and N. Weisbrod. 2014. “Impact of ambient conditions on evaporation from porous media.” *Water Resources Research* 50 (8): 6696–6712. doi:10.1002/2014WR015523.

Prichard, P., and J. Leylegian. 2011. *Introduction to Fluid Mechanics*. 8thed. New Jersey: John Wiley & Sons, Inc.

Prommas, R. 2011. “Theoretical and experimental study of heat and mass transfer mechanism during convective drying of multi-layered porous packed bed.” *International Communications in Heat and Mass Transfer* 38 (7): 900–905. doi:10.1016/j.icheatmasstransfer.2011.03.031.

Sakai, M., S. Jones, and M. Tuller. 2011. “Numerical evaluation of subsurface soil water evaporation derived from sensible heat balance.” *Water Resources Research*, no. 47. doi:10.1029/2010WR009866.

Scherer, G. 1990. “Theory of drying.” *Journal of the American Ceramic Society* 73 (1): 3–14. doi:10.1111/j.1151-2916.1990.tb05082.x.

Schultz, P. 1991. “On the falling-rate period.” *Chem. Eng. Technology*, 234–39. doi:10.1002/ceat.270140404.

Seymour, V., and T. Hsiao. 1984. “A soil surface psychrometer for measuring humidity and studying evaporation.” *Agric. For. Meteorol.*, no. 32: 61–70.

Shahraeeni, E., P. Lehmann, and D. Or. 2012. “Coupling of evaporative fluxes from drying porous surfaces with air boundary layer: Characteristics of evaporation from discrete pores: Coupling evaporation from discrete pores with boundary layer.” *Water Resources Research* 48 (9): n/a-n/a. doi:10.1029/2012WR011857.

Shahraeeni, E., and D. Or. 2010. “Thermo-evaporative fluxes from heterogeneous porous surfaces resolved by infrared thermography: evaporation fluxes from porous surfaces.” *Water Resources Research* 46 (9): n/a-n/a. doi:10.1029/2009WR008455.

Shokri, N., P. Lehmann, and D. Or. 2008. “Effects of hydrophobic layers on evaporation from porous media.” *Geophysical Research Letters* 35 (19). doi:10.1029/2008GL035230.

———. 2009. “Characteristics of evaporation from partially wettable porous media: Evaporation from wettable porous media.” *Water Resources Research* 45 (2): n/a-n/a. doi:10.1029/2008WR007185.

Shokri, N., and D. Or. 2011. “What determines drying rates at the onset of diffusion controlled stage-2 evaporation from porous media?: Drying rate at the onset of stage-2 evaporation.” *Water Resources Research* 47 (9): n/a-n/a. doi:10.1029/2010WR010284.

———. 2013. “Drying patterns of porous media containing wettability contrasts.” *Journal of Colloid and Interface Science* 391 (February): 135–41. doi:10.1016/j.jcis.2012.08.074.

Smits, K. M., A. Cihan, T. Sakaki, and T. H. Illangasekare. 2011. “Evaporation from soils under thermal boundary conditions: experimental and modeling investigation to compare equilibrium- and nonequilibrium-based approaches.” *Water Resources Research* 47 (5). doi:10.1029/2010WR009533.

Smits, K. M., V. V. Ngo, A. Cihan, T. Sakaki, and T. H. Illangasekare. 2012. “An evaluation of models of bare soil evaporation formulated with different land surface boundary conditions and assumptions: Models of bare soil evaporation.” *Water Resources Research* 48 (12): n/a-n/a. doi:10.1029/2012WR012113.

Uclés, O., L. Villagarcía, Y. Cantón, and F. Domingo. 2013. “Microlysimeter station for long term non-rainfall water input and evaporation studies.” *Agricultural and Forest Meteorology* 182–183 (December): 13–20. doi:10.1016/j.agrformet.2013.07.017.

Veissman, W., G. Lewis, and J. Knapp. 1989. *Introduction to Hydrology*. 3rd ed. New York: Harper & Row.

Wecel, D., T. Chmielniak, and J. Kotowicz. 2008. “Experimental and numerical investigations of the averaging pitot tube and analysis of installation effects on the flow coefficient.” *Flow Measurement and Instrumentation*, 301–6.

Yiotis, A. G., Ioannis N. Tsimpanogiannis, A. K. Stubos, and Y. C. Yortsos. 2007. “Coupling between external and internal mass transfer during drying of a porous medium: coupling external and internal mass transfer.” *Water Resources Research* 43 (6): n/a-n/a. doi:10.1029/2006WR005558.

Zhang, H., L. Simmonds, J. Morrison, and D. Payne. 1997. “Estimation of transpiration by single trees: comparison of sap flow measurements with a combination equation,” *Agricultural and Forest Meteorology* 156–69.

VITA AUCTORIS

NAME:	Rafal Marynowski
PLACE OF BIRTH:	Kielce, Poland
YEAR OF BIRTH:	1989
EDUCATION:	St. Clair College of Applied Arts and Technology, Windsor, ON, 2007 – 2010, Civil Engineering Technology Diploma
	University of Windsor, Windsor, ON, 2010 – 2013, B.A.Sc, Civil Engineering
	University of Windsor, Windsor, ON, 2013 – 2016, M.A.Sc, Civil Engineering